九州大学学術情報リポジトリ
Kyushu University Institutional Repository

Effect of a Density Structure of Solvent Particles on Solute Dynamics

原, 諒平

https://doi.org/10.15017/1806806

出版情報：九州大学, 2016, 博士（理学）, 課程博士
バージョン：
権利関係：全文ファイル公表済

A Thesis Submitted to Kyushu University for the Degree of Doctor of Science

Effect of a Density Structure of Solvent Particles on Solute Dynamics

Ryohei Hara

Department of Physics,
Graduate School of Science, Kyushu University,
Japan

December, 2016

Abstract

The purpose of the present thesis is to establish the relationship between the solute dynamics and the density distribution of solvent particles. For this purpose, the relationship is clarified by two studies. One is the solute dynamics affected by the equilibrium density distribution of solvent particles. Another is the nonequilibrium density distribution of solvent particles on a moving solute particle. Two studies are carried out in an insertion process of a large sphere (a solute particle) into a cylindrical vessel, which is immersed in small spheres (solvent particles). The insertion process of a solute particle is well observed in the biological process and fundamental phenomenon for understanding of biological functions.

The purpose of the first study is to clarify the solute dynamics under the assumption of the equilibrium density distribution of solvent particles. The solute dynamics is calculated by the Fokker-Planck (FP) equation with the potential of mean force (PMF) numerically. Under this assumption, effects of solvent particles on a solute particle are represented by the PMF between the solute particle and vessel. The PMF is calculated by the three-dimensional integral equation theory. As the result, the probability density of a solute particle is high in the center of the vessel cavity. In addition, a flux of a solute particle is higher at the central axis of a vessel entrance than at the side region.

The purpose of the second study is to clarify the nonequilibrium density distribution of solvent particles under the constraint of the trajectory of a moving solute particle. The nonequilibrium density distribution of solvent particles is calculated by the nonequilibrium theory formulated by incorporating the movement of a solute particle into time dependent density functional theory (TDDFT). The deviation from the equilibrium density distribution increases with the velocity of a solute particle. In particular, the discrepancy is large in the bottom of the vessel. Besides, the grand potential functional defined by TDDFT dramatically increases with the velocity of a solute particle. The relationship with the grand potential functional and number of solvent particles inside of the vessel cavity is discussed.

Contents

1 Introduction **4**

2 Studies of Equilibrium Solvent Effect on Biomolecules **7**
2.1 Grand Potential of Solvent Particles 7
2.2 Asakura-Oosawa Theory and Its Application to the Biological Systems 8
2.3 Density Functional Theory 9
2.4 Application of DFT to the Stability of a Protein 13
2.4.1 Purpose 13
2.4.2 Simple Expression of Free Energy 14
2.4.3 Results 15
2.5 Integral Equation Theory and Potential of Mean Force 15
2.6 Application of Integral Equation Theory to Chaperonin 18
2.6.1 Introduction 18
2.6.2 Model 18
2.6.3 Calculation Method 20
2.6.4 Results 20
2.6.5 Discussion and Conclusion 20
2.7 Summary 21

3 Equilibrium Effects of Solvent Particles on Solute Dynamics **25**
3.1 Introduction 25
3.2 Model 26
3.3 Theory 28
3.4 Results of model I 29
3.4.1 Spatial Distributions of Probability Density of the Large Sphere 29
3.4.2 Probability Density at the Local Minima of the Potential of Mean Force 29
3.4.3 Flux of the Probability Density 31
3.5 Size Dependence 33
3.6 Discussions 34
3.7 Summary 37

4 Nonequilibrium Effect of Solvent Particles on a Moving Solute 39
4.1 Introduction . . . 39
4.2 Theory . . . 41
4.2.1 Treatment of a Moving Solute Particle . . . 41
4.2.2 Time Dependent Density Functional Theory . . . 41
4.2.3 Grand Potential Functional . . . 42
4.3 Application to Insertion Process . . . 43
4.4 Density Distribution and Number of Solvent Particles in the Vessel 45
4.4.1 Results . . . 45
4.4.2 Discussions . . . 47
4.5 Grand Potential Functional . . . 48
4.5.1 Result for the Difference of the Grand Potential Functional . 49
4.5.2 Nonequilibrium part of Difference of Grand Potential Functional . . . 49
4.5.3 Dependence of the DGPF on Height of the Vessel . . . 50
4.5.4 Dependence of the DGPF on Inner Diameter of the Vessel . 50
4.5.5 Discussions . . . 51
4.6 Summary . . . 51

5 Summary 64

A Ornstein Zernike Equation and Hyper-netted Chain Approximation 66
A.1 Ornstein Zernike Equation . . . 66
A.2 Percus's Method . . . 67
A.3 Hyper-netted Chain (HNC) Approximation . . . 68

B Morita-Hiroike Formula 70

C Special Treatment of Number Density of Solvent Particles for the Hard-body Model 73

D Relationship with the Grand Potential Functional and Work 75

Chapter 1

Introduction

The living systems are sustained by biomolecule functions. The functions of biomolecules are closely related to the movement of the biomolecules. For examples, the F_1ATPase [1] is rotated when the F_1ATPase serves a function in the adenosine triphosphate (ATP) synthase [2]. A myosin V [3] slides over the actin filament when it acts as the transporter of the substance [4]. The GroEL assists a protein folding after an unfolded protein moves into the GroEL cavity [5–7].

Since these functions are performed in the water, the movement of biomolecules (solute particles) is affected by solvent particles. A typical example is the excluded volume effect. The repulsive potential between the solute and solvent particles excludes solvent particles, leading to a decrease in available volumes of the translational motion of solvent particles. When solute particles are contacting with each other, the excluded volumes of solute particles are overlapped. It leads to an increase of the available volumes for solvent particles and the corresponding entropy gain. Therefore, the effective attractive interaction between solute particles is induced by solvent particles. This effect has been studied by Asakura and Oosawa in the colloidal system [8, 9].

Though the solvent effect studied by Asakura-Oosawa theory is derived by assuming the homogeneous density distribution, the number density distribution around two biomolecules has an inhomogeneous structure due to the solvent-solvent interaction. In particular, number density at a position contacting with biomolecules becomes over six times higher than that in the bulk, given the size ratio and average number density ρ_0 by 10 and $\rho_0 d_{\mathrm{S}}^3 = 0.7317$[1]. Here, d_{S} is the diameter of a solvent particle. Because the attractive interaction increases with number density at the position contacting with biomolecules, the inhomogeneous distribution around the biomolecules makes the effective biomolecule-biomolecule interaction more attractive.

The effects of the inhomogeneous density distribution of solvent particles on

[1] This result is obtained by the integral equational theory. The solute and solvent particles are modeled by hard sphere model. A size ratio between solute and solvent particles is 10 : 1. Average number density ρ_0 is given by $\rho_0 d_{\mathrm{S}}^3 = 0.7317$, where d_{S} is the diameter of a solvent particle.

solute particles have been studied on the basis of equilibrium statistical mechanics. The effects of solvent particles on solute particles are represented by the grand potential of solvent particles. Examples of the theories for calculating the grand potential are density functional theory (DFT) [10] and integral equation theory (IET) [11]. In these theories, the inhomogeneous density distribution of solvent particles can be taken into consideration. These theories have been applied to the biological systems. For instance, the DFT has been applied to the stability of the configuration of a protein [12], the rotation of ATPase [13, 14], and the tripartite efflux system [15] with the help of the morphometric thermodynamic approach (MTA) [16]. The IET has also been applied to the chaperonin [17–20], the motor protein [21], and the tripartite efflux system [22, 23]. The theoretical results can describe the stability of the configuration of biomolecules.

Little is known about the movement of biomolecules on the inhomogeneous density distribution, though the functions of biomolecules are closely related to the movement of biomolecules. An example of importance of dynamics is the function of the chaperonin, which assists an unfolded protein fold. When the chaperonin assists the protein fold, an unfolded protein is inserted into the chaperonin cavity. The efficiency of the folding function depends on the protein position, such as bottom, top, and center of the chaperonin cavity. The analysis of equilibrium theory has shown that the protein is most stable at the bottom of the chaperonin cavity [17–20]. The equilibrium theory has also predicted that the protein is trapped at the center of the chaperonin due to the PMF barrier [17]. However, the time which it takes for the protein to be trapped at the center of the chaperonin cavity can not be obtained by the equilibrium theory.

The nonequilibrium effects of solvent particles have never been studied because the diffusion coefficient of a biomolecule is 10 times as large as that of a water molecule (solvent particle). Because of the large ratio of the diffusion coefficient, the relaxation time of solvent particles is sufficiently short compared to a translational motion of biomolecules. Therefore, most studies have been studied in equilibrium theory. However, the short relaxation time of solvent particles does not always hold. A typical example is an insertion process of an unfolded protein into a chaperonin. It may take a long time for solvent particles to relax when a motion of solvent particles becomes restricted on the space between the protein and chaperonin. If the relaxation time in the restricted space becomes 10 times longer than that in the bulk, solvent particles are in a nonequilibrium state. To discuss the validity of assumption of equilibrium state, the calculation of nonequilibrium distribution is needed.

The purpose of this thesis is to develop the method of studying the biomolecule dynamics including the effect of the number density distribution of solvent particles in the equilibrium state. For this purpose, the method is formulated using the Fokker-Plunk (FP) equation [24] with the potential of mean force (PMF). The PMF is calculated by the IET [11]. The formulated method is applied to the system consisting of a solute particle, a cylindrical vessel, and solvent particles. By the formulated method, the time development of the spatial distribution of

probability density of solute particle can be calculated numerically. This system mimics the insertion of an unfolded protein into the chaperonin. I discuss the mechanism of the insertion by comparing the calculated time scale of the solute insertion with the time scale speculated by the experimental result.

The other purpose of this thesis is to develop the theory of calculating solvent nonequilibrium distribution on a moving solute particle. The nonequilibrium distribution of solvent particles on a moving solute particle is studied by a theory incorporating the movement of a solute particle into time development density functional theory (TDDFT) [25–27]. By TDDFT, the time development of the density distribution can be obtained. Applying the theory to the solute insertion process into the cylindrical vessel with the constant velocity of a solute particle, the nonequilibrium distribution of solvent particles is calculated. In addition, the relationship between the grand potential functional and the effect of solvent particle on a moving solute particle is discussed.

The thesis is organized as follows. In Chapter 2, I review the equilibrium theories to calculate the effects of solvent particles on biomolecules. In addition, I review the application of the theories to the biological systems. In Chapter 3, I develop a nonequilibrium theory formulated using the Fokker-Planck equation, assuming the equilibrium density distribution of small spheres. Moreover, I apply the theory to a solute insertion process into a cylindrical vessel, immersed in small spheres. In Chapter 4, I formulate a nonequilibrium theory by incorporating the movement of a large-sphere into TDDFT. Furthermore, I apply the theory to the dynamics of solvent particles, when a solute particle is inserted into a cylindrical vessel with a constant velocity. In Chapter 5, I summarize this thesis.

Chapter 2

Studies of Equilibrium Solvent Effect on Biomolecules

In this chapter, I review the study of the effect of solvent particles on the biomolecules. The effect of solvent particles on the biomolecules has been studied by the grand potential of solvent particles. As the theories for calculating the grand potential, I will show the three theories, which are the Asakura-Oosawa (AO) theory, density functional theory (DFT), and integral equation theory (IET). I also show applications of these theories to biological systems.

2.1 Grand Potential of Solvent Particles

An effect of solvent particles on biomolecules has an important role in mechanism of biomolecule functions, such as the adsorption phenomenon on a protein, native structure of a protein, and the insertion process of a protein into the chaperonin. The equilibrium effect of solvent particles on biomolecules is represented by the grand potential of solvent particle with the configuration of biomolecules being fixed. The grand potential of solvent particles depends on the configuration of biomolecules. When the grand potential of solvent particles takes a local minimum value, the configuration of biomolecules becomes stabilized. When the grand potential is minimized, the biomolecule configuration becomes most stable.

To describe the grand potential of solvent particles, a macroscopic system consisting of solvent particles of mass m enclosed in a volume V and chemical potential μ is considered. The degree of freedom of the biological molecule is not considered. The restriction is represented by the external field $\Phi_{\mathrm{ext}}(\boldsymbol{r})$ depending on the configuration of a biomolecule. In addition, I consider the grand canonical ensemble. The Hamiltonian $\mathcal{H}$ of the system consisting of N solvent particles is defined as

$$\mathcal{H}(\boldsymbol{r}^N, \boldsymbol{p}^N) \equiv \sum_{i=1}^{N} \frac{|\boldsymbol{p}_i^2|}{2m} + \sum_{i>j=1}^{N} v(\boldsymbol{r}_{i,j}) + \sum_{i=1}^{N} \Phi_{\mathrm{ext}}(\boldsymbol{r}_i). \tag{2.1}$$

Here, $\boldsymbol{r}^N$ and $\boldsymbol{p}^N$ are the $3N$ coordinates and $3N$ momenta of the solvent particles.

Moreover, $v(\boldsymbol{r}_{i,j})$ is the interaction between solvent particles, where $\boldsymbol{r}_{i,j}$ is the relative position of solvent particle i and j. And then, $\Phi_{\mathrm{ext}}(\boldsymbol{r}_i)$ is the interaction between solvent particle i and a biomolecule.

The interaction between solvent particle i and a biomolecule $\Phi_{\mathrm{ext}}(\boldsymbol{r}_i)$ is represented by the sum of the interaction between an atom of a biomolecule and a solvent particle. When a biomolecule consists of N_{solu} atoms, $\Phi_{\mathrm{ext}}(\boldsymbol{r}_i)$ can be rewritten as

$$\Phi_{\mathrm{ext}}(\boldsymbol{r}_i) \equiv \sum_{n=1}^{N_{\mathrm{solu}}} v_{\mathrm{solv,solu}}(\boldsymbol{r}_{i,n}). \tag{2.2}$$

Here, $\boldsymbol{r}_{i,n}$ is the relative position between solvent particle i and an atom of biomolecule n.

The grand potential of solvent $\Omega(T, V, \mu)$ can be related to the Hamiltonian by

$$e^{-\beta\Omega(T,V,\mu)} = \sum_{N=1}^{\infty} \frac{e^{\beta\mu N}}{N! h^{3N}} \int \exp[-\beta\mathcal{H}(\boldsymbol{r}^N, \boldsymbol{p}^N)] \mathrm{d}\boldsymbol{r}^N \mathrm{d}\boldsymbol{p}^N. \tag{2.3}$$

Here, h is Planck's constant and $\beta = 1/(k_{\mathrm{B}}T)$, where k_{B} is Boltzmann's constant and T is the absolute temperature.

2.2 Asakura-Oosawa Theory and Its Application to the Biological Systems

Asakura-Oosawa (AO) theory [8, 9] can be rederived by the theory based on the equilibrium statics mechanics [28] in the condition when the interaction between solvent particles is ignored and the interaction between a solvent particle and biomolecules is modeled in hard body potential. In this condition, since N-fold integral can be calculated independently, one obtains grand potential of solvent particles

$$\begin{aligned}
e^{-\beta\Omega(T,V,\mu)} &= \sum_{N=0}^{\infty} \frac{e^{\beta\mu N}}{N!} \int \exp\left[-\beta\left\{\sum_{i=1}^{N} \frac{\boldsymbol{p}^2}{2m} + \sum_{i=1}^{N} \Phi_{\mathrm{ext}}(\boldsymbol{r}_i)\right\}\right] \mathrm{d}\boldsymbol{r}^N \mathrm{d}\boldsymbol{p}^N \\
&= \sum_{N=0}^{\infty} \frac{e^{\beta\mu N}}{N! \Lambda^{3N}} \int e^{-\beta\sum_{i=1}^{N}\Phi_{\mathrm{ext}}(\boldsymbol{r}_i)} \mathrm{d}\boldsymbol{r}^N \\
&= \sum_{N=0}^{\infty} \frac{1}{N!} \left[\frac{e^{\beta\mu}}{\Lambda^3} \int e^{-\beta\Phi_{\mathrm{ext}}(\boldsymbol{r})} \mathrm{d}\boldsymbol{r}\right]^N \\
\beta\Omega(T, V, \mu) &= -\frac{e^{\beta\mu}}{\Lambda^3} \int e^{-\beta\Phi_{\mathrm{ext}}(\boldsymbol{r})} \mathrm{d}\boldsymbol{r}.
\end{aligned} \tag{2.4}$$

Here, $\Lambda = (h^2/2\pi m k_{\mathrm{B}}T)^{\frac{1}{2}}$ is de Broglie wavelength. Since number density of solvent particles is written as $\rho \equiv \langle N\rangle/(V - V_{\mathrm{ex}}) = e^{\beta\mu}/\Lambda^3$, the grand potential is obtained by

$$\beta\Omega = -\rho(V - V_{\mathrm{ex}}). \tag{2.5}$$

Here, $V_{\mathrm{ex}} \equiv V - \int \exp[-\beta\Phi_{\mathrm{ext}}(\boldsymbol{r})]\mathrm{d}\boldsymbol{r}$ is the excluded volumes for the interaction between the biomolecule and solvent particle $\Phi_{\mathrm{ext}}(\boldsymbol{r})$.

To apply the theory to the adsorption phenomenon of a xenon atom on a protein, the grand potential in the binding case of a protein and a xenon is compared with that in the unbinding case. The external field $\Phi_{\mathrm{ext}}(\boldsymbol{r})$ in the binding case differs from that in the unbinding case. Thus, the excluded volumes are also changed. The excluded volumes of binding and unbinding cases are denoted by $V_{\mathrm{ex,bind}}$ and $V_{\mathrm{ex,unbind}}$. One can obtain the difference of grand potential $\Delta\Omega$ from

$$\beta\Delta\Omega = -\rho(V_{\mathrm{ex,unbind}} - V_{\mathrm{ex,bind}}) \equiv -\rho V_{\mathrm{overlap}}. \tag{2.6}$$

Here, V_{overlap} is the overlapped volumes between the excluded volume of a protein and a xenon.

One can interpret the AO theory that the effective attractive interaction is induced by the effects of solvent particles. In the binding of a xenon to a protein, the excluded volumes of solvent particles overlap. It leads to an increase in the total volume available for the translational displacement of solvent particles. The entropy corresponding to the increase in the total volume increases. Thus, the binding state is more stable than unbinding state. The effect by excluded volume is called as depletion effect and has often been discussed in phase separation of colloidal suspension [29].

Akiyama *et al.* have calculated the difference of grand potential between the binding and unbinding cases from the AO theory [28]. To use the AO theory, the interaction between a solvent particle and a protein is approximated by the hard body potential. In their model, all the atoms in the protein is modeled by hard sphere with the diameter 3.16Å, which is determined by molecular dynamics simulation. Given the diameter of the atoms, the excluded volumes can be obtained. From the excluded volumes, the overlapped volume can be calculated.

They have compared the locations and stability of stable points obtained by the AO theory with that obtained by experimental result. In the AO theory, the locations of stable points for the binding of a xenon atom are represented by the positions of the local minima in $\Delta\Omega$. The predicted stable points are well agree with the binding sites obtained by the X-ray crystallographic data [30]. The calculated stability of most stable point, which is represented by $\Delta\Omega$, is -3.7 kcal mol^{-1} by using the AO theory. Since $\Delta\Omega$ is -4.2 kcal mol^{-1} in the experimental result [31] (manometric method), the error is about only 12% in spite of the simple calculation.

2.3 Density Functional Theory

Let us consider the system with the virtual external field $u(\boldsymbol{r})$. The Hamiltonian in the system is

$$\mathcal{H}_{\mathrm{total}}(\boldsymbol{r}^N, \boldsymbol{p}^N) = \mathcal{H}(\boldsymbol{r}^N, \boldsymbol{p}^N) + \int \hat{\rho}(\boldsymbol{r})u(\boldsymbol{r})\mathrm{d}\boldsymbol{r}, \tag{2.7}$$

where

$$\hat{\rho}(\boldsymbol{r}) \equiv \sum_{i=1}^{N} \delta(\boldsymbol{r} - \boldsymbol{r}_i). \tag{2.8}$$

Here, $\hat{\rho}(\boldsymbol{r})$ is microscopic number density and $\mathcal{H}(\boldsymbol{r}^N, \boldsymbol{p}^N)$ is defined by Eq. (2.1). The grand potential in the presence of the virtual external field $\Omega[u(\boldsymbol{r})]$ is defined by

$$e^{-\beta\Omega[u(\boldsymbol{r})]} \equiv \sum_{N=1}^{\infty} \frac{e^{N\beta\mu}}{N!h^{3N}} \int \exp\left[-\beta\left\{\mathcal{H}(\boldsymbol{r}^N, \boldsymbol{p}^N) + \int \hat{\rho}(\boldsymbol{r}')u(\boldsymbol{r}')\mathrm{d}\boldsymbol{r}'\right\}\right] \mathrm{d}\boldsymbol{r}^N \mathrm{d}\boldsymbol{p}^N. \tag{2.9}$$

From Eq. (2.9), one can obtain the variational equation as follows.

$$\frac{\delta\Omega[u(\boldsymbol{r})]}{\delta u(\boldsymbol{r})} = \langle\hat{\rho}(\boldsymbol{r})\rangle_{\mathcal{H}_{\mathrm{total}}} \equiv \rho(\boldsymbol{r}) \tag{2.10}$$

Here, $\rho(\boldsymbol{r})$ is equilibrium number density in the presence of the virtual external field and $\langle ... \rangle_{\mathcal{H}_{\mathrm{total}}}$ is the grand canonical ensemble average with the Hamiltonian $\mathcal{H}_{\mathrm{total}}(\boldsymbol{r}^N, \boldsymbol{p}^N)$. For a given $u(\boldsymbol{r})$, the density $\rho(\boldsymbol{r})$ is uniquely determined.

The grand potential functional as the function of $\rho(\boldsymbol{r})$ is defined by Legendre transformation of $\Omega[u(\boldsymbol{r})]$ as the functional of $u(\boldsymbol{r})$

$$\Omega[\rho(\boldsymbol{r})] \equiv \Omega[u(\boldsymbol{r})] - \int \rho(\boldsymbol{r})u(\boldsymbol{r})\mathrm{d}\boldsymbol{r}. \tag{2.11}$$

The variation of the grand potential functional $\Omega[\rho(\boldsymbol{r})]$ is expressed in

$$\begin{aligned} \delta\Omega[\rho(\boldsymbol{r})] &= \delta\Omega[u(\boldsymbol{r})] - \int u(\boldsymbol{r})\delta\rho(\boldsymbol{r})\mathrm{d}\boldsymbol{r} - \int \rho(\boldsymbol{r})\delta u(\boldsymbol{r})\mathrm{d}\boldsymbol{r} \\ &= \delta\Omega[u(\boldsymbol{r})] - \int u(\boldsymbol{r})\delta\rho(\boldsymbol{r})\mathrm{d}\boldsymbol{r} - \int \frac{\delta\Omega[u(\boldsymbol{r})]}{\delta u(\boldsymbol{r})}\delta u(\boldsymbol{r})\mathrm{d}\boldsymbol{r} \\ &= -\int u(\boldsymbol{r})\delta\rho(\boldsymbol{r})\mathrm{d}\boldsymbol{r}. \end{aligned} \tag{2.12}$$

As the result, one can obtain

$$\frac{\delta\Omega[\rho(\boldsymbol{r})]}{\delta\rho(\boldsymbol{r})} = -u(\boldsymbol{r}). \tag{2.13}$$

For a given $\rho(\boldsymbol{r})$, the virtual external field $u(\boldsymbol{r})$ is uniquely determined.

For $u(\boldsymbol{r}) = 0$, one can obtain number density in equilibrium state

$$\left.\frac{\delta\Omega[\rho(\boldsymbol{r})]}{\delta\rho(\boldsymbol{r})}\right|_{\rho(\boldsymbol{r})=\rho_{\mathrm{eq}}(\boldsymbol{r})} = 0. \tag{2.14}$$

Here, $\rho_{\mathrm{eq}}(\boldsymbol{r})$ is equilibrium number density in the system with the Hamiltonian $\mathcal{H}$. The theory for obtaining the equilibrium number density from the equation (2.14)

is called the density functional theory (DFT) [10, 32]. Moreover, one can derive that $\Omega[\rho(\boldsymbol{r})]$ is convex [26]. If the grand potential function $\Omega[\rho(\boldsymbol{r})]$ is given, one can obtain number density in the equilibrium state.

An expression of the grand potential functional is difficult to obtain when there are interactions between particles. If there are no contribution of interactions to the Hamiltonian, the grand potential can analytically be obtained from Eq. (2.4). In the absence of interactions, the grand potential in the presence of the virtual external field $u(\boldsymbol{r})$ and external field $\Phi_{\rm ext}(\boldsymbol{r})$ is given by

$$\beta\Omega^{\rm id}[u(\boldsymbol{r}),\Phi_{\rm ext}(\boldsymbol{r})] = -\frac{e^{\beta\mu^{\rm id}}}{\Lambda^3}\int \exp[-\beta\{\Phi_{\rm ext}(\boldsymbol{r})+u(\boldsymbol{r})\}]{\rm d}\boldsymbol{r}. \tag{2.15}$$

One can find that number density $\rho(\boldsymbol{r})$ have a relationship with the virtual external field $u(\boldsymbol{r})$ from the variation equation [Eq. (2.10)] by

$$\rho(\boldsymbol{r}) = \frac{\delta\Omega[u(\boldsymbol{r}),\Phi_{\rm ext}(\boldsymbol{r})]}{\delta u(\boldsymbol{r})} = \frac{e^{\beta\mu^{\rm id}}}{\Lambda^3}\exp[-\beta\{\Phi_{\rm ext}(\boldsymbol{r})+u(\boldsymbol{r})\}]. \tag{2.16}$$

Eliminating $u(\boldsymbol{r})$ by using this equation, the grand potential functional of $\rho(\boldsymbol{r})$ is obtained from Eqs. (2.11) and (2.15) as

$$\begin{aligned}\beta\Omega^{\rm id}[\rho(\boldsymbol{r}),\Phi_{\rm ext}(\boldsymbol{r})] &= \int \rho(\boldsymbol{r})\ln[\Lambda^3\rho(\boldsymbol{r})/e]{\rm d}\boldsymbol{r} \\ &\quad + \int \beta\Phi_{\rm ext}(\boldsymbol{r})\rho(\boldsymbol{r}){\rm d}\boldsymbol{r} - \beta\mu^{\rm id}\int\rho(\boldsymbol{r}){\rm d}\boldsymbol{r}.\end{aligned} \tag{2.17}$$

Thus, in the case of the absence of interactions, the grand potential functional can be obtained analytically.

When the interactions are present, the grand potential functional can not be obtained analytically. The contribution of interactions to the grand potential functional $\Omega^{\rm ex}[\rho(\boldsymbol{r})]$, which is called the excess part of grand potential functional, is defined by

$$\Omega^{\rm ex}[\rho(\boldsymbol{r}),\Phi_{\rm ext}(\boldsymbol{r})] \equiv \Omega[\rho(\boldsymbol{r}),\Phi_{\rm ext}(\boldsymbol{r})] - \Omega^{\rm id}[\rho(\boldsymbol{r}),\Phi_{\rm ext}(\boldsymbol{r})]. \tag{2.18}$$

The excess part of the grand potential functional $\Omega^{\rm ex}[\rho(\boldsymbol{r})]$ is expanded up to the second order of $\Delta\rho(\boldsymbol{r}) \equiv \rho(\boldsymbol{r}) - \rho_0$,

$$\begin{aligned}\Omega^{\rm ex}[\rho(\boldsymbol{r}),\Phi_{\rm ext}(\boldsymbol{r})] &= \Omega^{\rm ex}[\rho_0,\Phi_{\rm ext}(\boldsymbol{r})] + \int \left.\frac{\delta\Omega^{\rm ex}[\rho(\boldsymbol{r}),\Phi_{\rm ext}(\boldsymbol{r})]}{\delta\rho(\boldsymbol{r})}\right|_{\Delta\rho=0}\Delta\rho(\boldsymbol{r}){\rm d}\boldsymbol{r} \\ &\quad + \frac{1}{2}\int\int \left.\frac{\delta^2\Omega^{\rm ex}[\rho(\boldsymbol{r}),\Phi_{\rm ext}(\boldsymbol{r})]}{\delta\rho(\boldsymbol{r})\delta\rho(\boldsymbol{r}')}\right|_{\Delta\rho=0}\Delta\rho(\boldsymbol{r})\Delta\rho(\boldsymbol{r}',t){\rm d}\boldsymbol{r}{\rm d}\boldsymbol{r}'.\end{aligned} \tag{2.19}$$

Here, ρ_0 is average number density.

One can obtain the coefficient of the functional Taylor expansion, connecting the grand potential functional in the presence of the external field $\Phi_{\rm ext}(\boldsymbol{r})$ to that in the absence of the external field. Because microscopic density is represented by $\hat{\rho}(\boldsymbol{r}) \equiv \sum_{i=1}^{N} \delta(\boldsymbol{r}-\boldsymbol{r}_i)$, the Hamiltonian in the presence of the virtual external field $u(\boldsymbol{r})$ is written as

$$\begin{aligned} \mathcal{H}(\boldsymbol{r}^N, \boldsymbol{p}^N) &+ \int \hat{\rho}(\boldsymbol{r}) u(\boldsymbol{r}) \mathrm{d}\boldsymbol{r} \\ &= \sum_{i=1}^{N} \frac{\boldsymbol{p}_i^2}{2m} + \sum_{i>j}^{N} \sum_{j=1}^{N} v(\boldsymbol{r}_{i,j}) + \int \hat{\rho}(\boldsymbol{r}) \left\{ \Phi_{\rm ext}(\boldsymbol{r}) + u(\boldsymbol{r}) \right\} \mathrm{d}\boldsymbol{r} \end{aligned} \tag{2.20}$$

Thus, the grand potential $\Omega[u(\boldsymbol{r}), \Phi_{\rm ext}(\boldsymbol{r})]$ is equivalent to $\Omega[\Phi_{\rm ext}(\boldsymbol{r}) + u(\boldsymbol{r}), 0]$. From Eq. (2.11), one can obtain

$$\Omega[\rho(\boldsymbol{r}), \Phi_{\rm ext}(\boldsymbol{r})] = \Omega[\rho(\boldsymbol{r}), 0] + \int \rho(\boldsymbol{r}) \Phi_{\rm ext}(\boldsymbol{r}) \mathrm{d}\boldsymbol{r}. \tag{2.21}$$

Therefore, the coefficient of the functional Taylor expansion can be represented by the grand potential functional for $\Phi_{\rm ext}(\boldsymbol{r}) = 0$. In $\Phi_{\rm ext}(\boldsymbol{r}) = 0$, number density becomes homogeneous ρ_0 due to symmetry. This system is called the homogeneous system.

Using Eq. (2.21), the constant, linear, and quadratic terms of the functional Taylor expansion are given. The constant term is written as

$$\begin{aligned} \Omega^{\rm ex}[\rho_0, \Phi_{\rm ext}(\boldsymbol{r})] &= \Omega[\rho_0, \Phi_{\rm ext}(\boldsymbol{r})] - \Omega^{\rm id}[\rho_0, \Phi_{\rm ext}(\boldsymbol{r})] \\ &= \Omega[\rho_0, 0] - \Omega^{\rm id}[\rho_0, 0] = \Omega^{\rm ex}[\rho_0, 0]. \end{aligned} \tag{2.22}$$

The linear term is written as

$$\left. \frac{\delta \Omega^{\rm ex}[\rho(\boldsymbol{r}), \Phi_{\rm ext}(\boldsymbol{r})]}{\delta \rho(\boldsymbol{r})} \right|_{\Delta\rho=0} = \left. \frac{\delta \Omega^{\rm ex}[\rho(\boldsymbol{r}), 0)]}{\delta \rho(\boldsymbol{r})} \right|_{\Delta\rho=0} = 0. \tag{2.23}$$

The quadratic term is defined as

$$\frac{\delta^2 \beta \Omega^{\rm ex}[\rho(\boldsymbol{r}), \Phi_{\rm ext}(\boldsymbol{r})]}{\delta \rho(\boldsymbol{r}) \delta \rho(\boldsymbol{r}')} = \frac{\delta^2 \beta \Omega^{\rm ex}[\rho(\boldsymbol{r}), 0]}{\delta \rho(\boldsymbol{r}) \delta \rho(\boldsymbol{r}')} \equiv -c_{0,\rm SS}(|\boldsymbol{r}'-\boldsymbol{r}|), \tag{2.24}$$

where the argument of $c_{0,\rm SS}(|\boldsymbol{r}'-\boldsymbol{r}|)$ is reduced from $\boldsymbol{r}$ and $\boldsymbol{r}'$ to $\boldsymbol{r}'-\boldsymbol{r}$ for the symmetry of the homogeneous system. In addition, $c_{0,\rm SS}(|\boldsymbol{r}'-\boldsymbol{r}|)$ is called the direct correlation function.

Finally, the grand potential functional $\Omega[\rho(\boldsymbol{r})]$ can be written as

$$\begin{aligned} \beta\Omega[\rho(\boldsymbol{r}), \Phi_{\rm ext}(\boldsymbol{r})] &= \beta\Omega_0 + \int \rho(\boldsymbol{r}) \ln[\rho(\boldsymbol{r})/\rho_0] \mathrm{d}\boldsymbol{r} \\ &\quad + \int \beta \Phi_{\rm ext}(\boldsymbol{r}) \rho(\boldsymbol{r}) \mathrm{d}\boldsymbol{r} - \int \Delta\rho(\boldsymbol{r}) \mathrm{d}\boldsymbol{r} \\ &\quad - \frac{1}{2} \int \int c_{0,\rm SS}(|\boldsymbol{r}'-\boldsymbol{r}|) \Delta\rho(\boldsymbol{r}) \Delta\rho(\boldsymbol{r}') \mathrm{d}\boldsymbol{r} \mathrm{d}\boldsymbol{r}', \end{aligned} \tag{2.25}$$

by using $\mu^{\mathrm{id}} = \mu_0^{\mathrm{id}} = \ln[\lambda^3 \rho_0]$. Here, $\Omega_0 = \Omega_0^{\mathrm{id}} + \Omega_0^{\mathrm{ex}}$ is the grand potential functional in the homogeneous system, where $\Omega_0^{\mathrm{id}} = -\int \rho_0 \mathrm{d}\boldsymbol{r}$. It is called the Ramakrishnan-Yussouff approximation [33]. Inserting the equilibrium number density $\rho(r)$ into Eq. (2.25), one can obtain the grand potential.

Number density of solvent particles can be obtained by insertion of Eq. (2.25) into Eq. (2.14).

$$\rho(\boldsymbol{r}) = \rho_0 \exp\left\{-\beta\Phi_{\mathrm{ext}}(\boldsymbol{r}) + \int c_{0,\mathrm{SS}}(|\boldsymbol{r}' - \boldsymbol{r}|)\Delta\rho(\boldsymbol{r})\mathrm{d}\boldsymbol{r}'\right\}. \tag{2.26}$$

Thus, $\rho(\boldsymbol{r})$ can be calculated by the correlation function in the homogenous system $c_{0,\mathrm{SS}}(|\boldsymbol{r}' - \boldsymbol{r}|)$. A method for calculating $c_{0,\mathrm{SS}}(\boldsymbol{r})$ is formulated by the combination of the Ornstein- Zernike (OZ) equation [10, 32] and hyper-netted chain (HNC) approximation [34–36] (Appendix A).

The Morita-Hiroike formula is the expression of the chemical potential of an arbitrary shaped particle (e.g. protein) as the functional of the correlation between an arbitrary shaped particle and solvent particle. The Morita-Hiroike formula is derived by RY approximation (Appendix B). It is written as

$$\beta\mu = \rho_0 \int \left[\frac{1}{2}\{h_{\mathrm{P,S}}(\boldsymbol{r})\}^2 - \frac{1}{2}h_{\mathrm{P,S}}(\boldsymbol{r})c_{\mathrm{P,S}}(\boldsymbol{r}) - c_{\mathrm{P,S}}(\boldsymbol{r})\mathrm{d}\boldsymbol{r}\right], \tag{2.27}$$

where $h_{\mathrm{P,S}}(\boldsymbol{r})$ is the pair correlation function between an arbitrary shaped particle and solvent particle, $c_{\mathrm{P,S}}(\boldsymbol{r})$ is the direct correlation function between an arbitrary shaped particle and solvent particle.

2.4 Application of DFT to the Stability of a Protein

In this section, the effect of solvent particles is described through the review of ref 38.

2.4.1 Purpose

A function of a protein depends on its three-dimensional structure. To predict the three-dimensional structure from an amino acid sequence, the effect of intramolecular potential energy of a protein or the entropy gain of the intramolecular motion of a protein has been studied. In these studies, water molecules as a solvent are neglected while proteins are surrounded in a solvent. Therefore, effects of solvent particles on the protein folding also should be investigated.

To obtain effects of solvent particles in all-atom calculations considered all atoms of a protein and solvent particles, a heavy calculation cost is needed. A large protein is poorly understood owing to a heavy cost, though a small protein has been studied [37]. In order to calculate the effect of solvent particles by the

reasonable cost, the intramolecular motion of a protein is ignored. In addition, atoms of a protein are modeled by hard spheres. Under the two assumptions, the simple method for calculating the effects of solvent particles has been developped [38, 39]. The simple method is expressed by a combination of the morphometric thermodynamic approach (MTA) [16] and density functional theory (DFT) [10,32].

Hamano *et al* have proposed a simple expression of the free energy to calculate the free energy with the minor computational effort [40]. They simplified the free energy to satisfy that the free energy of native configuration is smallest in the all configuration. To obtain the simple expression of the free energy, they used a lot of assumptions.

2.4.2 Simple Expression of Free Energy

The free energy of the system is represented by the sum of the protein intramolecular interactions, conformational entropy of a protein, protein-water interactions, water-water interactions, and entropy of water molecules. Hamano *et al* considered the structural change from a protein of native structure to a misfolded protein, which is the local minimum state. First, an assumption is that conformational entropy of a protein of native structure is almost the same as that of misfolded structure. Secondly, they also assumed that the change in the sum of the protein intramolecular interactions, protein-water interactions, and water-water interactions depends on the number of the hydration bond. The validity of the second assumption has been confirmed by the RISM theory in all atoms calculation [41]. with the two assumptions, the change in the free energy from the native structure to the misfolded structure is represented by the change in the sum of the entropy of water molecules S and the energy for the hydration bond ξ. Therefore, they suggested that a new expression of the free energy is represented by a sum of the entropy of water molecules S and the energy for hydration bond ξ.

To calculate the entropy of solvent particles S, they modeled an atom constituting a protein as the hard sphere. Generically, the potential between atoms constituting the protein and solvent particle has the attractive part, such as Leonard Jones potential. The result by early work of 39 about a small protein has shown that the entropy in the LJ potential system was almost the same as that in the hard-body system [41]. In this calculation, the diameters of atoms ware chosen as the distance where the LJ potential is equal to $k_{\mathrm{B}}T$. This approximated potential is now widely accepted to calculate the entropy of solvent particles.

The entropy S of a protein can be calculated by

$$S = -\left(\frac{\partial \mu}{\partial T}\right), \tag{2.28}$$

where the chemical potential μ can be obtained by the Morita-Hiroike fomula [34,35] [Eq (2.27)]. They used the MTA [16] to calculate with the reasonable cost.

The free energy of hydrogen bond ξ is calculated by

$$\xi = P \times N, \tag{2.29}$$

where P is the free energy of the hydrogen bond per one, which is set at $7k_{\mathrm{B}}T_0$ from the result of the computer simulation. Here, $T_0 = 298$ K and N is the number of the hydrogen bond.

They calculated the difference in the total energy of hydrogen bond ξ between misfolded structure and native structure

$$X = \xi/(k_{\mathrm{B}}T_0) - \{\xi/(k_{\mathrm{B}}T_0)\}_{\mathrm{Native}} \tag{2.30}$$

and the difference in the entropy of solvent particles S between misfolded structure and native structure

$$Y = -TS/(k_{\mathrm{B}}T_0) - \{-TS/(k_{\mathrm{B}}T_0)\}_{\mathrm{Native}}. \tag{2.31}$$

They examined the seven native structures, which are chosen as the vitamin B-dependent calcium binding protein (3icb), the amino terminal domain of 434 repressor (1r69), the 434 Cro protein (2cro), the C-terminal domain of ribosomal protein (1ctf), the scorpion neurotoxin (1sn3), the trypsin inhibitor (4pti), and the rubredoxin (4rxn). They examined over 600 misfolded structures of each protein.

2.4.3 Results

As the result of their calculations, the simple expression of the free energy $(-TS + \xi)/(k_B T_0)$ of native structure is lowest in all structure (Fig. 2.1). The difference in $-TS$ and ξ between native structure and misfolded structure is almost same. Thus, both of two quantities, which are the entropy of solvent particles and total loss of hydrogen bond, has an important role for the stability of native structure of proteins. In addition, the protein does not become stabilized only by the entropy of solvent particles because of existing of $Y < 0$. Moreover, the protein does not become stabilized only by the free energy loss of hydrogen bond because of existing of $X < 0$. This study indicates the importance of solvent particles on the mechanism of biomolecule functions.

2.5 Integral Equation Theory and Potential of Mean Force

The potential of mean force (PMF) has been used in many feilds, such as phase separation of colloidal suspension [29], self-assembly of peptide [42] and DNA [43], motion of proteins [17–19, 22, 23]. The PMF represents the effective potential of macromolecules, which is induced by the effects of smaller particles.

For a simple explanation of PMF, I consider a system consisting of three components, namely an arbitrary shaped solute (denote A), a spherical solute (denote B), and a small spherical solvent (denote S). Due to the symmetry of spherical solute, the relative position between solute A and B can be represented by the relative position $\boldsymbol{r}$. Using the relative position $\boldsymbol{r}$, the PMF is written by

$$\Phi_{\mathrm{A,B}}(\boldsymbol{r}) \equiv -k_{\mathrm{B}}T \ln[g_{\mathrm{A,B}}(\boldsymbol{r})]. \tag{2.32}$$

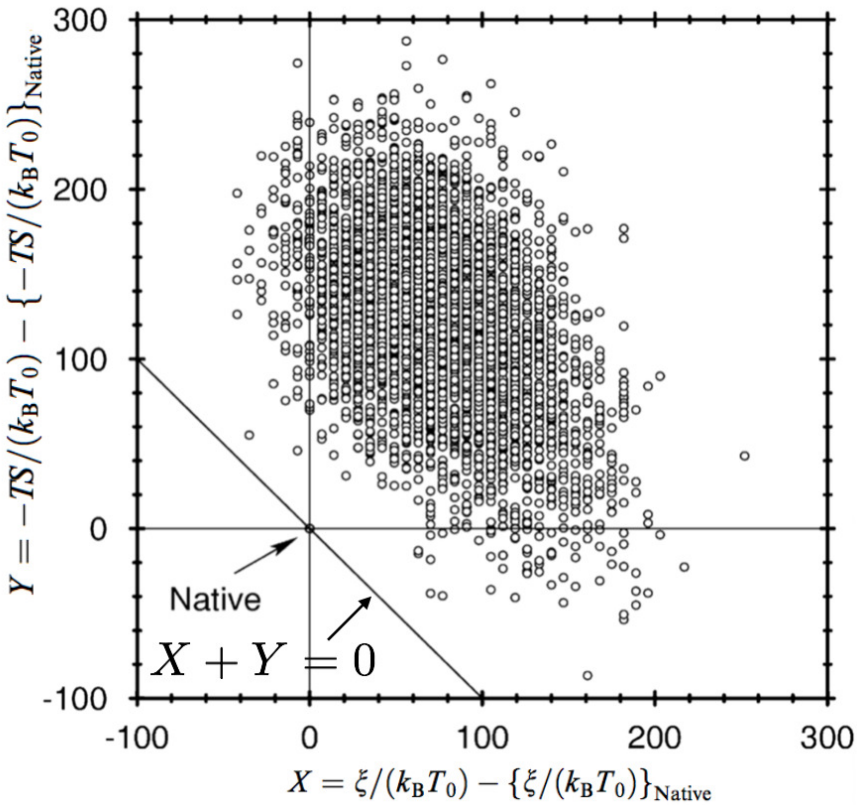

Figure 2.1: The difference of the hydration entropy between misfolded structure and native structure Y plotted against the difference of the total dehydration penalty between misfolded structure and native structure X [40].

Here, $g_{\mathrm{A,B}}(\boldsymbol{r})$ is the pair distribution function of particles of species A and B, which is defined by

$$x_{\mathrm{A}} x_{\mathrm{B}} \rho g_{\mathrm{A,B}}(\boldsymbol{r}) \equiv \left\langle \frac{1}{N} \sum_{i=1}^{N_{\mathrm{A}}} \sum_{j=1}^{N_{\mathrm{B}}} \delta(\boldsymbol{r} - \boldsymbol{r}_i^{\mathrm{A}} + \boldsymbol{r}_j^{\mathrm{B}}) \right\rangle . \tag{2.33}$$

Here, N_{A} is the number of specie A particles, $\boldsymbol{r}_i^{\mathrm{A}}$ is the position of specie A particle i, and $x_{\mathrm{A}} = N_{\mathrm{A}}/N$, where $N \equiv \sum_{c=A,B,S} N_c$. $\langle ... \rangle$ is the ensemble average.

The PMF can be rewritten from Eq. (2.32) by

$$\Phi_{\mathrm{A,B}}(\boldsymbol{r}) = \Omega_{\mathrm{A,B}}(\boldsymbol{r}) - \Omega_{\mathrm{A,B}}(\infty), \tag{2.34}$$

where $\Omega_{\mathrm{A,B}}(\boldsymbol{r})$ is the grand potential of the system when a solute A and a solute B are fixed at the relative distance $\boldsymbol{r}$.

The PMF between biomolecules can also be obtained by the definition of the pair distribution function $g_{AB}(\boldsymbol{r})$ [Eq. (2.32)]. $g_{AB}(\boldsymbol{r})$ is often calculated by using a combination of Ornstein-Zernike (OZ) equation

$$h_{\mu,\nu}(\boldsymbol{r}) = c_{\mu,\nu}(\boldsymbol{r}) + \sum_{\gamma} \rho_{\gamma} \int c_{\mu,\gamma}(\boldsymbol{r}' - \boldsymbol{r}) h_{\gamma,\nu}(\boldsymbol{r}') \mathrm{d}\boldsymbol{r}' \qquad (\mu, \nu, \gamma = A, B, S) \tag{2.35}$$

and hyper-netted chain (HNC) approximation [34–36]

$$g_{\mu,\nu}(\boldsymbol{r}) = \exp\{-\beta v_{\mu,\nu}(\boldsymbol{r}) + h_{\mu,\nu}(\boldsymbol{r}) - c_{\mu,\nu}(\boldsymbol{r})\} \qquad (\mu,\nu = A, B, S). \tag{2.36}$$

Here, $c_{\mu,\nu}(\boldsymbol{r})$ is the direct correlation function and $h_{\mu,\nu}(\boldsymbol{r}) \equiv g_{\mu,\nu}(\boldsymbol{r}) - 1$ is pair correlation function. The OZ equation [10, 32] and hyper-netted chain (HNC) approximation [34–36] are derived by the same method as those in the one component system (Appendix A).

In the application of the biological system, it can be assumed in many cases that the solute particles are at dilution limit ($x_{\mathrm{A}}/x_{\mathrm{S}}, x_{\mathrm{B}}/x_{\mathrm{S}} << 1$). Since the solute effects on the solvent particles can be ignored in dilution limit, the OZ equation [Eq. (2.35))] and HNC approximation [Eq. (2.36)] can be rewritten by

$$h_{\mathrm{S,S}}(r) = c_{\mathrm{S,S}}(r) + \rho_{\mathrm{S}} \int c_{S,S}(|\boldsymbol{r}' - \boldsymbol{r}|) h_{\mathrm{S,S}}(r') 4\pi r'^2 \mathrm{d}r' \tag{2.37}$$

and

$$g_{\mathrm{S,S}}(r) = \exp\{-\beta v_{\mathrm{S,S}}(r) + h_{\mathrm{S,S}}(r) - c_{\mathrm{S,S}}(r)\}. \tag{2.38}$$

Here, ρ_{S} is average density of solvent particles and $r = |\boldsymbol{r}|$. An argument of functions is reduced for symmetry. In addition, $v_{\mathrm{S,S}}(r)$ is the interaction between solvent particles. The solution of $c_{\mathrm{S,S}}(r)$ and $h_{\mathrm{S,S}}(r)$ can be obtained from an iterative numerical approach, such as Picard's method [44, 45] and Newton-Raphson method [45].

In dilution limit of solute particles, the correlation functions between a solute particle and a solvent particle can be represented by the interaction between a solute particle and a solvent particle $v_{\mathrm{A,S}}(\boldsymbol{r})$ and the direct correlation function between solvent particles $c_{\mathrm{S,S}}(r)$. It is because the effect of correlation function between the other solute particle and a solvent particle is ignored for $x_{\mathrm{B}}/x_{\mathrm{S}} << 1$. The OZ equation [Eq. (2.35)] and HNC approximation [Eq. (2.36)] for a solute A and a solvent particle are

$$h_{\mathrm{A,S}}(\boldsymbol{r}) = c_{\mathrm{A,S}}(\boldsymbol{r}) + \rho_{\mathrm{S}} \int c_{\mathrm{S,S}}(|\boldsymbol{r}' - \boldsymbol{r}|) h_{\mathrm{A,S}}(\boldsymbol{r}') \mathrm{d}\boldsymbol{r}' \tag{2.39}$$

and

$$g_{\mathrm{A,S}}(\boldsymbol{r}) = \exp\{-\beta v_{\mathrm{A,S}}(\boldsymbol{r}) + h_{\mathrm{A,S}}(\boldsymbol{r}) - c_{\mathrm{A,S}}(\boldsymbol{r})\}. \tag{2.40}$$

Using $c_{\mathrm{S,S}}(|\boldsymbol{r}' - \boldsymbol{r}|)$ calculated from Eqs. (2.37) and (2.38), an iterative numerical approach is taken for solution of Eqs. (2.39) and (2.40). Similarly to Eqs. (2.39) and (2.40), $h_{\mathrm{S,B}}(\boldsymbol{r})$ and $c_{\mathrm{S,B}}(\boldsymbol{r})$ can be obtained.

The PMF $\Phi_{\mathrm{A,B}}(\boldsymbol{r})$ can be obtained from Eq. (2.32). Using HNC approximation [Eq. (2.36)] for solutes A and B

$$g_{\mathrm{A,B}}(\boldsymbol{r}) = \exp\{-\beta v_{\mathrm{A,B}}(\boldsymbol{r}) + h_{\mathrm{A,B}}(\boldsymbol{r}) - c_{\mathrm{A,B}}(\boldsymbol{r})\}, \tag{2.41}$$

and the OZ equation [Eq. (2.35)] for solutes A and B

$$h_{\mathrm{A,B}}(\boldsymbol{r}) - c_{\mathrm{A,B}}(\boldsymbol{r}) = \rho_{\mathrm{S}} \int c_{\mathrm{A,S}}(|\boldsymbol{r}' - \boldsymbol{r}|) h_{\mathrm{S,B}}(\boldsymbol{r}') \mathrm{d}\boldsymbol{r}', \tag{2.42}$$

one can derive

$$\beta\Phi_{\mathrm{A,B}}(\boldsymbol{r}) = \beta v_{\mathrm{A,B}}(\boldsymbol{r}) - \rho_{\mathrm{S}} \int c_{\mathrm{A,S}}(|\boldsymbol{r}' - \boldsymbol{r}|) h_{\mathrm{S,B}}(\boldsymbol{r}') \mathrm{d}\boldsymbol{r}'. \tag{2.43}$$

Insertion of the calculated $c_{\mathrm{A,S}}(\boldsymbol{r})$ and $h_{\mathrm{S,B}}(\boldsymbol{r})$ into Eq. (2.43) yields the PMF.

2.6 Application of Integral Equation Theory to Chaperonin

2.6.1 Introduction

A chaperonin is a group of protein complexes that help an unfolded protein to fold. A typical example is GroEL/GroES bacterial chaperonin complex, which shaped cylindrical vessel/cover [5, 6]. The process in help of an unfolded protein is as follows. First, an unfolded protein is inserted into a GroEL. And then, it is closed by GroES as the lid. Next, an unfolded protein is in a native structure by the assist of GroEL. After that, GroES is detached. Finally, a folded protein is released by GroEL. Among theses process, the protein insertion process into the GroEL cavity has been focused by several studies [5–7, 17–20].

Amano *et al.* have been studied the equilibrium effect of solvent particles by analyzing the PMF between an unfolded protein and a chaperonin [17–20]. They devised a minimum model required for the explanation of insertion. In their simple model, an unfolded protein and a solvent particle ware represented by the spherical particle. In addition, a chaperoinin was represented by a cylindrical vessel. They analyzed the parameter dependence on parameters, such as the size of the protein, solvent particle, and vessel, the magnitude of the attractive potential. Even if the interaction is hard core potential, the insertion of the protein can be explained by the PMF. Since they use the same model as the model that I used in my study, I introduce the study of Amano *et al.*.

2.6.2 Model

They have considered a large sphere, a cylindrical vessel, and small spheres(Fig. 2.2), which are models of an unfolded protein, a chaperonin, and water molecules, respectively [20]. The diameter of the large-sphere and small-sphere are denoted by d_{B} and d_{S}. Length, inner diameter, outer diameter and bottom wall thickness of the vessel are denoted by d_{Le}, d_{I}, $d_{\mathrm{I}} + 12d_{\mathrm{S}}$, and d_{S}, respectively. The vessel has rounded corners of the top and rounded fillets of the bottom, where their radii are d_{S}. The large sphere and the vessel are assumed at infinite dilution. In addition, number density of the small spheres ρ_{S} is given by $\rho_S d_{\mathrm{S}}^3 = 0.7317$, which is that of water at 298 K and 1 atm.

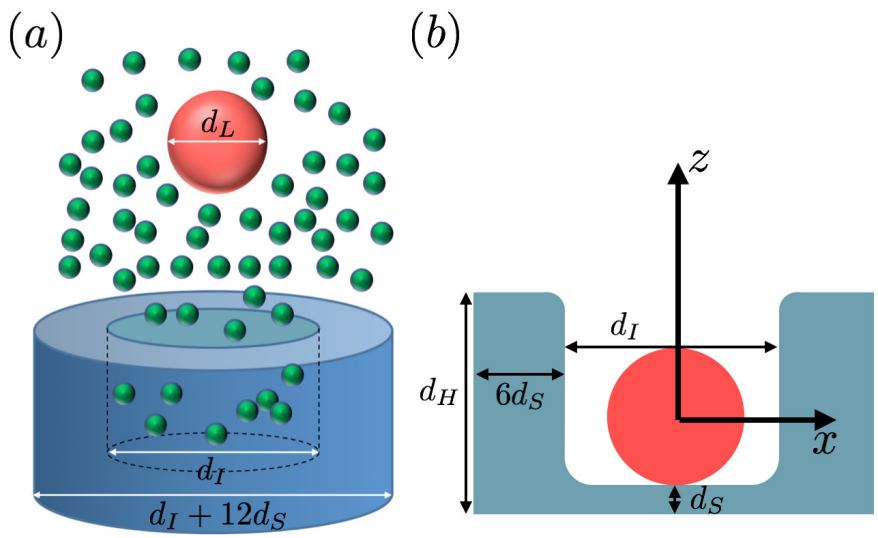

Figure 2.2: (a) Models of a large sphere, small spheres and a cylindrical vessel. The large sphere diameter, the vessel inner diameter and outer diameter are d_{L}, d_{I} and $d_{\mathrm{I}} + 12d_{\mathrm{S}}$ respectively, where d_{S} is the small sphere diameter. (b) The cross section of the vessel. The height, bottom-wall thickness and sidewall thickness of the vessel are d_{H}, d_{S} and $6d_{\mathrm{S}}$, respectively. The vessel has rounded corners of the top and rounded fillets of the bottom, where both of the radii are d_{S}. The thick solid lines represent the x-axis and z-axis. The y axis is vertical direction to a paper. The origin of the x- and y-axis is at the center of the vessel. The origin of the z-axis is at the center of the large sphere in contact with the bottom of the vessel.

2.6.3 Calculation Method

They considered the vessel-fixed Cartesian coordinate system (x, y, z) in order to use Fast Fourier Transform (Fig. 2.2) [20]. The origin of the x- and y-axis is the center of the vessel. At the origin of the z-axis, the center of the large sphere is in touch with the bottom of the vessel. The position (x, y, z) represents the center of the large sphere. In their calculation, the grid spacing (Δx, Δy and Δz) is set at $0.1d_S$, and the box size is ($51.2d_S$, $51.2d_S$, $51.2d_S$). The value of PMF is zero at the box surfaces.

There are two types of models for the parameters d_{L}, d_{H}, and d_{I}. One of models is set at $d_{\mathrm{L}} = 5d_{\mathrm{S}}$, $d_{\mathrm{H}} = 8d_{\mathrm{S}}$, and $d_{\mathrm{I}} = 9d_{\mathrm{S}}$ (denote model I). The other model is set at $d_{\mathrm{L}} = 8d_{\mathrm{S}}$, $d_{\mathrm{H}} = 11d_{\mathrm{S}}$, and $d_{\mathrm{I}} = 12d_{\mathrm{S}}$ (denote model II).

2.6.4 Results

They have calculated the PMF between the large sphere (denote 1) and the vessel (denote 2) $\Phi_{1,2}(\boldsymbol{r})$ [20]. In the small sizes of large-sphere and vessel, the PMF $\Phi_{1,2}(\boldsymbol{r})$ is shown by Fig. 2.3-(a). The PMF in the vessel is low when the large sphere is located in the center of the vessel ($r = 0$). The PMF is also low when the large sphere is in the touch with the inner surface ($r = 2d_{\mathrm{S}}$). The PMF in the large sizes of large sphere and vessel has similar characteristics to that in model I I (Fig. 2.3-(b)). It is also small at $r = 0$ and $r = 2d_{\mathrm{S}}$.

The geometry of the PMF is complex due to the effect of solvent particles. In the small sizes case, it has the characteristic six local minima, which are at the positions A ($r = 0, z = 0$), B ($r = 0, z = d_S$), C ($r = d_S, z = 0$), D ($r = d_{\mathrm{S}}, z = d_{\mathrm{S}}$), E ($r = 2d_{\mathrm{S}}, z = 0$), and F ($r = 2d_{\mathrm{S}}, z = d_{\mathrm{S}}$) (Fig. 2.2). These local minima are shown by Fig. 2.4 with the PMF along the z-axis at $r = 0$, $r = d_{\mathrm{S}}$, and $r = 2d_{\mathrm{S}}$.

The height of the PMF has the large size dependence. In particular, the magnitude of the barrier between the bottom ($r = 0$,$z = 0$) and the center ($r = 0$,$z = d_{\mathrm{S}}$) of the vessel is significantly different. The barrier in the large sizes of the large-sphere and vessel has the height of $\Phi_{1,2}(r, z)/k_{\mathrm{B}}T = 3.94$ (Fig. 2.5), while that in the small sizes has $\Phi_{1,2}(r, z)/k_{\mathrm{B}}T = 2.03$. These barriers are located at $r = 0.0$ and $z = 0.6d_{\mathrm{S}}$ for the minima A ($r = 0$,$z = 0$) and B ($r = 0$,$z = d_{\mathrm{S}}$) and at $r = 0.0$ and $z = 0.5d_{\mathrm{S}}$ for the minima A and B. They suggested that the size dependence of the barrier is caused by a change in the excluded volume of small spheres due to the large sphere and vessel.

2.6.5 Discussion and Conclusion

By the analysis of the PMF between the large sphere and cylindrical vessel, Amano *et al.* have evaluated the equilibrium effect of solvent particles. They calculated the PMF by using IET. The result have shown that the PMF is lowest when the large sphere is located in the bottom of the vessel. The PMF is also low in the position B ($r = 0, z = d_{\mathrm{S}}$). When the large sphere flows from the position B to the position

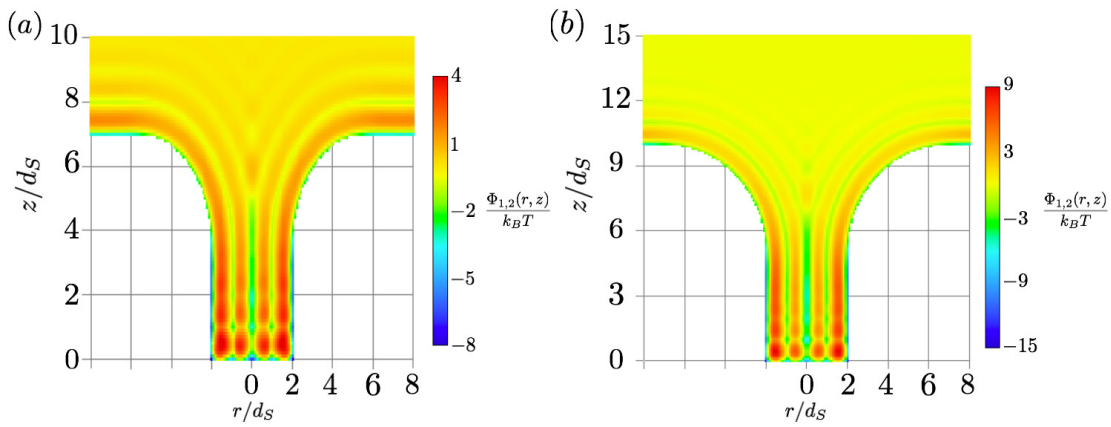

Figure 2.3: The spatial distribution of the potential of the mean force (PMF) between a large sphere and the vessel $\Phi_{1,2}(r, z)$ [20]. A contour map of (a) represents the PMF when the large-sphere and inner diameter of the vessel are $5d_{\mathrm{S}}$ and $9d_{\mathrm{S}}$. A contour map of (b) represents the PMF when the large-sphere and inner diameter of the vessel are $8d_{\mathrm{S}}$ and $12d_{\mathrm{S}}$. The x-axis and z-axis are shown by Fig.2.2. Here, d_{S} is the diameter of a small sphere, k_{B} is Boltzmann's constant and T is the absolute temperature. The PMF becomes lower, as the color approaches thick blue. The PMF becomes higher, as the color approaches thick red. The white area is the domain into which the center of the large sphere cannot enter. The numerical data of PMF is kindly provided from Amano and Kinoshita.

of the lowest PMF along the z-axis of the vessel, the PMF barrier is about $2k_{\mathrm{B}}T$. Therefore, they have suggested from the calculated PMF that the large sphere is trapped at the center of the vessel cavity. The experimental observation obtained from using cryo-electron microscopy have shown that a protein is not in touch with the inner surface of GroEL [7].

2.7 Summary

The effect of solvent particles has been evaluated in the grand potential of solvent particles [12–15, 17–23, 28, 38–41, 46–52]. The three theories for calculating the grand potential of solvent particle have been reviewed. In the Asakura-Oosawa (AO) theory, the interaction between solvent particles is ignored. However, the AO theory can well predict the binding site of a xenon atom. In spite of ignore of interactions between solvent particles, the value of the grand potential by AO theory is not far from that by experimental data.

The grand potential of solvent particle in the presence of interaction between solvent particles can be obtained from the combination of the density functional theory (DFT) and functional Taylor expansion of thermodynamics function. As the example of the functional Taylor expansion, Ramakrishnan-Yussouff approximation have been reviewed. Harano *et al.* have applied the theory to the native

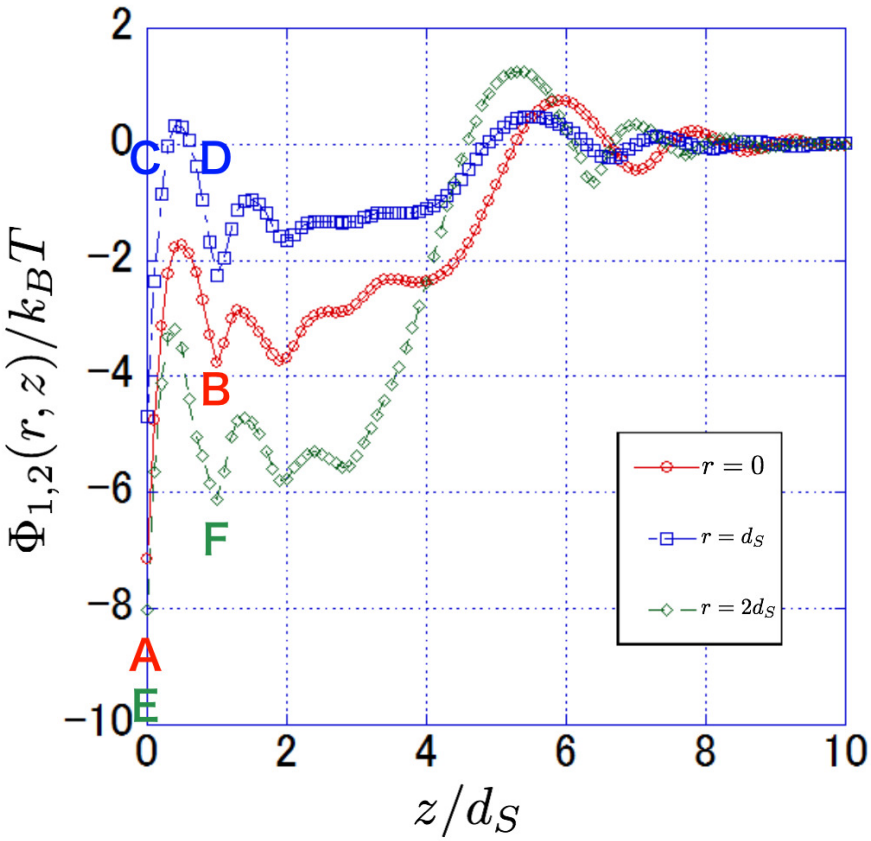

Figure 2.4: Potential of mean force (PMF) of a large sphere $\Phi_{1,2}(x, y, z)$ along the z-axis at $r = 0$ (red), $r = d_{\mathrm{S}}$ (blue), and $r = 2d_{\mathrm{S}}$ (green) for $d_{\mathrm{L}} = 5d_{\mathrm{S}}$ and $d_{\mathrm{I}} = 9d_{\mathrm{S}}$ [20]. The z-axis is shown by Fig.4.1. Here, d_{S} is the diameter of a small sphere, k_{B} is Boltzmann's constant and T is the absolute temperature. In addition, d_{L} and d_{I} are the diameter of the large sphere and inner diameter of the vessel. The positions A ($r = 0, z = 0$), B ($r = 0, z = d_{\mathrm{S}}$), C ($r = d_{\mathrm{S}}, z = 0$), D ($r = d_{\mathrm{S}}, z = d_{\mathrm{S}}$), E ($r = 2d_{\mathrm{S}}, z =$) and F ($r = 2d_{\mathrm{S}}, z = d_{\mathrm{S}}$) represent the local minima of the potential of mean force. The numerical data of PMF is kindly provided from Amano and Kinoshita.

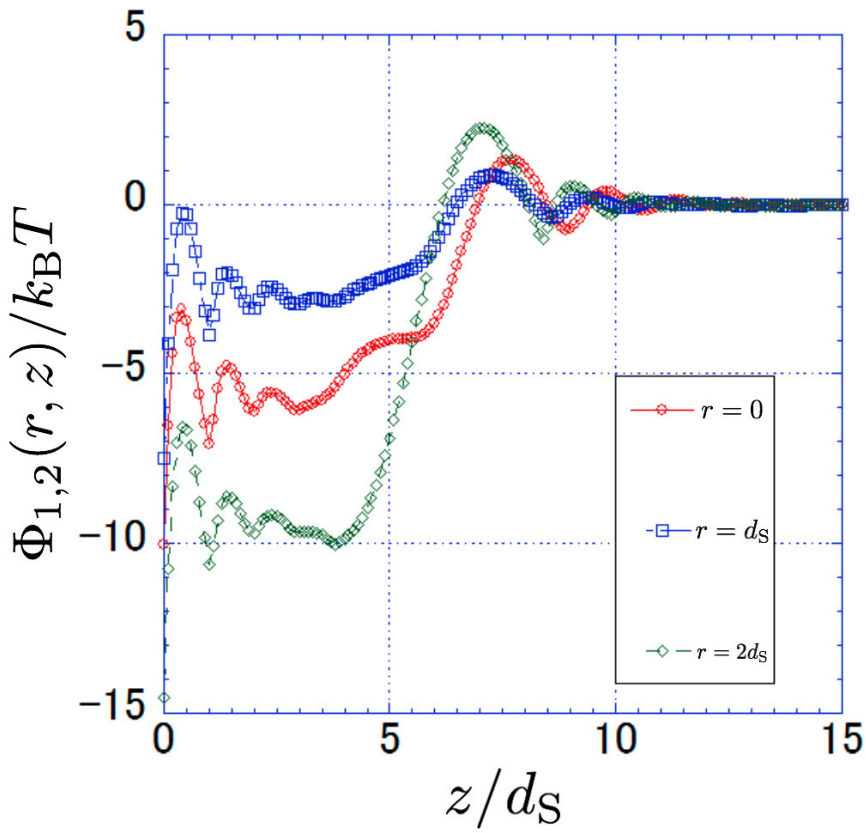

Figure 2.5: Potential of mean force (PMF) of a large sphere $\Phi_{1,2}(x, y, z)$ along the z-axis at $r = 0$ (red), $r = d_{\mathrm{S}}$ (blue), and $r = 2d_{\mathrm{S}}$ (green) for $d_{\mathrm{L}} = 8d_{\mathrm{S}}$ and $d_{\mathrm{I}} = 12d_{\mathrm{S}}$ [20]. The z-axis is shown by Fig.4.1. Here, d_{S} is the diameter of a small sphere, k_{B} is Boltzmann's constant and T is the absolute temperature. In addition, d_{L} and d_{I} are the diameter of the large sphere and inner diameter of the vessel. The positions A ($r = 0, z = 0$), B ($r = 0, z = d_{\mathrm{S}}$), C ($r = d_{\mathrm{S}}, z = 0$), D ($r = d_{\mathrm{S}}, z = d_{\mathrm{S}}$), E ($r = 2d_{\mathrm{S}}, z =$) and F ($r = 2d_{\mathrm{S}}, z = d_{\mathrm{S}}$) represent the local minima of the potential of mean force. The numerical data of PMF is kindly provided from Amano and Kinoshita.

structure of a protein [12]. They suggested that the sum of the entropy of solvent particles and the number of the hydrogen bond is minimalized in the native structure of a protein.

When the solutes pair is immersed in solvent particles, the grand potential of solvent particles in each configuration of the solutes pair is equivalent to the potential of mean force (PMF). The integral equational theory (IET) can calculate the correlation functions, such as the pair distribution function. From the calculated pair distribution function, the potential of mean force (PMF) can be calculated. Amano *et al.* have applied the IET to the insertion process of an unfolded protein into a chaperonin. The PMF was lower inside of the chaperoin than outside of the chaperonin. This result showed that an unfolded protein is inserted into the chaperonin.

Chapter 3

Equilibrium Effects of Solvent Particles on Solute Dynamics

In the present chapter, I study solute dynamics on a solute insertion process into a vessel with a cylindrical shape. Amano *et al.* have studied the same problem, considering the equilibrium effects of solvent particles. It was evaluated by the potential of mean force (PMF) between a large sphere (solute particle) and the vessel. Though the equilibrium effect of solvent particles are obtained, the solute dynamics have not been studied yet. In the present chapter, I develop a theoretical method for calculating the time deveopment of probability density of a solute particle.

3.1 Introduction

The equilibrium effect of solvent particles has been studied in biological functions, using the equilibrium statistical mechanics theory, such as integral equational theory (IET) [11], the method using the reference interaction site model (RISM) [53]. These theories provide the potential of mean force (PMF) between biomolecules. The analysis of the PMF provides the stable positions of biomolecules, considering the effects of solvent particles.

In the experimental aspect, the time for performing the function has been discussed. For instance, the time constant for an insertion of an unfolded protein into the GroEL cavity has been studied [54]. After the insertion, the GroEL assists a protein to be folded. However, the theoretical methods did not mention about the average time because the PMF gives only stability of biomolecules.

It is hard to analyze the dynamics of biomolecules by the molecular dynamics (MD) simulation due to the calculation cost. It is because the time scale of biomolecule motions differs from that of solvent particles. The time step of the MD simulation is about 10^{-15} sec for the water. In the insertion process of an unfolded protein into GroEL as the biological process, for instance, the time scale of the biological process is in the range from 10^{-3} sec to 10^{-1} sec. The time scale of

the biomolecules process is much longer than the time step of the MD simulation. Therefore, it takes huge time for the MD simulation to calculate the dynamics of biomolecules.

To make the calculation of the biomolecule movement feasible in cost and time, a modified theoretical method, which assumes the equilibrium density distribution of solvent particles, is required. Given that the relaxation time of solvent particles is sufficiently short, their motion can be considered as remained at equilibrium. Because the diffusion coefficient of a protein is 10 times as long as that of a water molecule, this approximation is currently accepted for biomolecules in the bulk and thus applicable to our study in order to reduce the cost of computation. Indeed this method allows us to calculate the time development of the biomolecule movement for up to 10^{-4} sec, which is close to the time for an insertion process of an unfolded protein into GroEL (10^{-3} sec). Though the computable time of a simulation is shorter than the time for the insertion process (biological process), the prediction of the movement of a biomolecule is expected to be obtained.

The purpose of this chapter is to clarify the equilibrium effects of solvent particles on the biomolecule dynamics. For the purpose, the Fokker-Planck (FP) equation is combined with the PMF calculated using the 3D integral equation theory. This theory has the assumption that solvent particles are always in the equilibrium state with each position of biomolecules. Applying the theory to the insertion of a large sphere into a cylindrical vessel, the time development of the probability density of the large-sphere is calculated. The flux of the large sphere is also calculated. In addition, the relevance to the behavior of a biological system is discussed.

3.2 Model

A large sphere, a cylindrical vessel, and small spheres are considered as the models of an unfolded protein, a chaperonin, and water molecules, respectively (Fig. 3.1). In these models, the shape of the large-sphere, vessel, and small-sphere are the same as the models of Amano *et al.* in §2.6.2. Number density of large-sphere, vessel, and small-sphere are also the same. The only difference from the system of Amano *et al.* is the coordinate system. In this section, the vessel-fixed cylindrical coordinate system (r, z) is selected (Fig. 3.1). The origin of the r-axis is the center of the vessel. At the origin of the z-axis, the center of the large sphere is in touch with the bottom of the vessel. The position of the center of the large sphere is represented by (r, z).

The model for two sets of the parameters d_{L}, d_{H}, and d_{I} is studied. One is $d_{\mathrm{L}} = 5d_{\mathrm{S}}$, $d_{\mathrm{H}} = 8d_{\mathrm{S}}$, and $d_{\mathrm{I}} = 9d_{\mathrm{S}}$ (denote model I). The other is $d_{\mathrm{L}} = 8d_{\mathrm{S}}$, $d_{\mathrm{H}} = 11d_{\mathrm{S}}$, and $d_{\mathrm{I}} = 12d_{\mathrm{S}}$ (denote model II). Inside of the vessel, the maximum value of r for the available area of entering in the center of the large sphere dependents on z. In model I, the large sphere is in touch with the inner surface of the vessel at $r = 2d_{\mathrm{S}}$ in $z < 3.5d_{\mathrm{S}}$. In $3.5d_{\mathrm{S}} < z < 7.0d_{\mathrm{S}}$, r of the large sphere position can

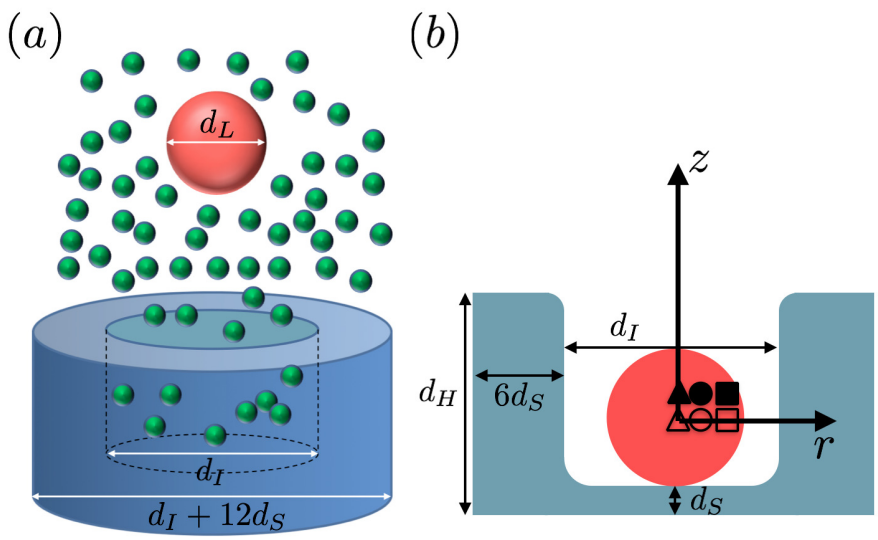

Figure 3.1: (a) Models of a large sphere, small spheres and a cylindrical vessel. The large sphere diameter, the vessel inner diameter and outer diameter are d_{L}, d_{I} and $d_{\mathrm{I}} + 12d_{\mathrm{S}}$ respectively, where d_{S} is the small sphere diameter. (b) The cross section of the vessel. The height, bottom-wall thickness and sidewall thickness of the vessel are d_{H}, d_{S} and $6d_{\mathrm{S}}$, respectively. The vessel has rounded corners of the top and rounded fillets of the bottom, where both of the radii are d_{S}. The thick solid lines represent the r-axis and z-axis. The origin of the r-axis is at the center of the vessel. The origin of the z-axis is at the center of the large sphere in contact with the bottom of the vessel. The open triangle, the closed triangle, the open circle, the closed circle, open square, and closed square represent the positions A ($r = 0, z = 0$), B ($r = 0, z = d_{\mathrm{S}}$), C ($r = d_{\mathrm{S}}, z = 0$), D ($r = d_{\mathrm{S}}, z = d_{\mathrm{S}}$), E ($r = 2d_{\mathrm{S}}, z = 0$), and F ($r = 2d_{\mathrm{S}}, z = d_{\mathrm{S}}$), respectively.

take a value slightly exceeding $2d_{\mathrm{S}}$ because the corner of the vessel is rounded. In particular, the large sphere is in touch with the inner surface of the vessel at $r = 2.1d_{\mathrm{S}}$ in $z = 4.5d_{\mathrm{S}}$. In model II, the large sphere is in touch with the inner surface of the vessel at $r = 2d_{\mathrm{S}}$ in $z < 6.5d_{\mathrm{S}}$. In $6.5d_{\mathrm{S}} < z < 10d_{\mathrm{S}}$, r of the large sphere position can take a value slightly exceeding $2d_{\mathrm{S}}$ because the corner of the vessel is rounded.

3.3 Theory

To study the large-sphere dynamics including the static effect of solvent particles, I formulate the Fokker-Plank (FP) equation combined with the PMF. The FP equation describes the time evolution of the probability density that the center of the large-sphere is on the position $\boldsymbol{r}$ at time t $P(\boldsymbol{r}, t)$ by

$$\frac{\partial P(\boldsymbol{r}, t)}{\partial t} = \nabla \cdot \left[D\nabla + \frac{D}{k_B T} \nabla \Phi_{1,2}(\boldsymbol{r}) \right] P(\boldsymbol{r}, t) \tag{3.1}$$

$$= -\nabla \cdot \boldsymbol{J}(\boldsymbol{r}, t). \tag{3.2}$$

Here, D is the diffusion coefficient of the large sphere, $\boldsymbol{J}(\boldsymbol{r}, t)$ is the flux of the probability density that the center of the large sphere is on position $\boldsymbol{r}$ at time t, and $\Phi_{1,2}(\boldsymbol{r})$ is the PMF between the large-sphere and the vessel. Equation (3.1) has a steady-state probability density $P(\boldsymbol{r}, t) \propto \exp[-\Phi_{1,2}(\boldsymbol{r})/k_B T]$ at $t \to \infty$.

In Eqs. (3.1) and (3.2), I assume the equilibrium state for the small spheres. This assumption is justified when the relaxation time of the small spheres is sufficiently shorter than that of the solute particle. To discuss the validity of the assumption, one needs to calculate the dynamics of solvent particles with a moving solute particle. The calculation is given by Chapter 4.

To solve FP equation (3.1) numerically, I employ the modified Euler method [55], with the time step $\Delta t = 10^{-6} d_{\mathrm{S}}^2/D$. For discretization of the space, I use a 2nd order central difference, where the spatial grid interval is set at $0.1d_{\mathrm{S}}$. In addition, I use the PMF calculated by Amano *et al.*. The theoretical method for calculating the PMF is shown in chapter 2.5.

The units of the length and the time are taken with d_{S} and d_{S}^2/D. Here, d_{S} is the diameter of the solvent particle and D is the diffusion coefficient of the large-sphere. If a small particle is assumed as a water molecule, d_{S} is about 0.28 nm. If a large sphere is assumed as a protein, the magnitude of D is the order of 10^{-6} cm^2/sec, according to the experiment [56]. By these values, the order of the magnitude can be estimated in d_S^2/D at 10^{-9} sec.

In model I, the maximum values of r and z are $8d_{\mathrm{S}}$ and $10d_{\mathrm{S}}$. At $r = 8d_{\mathrm{S}}$, $\partial\Phi_{1,2}(r, z)/\partial r$ approaches zero. At $z = 10d_{\mathrm{S}}$, the value of the PMF approaches zero. In model II, the maximum values of r and z are $8d_{\mathrm{S}}$ and $15d_{\mathrm{S}}$. At $r = 8d_{\mathrm{S}}$, $\partial\Phi_{1,2}(r, z)/\partial r$ approaches zero. At $z = 15d_{\mathrm{S}}$, the value of the PMF approaches zero.

In this calculation, the system has three types of the boundary condition. First, the boundary condition of $P(r, z, t) = P_{\mathrm{const}}$ is assumed at $z = 10d_{\mathrm{S}}$ in model I and at $z = 15d_{\mathrm{S}}$ in model II. Secondly, the condition of $\boldsymbol{J}(r, z, t) \cdot \boldsymbol{e_r} = 0$ at $r = 8d_{\mathrm{S}}$ is also assumed, where $\boldsymbol{e_r}$ is the unit vector of the r direction. Thirdly, the condition of $\boldsymbol{J} \cdot \boldsymbol{n} = 0$ is also assumed when the large sphere comes in contact with the wall of the vessel, $\boldsymbol{n}$ is the unit vector perpendicular to the vessel walls. The first condition shows that the particle bath of the large spheres is at $z = 10d_{\mathrm{S}}$ in model I and at $z = 15d_{\mathrm{S}}$ in model II. The reason of second condition is that the large-spheres are not supplied from $r > 8d_{\mathrm{S}}$. The reason of third condition is that the large sphere does not enter into the wall of the vessel. In addition, $P(r, z, t = 0)$ is initialized to zero in $z < 10d_{\mathrm{S}}$.

3.4 Results of model I

3.4.1 Spatial Distributions of Probability Density of the Large Sphere

Figure 3.2 shows spatial distributions of the probability density $P(\boldsymbol{r}, t)$ in several different times ($t = 3.0 \times 10^2 d_{\mathrm{S}}^2/D$, $1.0 \times 10^3 d_{\mathrm{S}}^2/D$, $1.0 \times 10^4 d_{\mathrm{S}}^2/D$ and $1.0 \times 10^5 d_{\mathrm{S}}^2/D$). In $t = 3.0 \times 10^2 d_{\mathrm{S}}^2/D$ (Fig. 3.2(a)), the probability density is high in the center region of the vessel ($r < d_{\mathrm{S}}$). In $t = 1.0 \times 10^3 d_{\mathrm{S}}^2/D$ (Fig. 3.2(b)), the high-density region expands along $r = 0$ and $r = d_{\mathrm{S}}$, although the probability density at the bottom ($z = 0$) is still low. In $t = 1.0 \times 10^4 d_{\mathrm{S}}^2/D$ (Fig. 3.2(c)), the probability density at the bottom increases in the center region ($r = z = 0$). Compared with the probability density distribution in $t = 1.0 \times 10^4 d_{\mathrm{S}}^2/D$, the color map of the probability density distribution in $t = 1.0 \times 10^5 d_{\mathrm{S}}^2/D$ (Fig.3.2(d)) is close to that in Fig. 2.3-(a). Because the probability density distribution becomes $\ln[P(\boldsymbol{r}, t)/P_{\mathrm{const}}] = -\Phi_{1,2}(\boldsymbol{r})/k_{\mathrm{B}}T$ in the infinity limit of time, the probability density approaches the equilibrium value.

A high probability at $r = 0$ in short time indicates that the large sphere is inserted into the center region of the vessel. The probability density at $r = 0$ exceeds P_{const} (the boundary value at $z = 10d_{\mathrm{S}}$) for a short time ($t = 3.0 \times 10^2 d_{\mathrm{S}}^2/D$), while it takes a long time ($t = 8.1 \times 10^2 d_{\mathrm{S}}^2/D$) at $r = 2d_{\mathrm{S}}$. This result also shows that probability is first spread to the bottom of the vessel, then to sidewall of the vessel. I considered that the long time is due to a high barrier of the PMF. This result is consistent with the prediction of Amano *et al.* [17–19].

3.4.2 Probability Density at the Local Minima of the Potential of Mean Force

Since the probability density at the local minima of the PMF is expected to be high, I focus attention on the time evolution of the probability density at the local minima (Fig. 3.3). Although the PMF is lower at the minimum A ($r = 0, z = 0$)

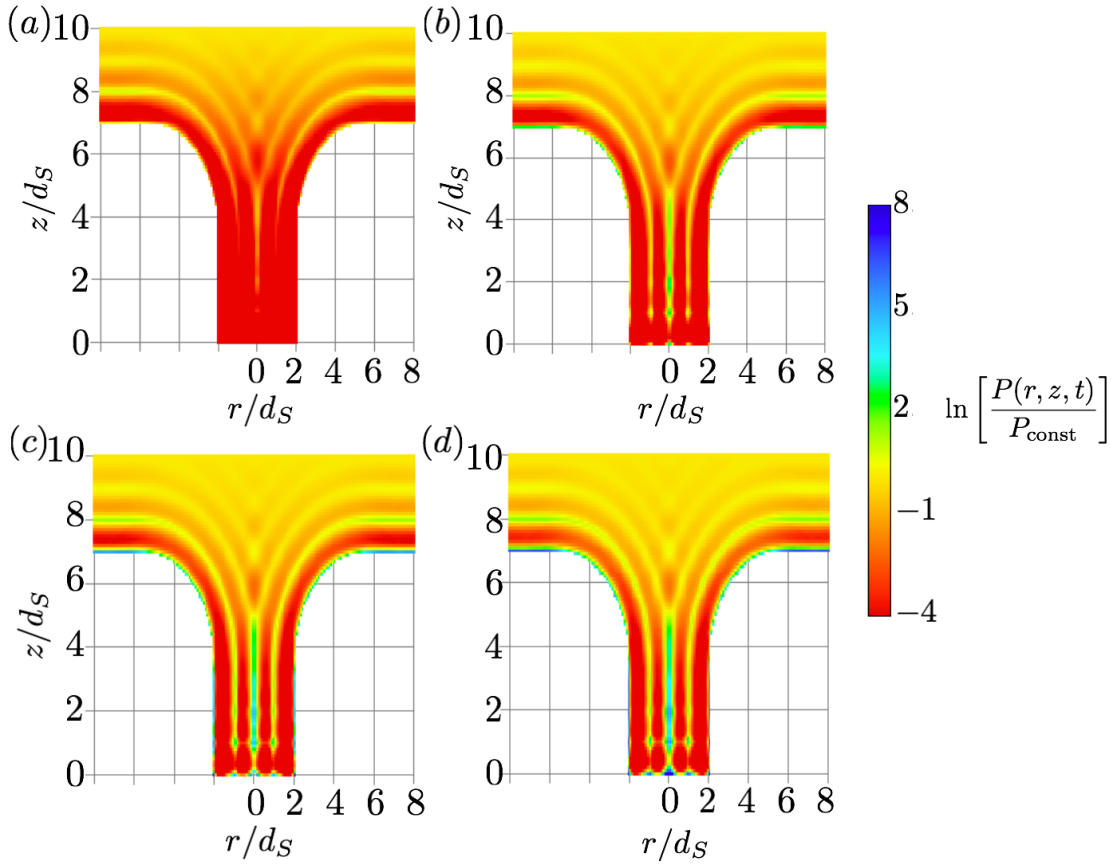

Figure 3.2: Spatial distributions of the probability density that the large sphere is on position $\boldsymbol{r}$ at time t for several different times: (a) $t = 3.0 \times 10^2 d_{\mathrm{S}}^2/D$, (b) $t = 1.0 \times 10^3 d_{\mathrm{S}}^2/D$, (c) $t = 1.0 \times 10^4 d_{\mathrm{S}}^2/D$, (d) $t = 1.0 \times 10^5 d_{\mathrm{S}}^2/D$. Here, d_{S} is the diameter of a small sphere, D is the diffusion coefficient of a large sphere, and P_{const} is probability density of particle bath at $z \geq 10 d_{\mathrm{S}}$. The r-axis and z-axis are shown by Fig. 3.1. Probability density becomes lower, as the color approaches thick red. Probability density becomes higher, as the color approaches thick blue. The white area is the domain into which the center of the large sphere cannot enter.

than at the minimum B ($r = 0, z = d_{\mathrm{S}}$), the probability density at B is the highest for $t < 8.3 \times 10^2 d_{\mathrm{S}}^2/D$. The high probability density at the minimum B shows that the large sphere is trapped at the minimum B until the reach of the large sphere to the bottom of the vessel ($r = z = 0$). I consider that the trap at the minimum B is caused by a large barrier between the minima A and B (Fig. 2.4). The probability density at these local minima depends on the geometric position as well as on the values of the PMF.

The probability density is higher at positions in the center of the vessel (Positions A and B) than at positions in the inner surface (Positions E and F) in a short time. The probability density at the minimum A is higher than at the other minima in $tD/d_{\mathrm{S}}^2 < 10^5$. In addition, the probability density at the minimum B

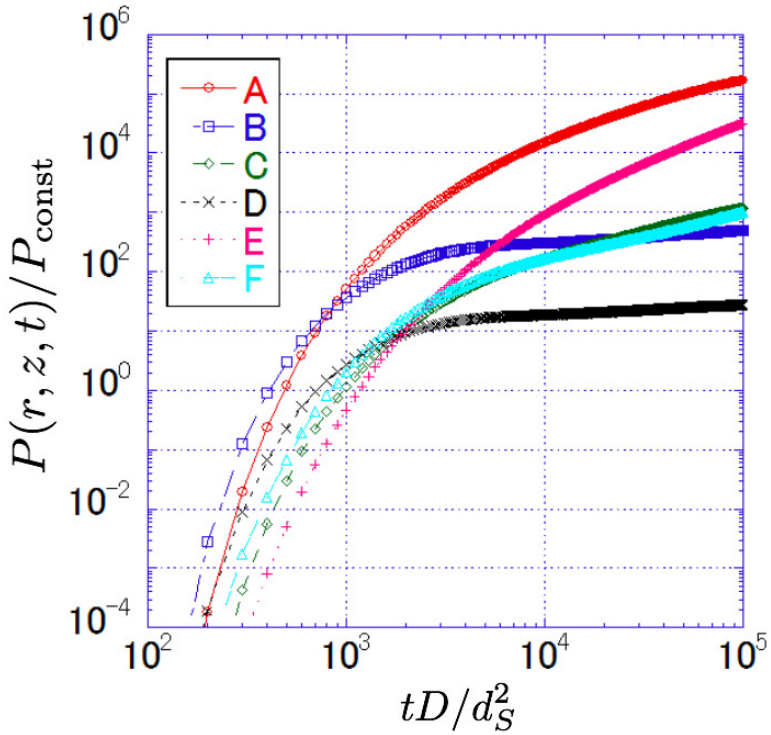

Figure 3.3: Time evolution of the probability density that the large sphere is on position $\boldsymbol{r}$ at time t $P(r,z,t)$ at local minima in the potential of mean force. A red curve represents the density at A ($r=0, z=0$); a blue curve represents the density at B ($r=0, z=1d_{\rm S}$); a green curve represents the density at C ($r=d_{\rm S}, z=0$); a black curve represents the density at D ($r=d_{\rm S}, z=d_{\rm S}$); a pink curve represents the density at E ($r=2d_{\rm S}, z=0$); an aqua curve represents the density at F ($r=2d_{\rm S}, z=d_{\rm S}$). The positions A, B, C, D, E, and F are shown by Fig. 3.1. The r-axis and z-axis are also shown by Fig. 3.1. Here, D is the diffusion coefficient of a large sphere, $d_{\rm S}$ is the diameter of a small sphere, and $P_{\rm const}$ is probability density of the particle bath at $z \geq 10d_{\rm S}$.

is higher than that at the minima E and F in $tD/d_{\rm S}^2 < 3.0 \times 10^4$. In contrast, the PMF has lower values at the minima E and F than at the minima A and B. The high density at the minima A and B also show a high probability that the large sphere is inserted into the region at $r = 0$. To clarify the position of an insertion of the large sphere, I discuss the flux of the probability density in the next subsection.

3.4.3 Flux of the Probability Density

In order to clarify the path of the large-sphere insertion, I calculate the flux of the probability density $\boldsymbol{J}(\boldsymbol{r},t)$ defined by Eq. (3.2). The flux in the direction of entering the vessel $-J_z(r,z,t)$ is shown by Fig. 3.4 for $t = 5.0 \times 10^2 d_{\rm S}^2/D$ and $z = 4.5d_{\rm S}$. At the z-value, $-J_z(r,z,t)$ has the local maximal values at $r = 0.1d_{\rm S}$, $r = 1.1d_{\rm S}$, and $r = 2.1d_{\rm S}$. The positions of these local maxima are correlated with

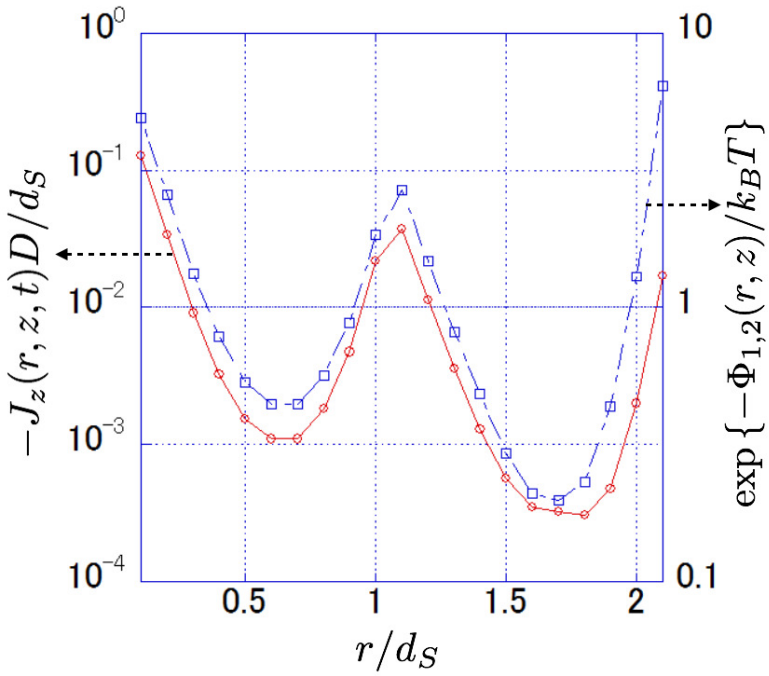

Figure 3.4: A z-component of probability density flux $J_z(r, z, t)$ (red line) and the potential of mean force $\Phi_{1,2}(r, z)$ (blue line) at $z = 4.5d_S$ along the r-axis for $t = 5.0\times10^2 d_S^2/D$. Here d_S is the diameter of a small sphere and D is the diffusion coefficient of a large sphere. The r-axis and z-axis are shown by Fig. 3.1. At $z = 4.5d_S$, the maximal value of the r-axis ($r = 2.1d_S$) is the positioin where the large sphere is in touch with the vessel due to the rounded corner of the vessel.

low values of the PMF.

Since the value of $-J_z(r, z, t)$ is largest at $r = 0.1d_S$ for $t = 3.0 \times 10^2 d_S^2/D$, one can find that a probability that the large sphere is inserted into the center of the vessel ($r = 0$) is high. In contrast to the flux, the PMF has the lowest value at $r = 2.1d_S$. This discrepancy is considered to be caused by the high barrier of the PMF between the wall of the vessel and the position $2d_S$ vertically away from the wall.

To understand the path that large-sphere moves until equilibrium state, the time evolution of the probability density flux at $z = 4.5d_S$ is calculated (Fig. 3.5). At $r = 0.1d_S$, $J_z(r, z, t)$ is larger than at the other values of r for $t < 7.9\times10^3 d_S^2/D$. For $t > 7.9\times10^3 d_S^2/D$, $J_z(r, z, t)$ at $r = 2.1d_S$ exceeds that at $r = 0.1d_S$. Thus, the probability that the large sphere is inserted along the inner surface ($r = 0.1d_S$) is high for $t < 7.9 \times 10^3 d_S^2/D$. Again, the calculation result of $J_z(r, z, t)$ shows that the large sphere is inserted into the center region of the vessel ($r = 0.1d_S$).

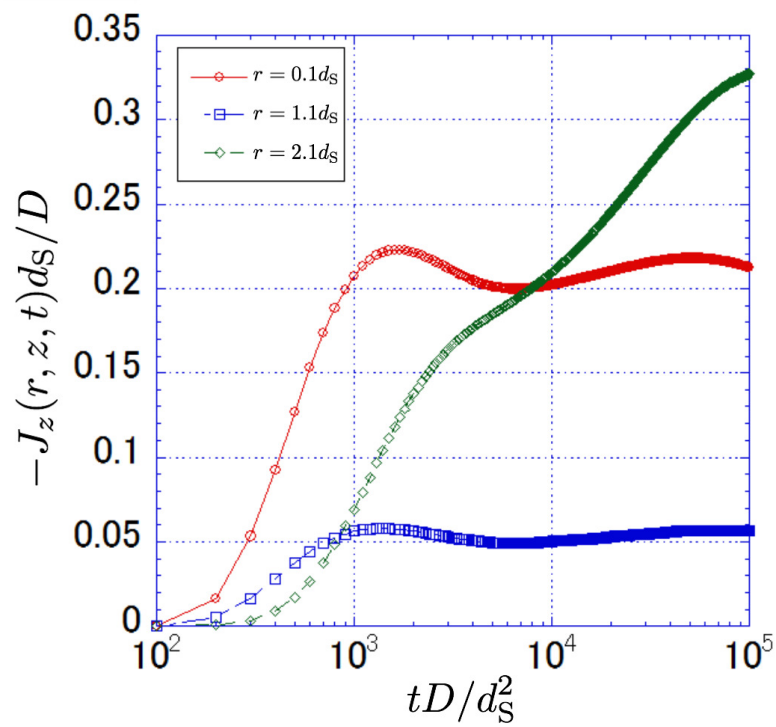

Figure 3.5: Time evolution of probability density flux of large sphere $J_z(r, z, t)$ at $z = 4.5d_S$ for $r = 0.1d_S$(Red line), $r = 1.1d_S$ (Blue line) and $r = 2.1d_S$ (Green line). Here d_S is the diameter of a small sphere, and D is the diffusion coefficient of a large sphere. The large sphere is in touch with the vessel at $r = 2.1d_S$ because the corner of the vessel at $z = 4.5d_S$ is rounded.

3.5 Size Dependence

To study dependence on sizes of the large sphere and vessel inner diameter, I compare model I (small sizes of the large-sphere and vessel) and II (large sizes of the large-sphere and vessel). Spatial distributions of the probability density $P(\boldsymbol{r}, t)$ calculated in model II are shown by Fig. 3.6. A high probability at $r = 0$ in $t = 3.0 \times 10^2 d_S^2/D$ indicates that the large sphere is inserted into the center region of the vessel. This result is same as the result of the case in model I. The distributions of the case in model II are similar to that of the case in model I.

Figure 3.7 shows the time evolution of probability density $P(\boldsymbol{r}, t)$ at the two local minima A' ($r = 0, z = 0$) and B' ($r = 0, z = d_S$). The probability density at the minimum B' is higher than that at the minimum A' for $t < 1.4 \times 10^4 d_S^2/D$. This shows that the large sphere is trapped at the minimum B' until $t < 1.4 \times 10^4 d_S^2/D$. The trapping time for model I (large sizes case) is 18 times longer than that for model II (small sizes case).

The trapping time has the size dependence, which is caused by that of the barrier height of PMF between the bottom ($r = 0, z = 0$) and the center ($r = 0, z = d_S$) of the vessel. The trapping time increases with an increase in the hight

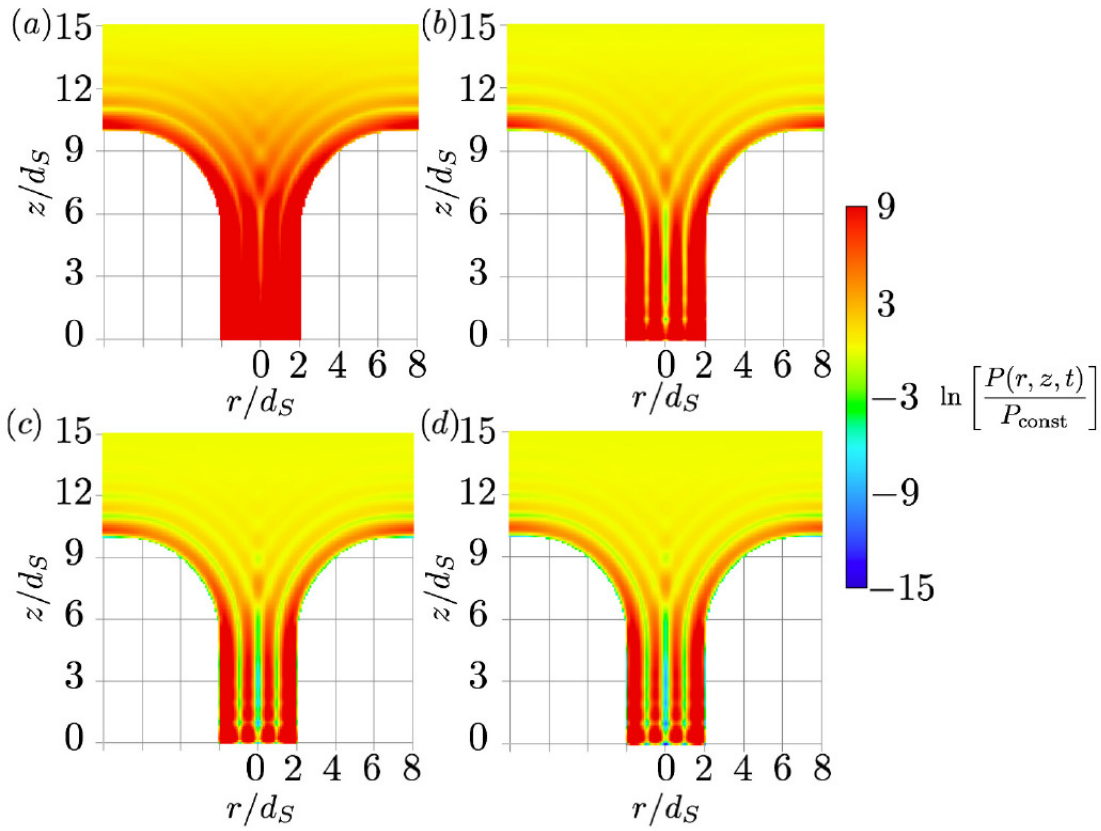

Figure 3.6: Spatial distributions of the probability density that the large sphere is on position $\boldsymbol{r}$ at time t for several different times: (a) $t = 3.0 \times 10^2 d_{\mathrm{S}}^2/D$, (b) $t = 1.0 \times 10^3 d_{\mathrm{S}}^2/D$, (c) $t = 1.0 \times 10^4 d_{\mathrm{S}}^2/D$, (d) $t = 1.0 \times 10^5 d_{\mathrm{S}}^2/D$. Here, d_{S} is the diameter of a small sphere and D is the diffusion coefficient of a large sphere. The r-axis and z-axis are shown by Fig. 3.1. Probability density becomes lower, as the color approaches thick red. Probability density becomes higher, as the color approaches thick blue. The white area is the domain into which the center of the large sphere cannot enter.

of PMF barrier. The height of the PMF barrier increases with an increase in the sizes of the-large sphere and vessel. Thus, as the sizes of the large-sphere and vessel are larger, the trapping time is also longer.

3.6 Discussions

The calculated result shows a high probability that the large sphere is in the central region of the vessel cavity and does not touch with the inner surface of the vessel cavity in $tD/d_{\mathrm{S}}^2 < 8.3 \times 10^2$ at $d_{\mathrm{L}} = 5d_{\mathrm{S}}$ (Fig. 3.3). For $tD/d_{\mathrm{S}}^2 > 8.3 \times 10^2$, a probability that the large sphere is in the bottom of the vessel cavity becomes high (Fig. 3.3). The time when the large sphere is trapped at the center of the vessel τ depends on the sizes of the large sphere and vessel. For $d_{\mathrm{L}} = 8d_{\mathrm{S}}$ and $d_{\mathrm{I}} = 12d_{\mathrm{S}}$, τ is $\tau D/d_{\mathrm{S}}^2 = 1.4 \times 10^4$ (Fig. 3.7).

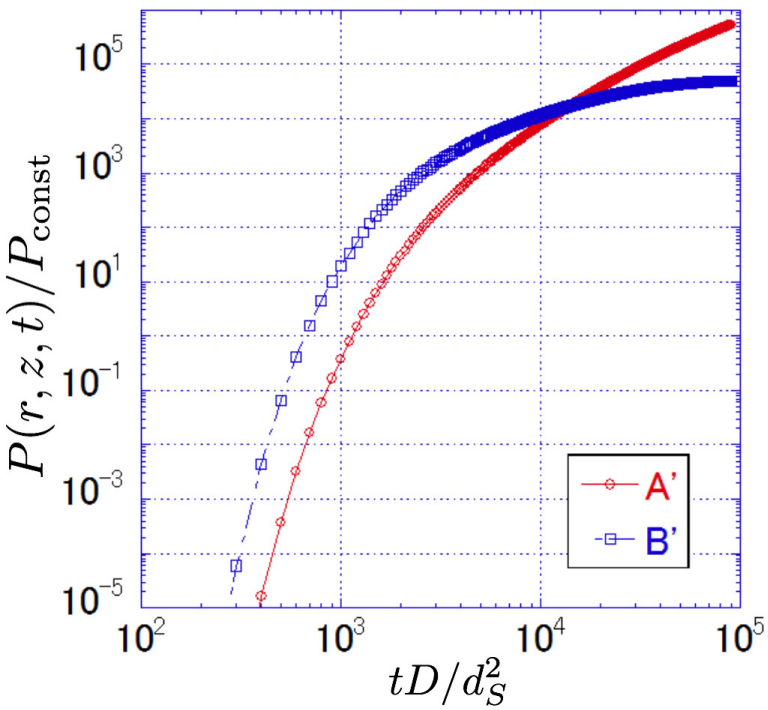

Figure 3.7: Time evolution of the probability density that the large sphere is on position $\boldsymbol{r}$ at time t $P(\boldsymbol{r},t)$ for the vessel inner diameter of $12d_{\mathrm{S}}$ and the large-sphere diameter of $8d_{\mathrm{S}}$. Here, d_{S} is the diameter of a small sphere, and D is the diffusion coefficient of a large sphere. Red and blue curves represent the density at A'($r = 0z = 0$) and B'($r = 0, z = d_{\mathrm{S}}$), respectively. The positions A' and B' represent the local minima in the potential of mean force.

To make the calculation reasonably in cost and time, a simplified model is used to analyze the whole process that an unfolded protein is inserted into the GroEL cavity. Though the large-sphere sizes investigated in a simplified model are $5d_{\mathrm{S}}$ and $8d_{\mathrm{S}}$, the size of an observed small protein is larger than $8d_{\mathrm{S}}$. Here, d_{S} is set at 0.28 nm, whose size is the molecular diameter of water. For instance, the natural structure of apoplastocyanin whose amino acid residues are 99 has roughly the diameter 3.5 nm [57]. Therefore, the diameter of the large sphere d_{L} becomes about $12.5d_{\mathrm{S}}$.

The trapping time at the center of the vessel τ is extrapolated until the observed size of an unfolded protein ($d_{\mathrm{L}} = 12.5d_{\mathrm{S}}$). An extrapolation equation is obtained from an assumption that the solute particle overcomes the PMF barrier between the positions A and B by an activation process. By the assumption, τ is written in the form of

$$\tau D/d_{\mathrm{S}}^2 = a\exp[b\Phi], \tag{3.3}$$

where a and b are the constants and Φ is height of the PMF barrier.

One can find $\Phi \propto d_{\mathrm{L}}/d_{\mathrm{S}}$ from the result of Amano *et al* (Fig. 2.4 and Fig. 2.5).

Hence, one obtains

$$\tau D/d_{\mathrm{S}}^2 = a\exp[c(d_{\mathrm{L}}/d_{\mathrm{S}})], \tag{3.4}$$

where c is the constant. The equation has the parameters a and c required for the extrapolation. The parameters are given in $a = 7.5$ and $c = 0.94$, which are obtained from the calculated results [$\tau D/d_{\mathrm{S}}^2 = 8.3 \times 10^2$ at $d_{\mathrm{L}}/d_{\mathrm{S}} = 5$ (Fig. 3.3) and $\tau D/d_{\mathrm{S}}^2 = 1.4 \times 10^4$ at $d_{\mathrm{L}}/d_{\mathrm{S}} = 8$ (Fig. 3.7)].

Moreover, the diffusion coefficient of a protein D is required for an estimation of the trapping time at the center of the vessel τ. The diffusion coefficient of a protein D has been estimated to be $\sim 10^{-6}$ cm^2/ sec (it is not strongly dependent on the protein size) [56]. Setting D at 10^{-6} cm^2/sec and d_{S} at 0.28 nm (the molecular diameter of water), τ can be estimated at $\tau = 1.1 \times 10^{-3}$ sec in the case of the diameter of apoplastocyanin ($d_{\mathrm{L}} = 12.5 d_{\mathrm{S}}$) by the extrapolation equation [Eq. 3.4].

The calculated result shows that the large sphere is in the central region of the vessel cavity until the trapping time τ. The experimental observation obtained using the cryo-electron microscopy has shown that a protein is within the GroEL cavity and not in touch with the inner surface of GroEL [7]. Until the trapping time τ, the theoretical result is quite consistent with experimental results. On the other hand, the authors of the experimental study have predicted the presence of a repulsive interaction between the protein and the inner surface of the GroEL from the average position of an unfolded protein. In contrast, the theoretical result shows that an unfolded protein is trapped at the central region of the vessel cavity without the introduction of a repulsive interaction predicted by the authors of ref.7 until the trapping time τ.

The time when the large sphere is in the central region of the vessel cavity is predicted from experimental results. This time is considered to be almost the same as the time required for a small protein to fold into its native structure. It is in the range of $10^{-6} \sim 10^{-3}$ sec [58–60]. If it is shorter than τ estimated by the theoretical method, the introduction of a repulsive interaction may not be necessary.

The relevance of $\Phi \propto d_{\mathrm{L}}/d_{\mathrm{S}}$ is discussed by a simple picture. Only the wall and the large sphere are considered (Fig. 3.8). When the distance between the wall and the front of the large sphere is $0.5 d_{\mathrm{S}}$, the excluded volume, which is not be available for translational motions of a solvent particle, is generated. A decrease of this volume is assumed to correspond to the PMF barrier. It can be estimated by

$$\Phi/(k_{\mathrm{B}}T) \sim \rho_{\mathrm{S}} V_{\mathrm{vacant}}, \tag{3.5}$$

where ρ_{S} is the average number density of solvent particles and V_{vacant} is the volume of the vacant space. It is defined by the space where the distance between the wall and the large sphere is less than d_{S}.

Given V_{vacant} as a cylindrical space with a height $d_{\mathrm{H}} = d_{\mathrm{S}}/2$ approximately,

$$V_{\mathrm{vacant}} = d_{\mathrm{S}}/2 \times \pi d_{\mathrm{R}}^2. \tag{3.6}$$

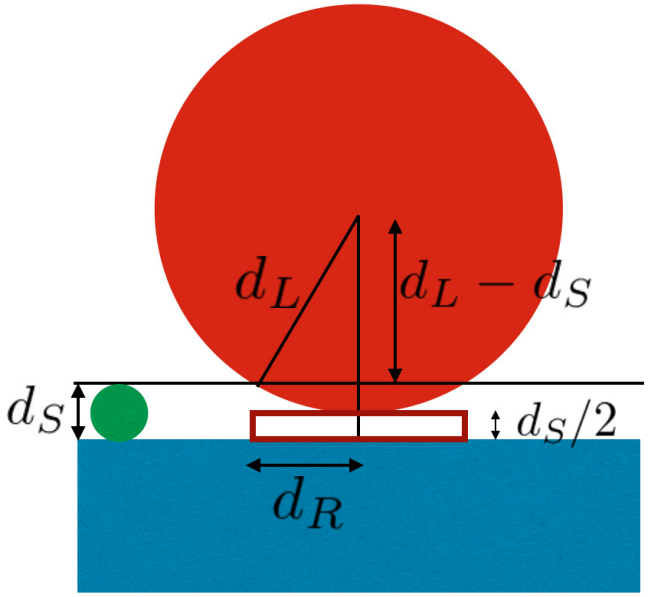

Figure 3.8: The vacant space between large sphere and wall when the distance between the wall and the front of the large sphere is $0.5d_{\mathrm{S}}$.

Here, d_{R} is represented by Fig. 3.8 and is satisfied with $d_{\mathrm{R}}^2 = d_{\mathrm{L}}^2 - (d_{\mathrm{L}} - d_{\mathrm{S}})^2$. The PMF barrier is

$$\frac{\Phi}{k_{\mathrm{B}}T} \sim \rho_{\mathrm{S}} \times \frac{d_{\mathrm{S}}}{2} \times \pi d_{\mathrm{R}}^2 = \rho_{\mathrm{S}} \frac{d_{\mathrm{S}}}{2} \times \pi \left\{ d_{\mathrm{L}} - (d_{\mathrm{L}} - d_{\mathrm{S}})^2 \right\} = \pi \rho_{\mathrm{S}} d_{\mathrm{S}}^3 \times \left(\frac{d_{\mathrm{L}}}{d_{\mathrm{S}}} - \frac{1}{2} \right). \quad (3.7)$$

Therefore, the height of the PMF barrier Φ is proportional to $d_{\mathrm{L}}/d_{\mathrm{S}}$ if the volume fraction $\phi_{\mathrm{volume}} \equiv \pi \rho_{\mathrm{S}} d_{\mathrm{S}}^3/6$ is a constant value.

3.7 Summary

The dynamics for a insertion of a large hard sphere into a large rigid cylinder has been analyzed. The large hard sphere and large rigid cylinder, which correspond to a solute particle and vessel, respectively, are immersed in small hard spheres forming the solvent. The time evolution of the probability density $P(\boldsymbol{r}, t)$ has been calculated by solving the Fokker-Plank equation [24] in the presence of the potential field, which is represented by the equilibrium effect of solvent particles. Here, $P(\boldsymbol{r}, t)$ denotes the probability density of finding the solute particle at position $\boldsymbol{r}$ at time t. The potential field has been calculated beforehand using the three-dimensional integral equation theory [11].

The analysis shows that the large-sphere is trapped at the center of the vessel. After being trapped, it moves to the bottom of the vessel. The trapping time can be calculated by solving the Fokker-Plank equation. Though the realistic size of the small protein and GroEL can not be calculated, the trapping time in the case

of the size of a small protein is predicted by an extrapolation method. When an unfolded protein can be regarded as the hard sphere with the diameter $d_L > 3.5$ nm, the estimated time is longer than the time required for a small protein to fold into its native structure. Thus, our result may be relevant to the experimental result that an unfolded protein is not touch with the inner surface of the GroEL cavity.

Chapter 4

Nonequilibrium Effect of Solvent Particles on a Moving Solute

In chapter 3, equilibrium effect of solvent particles on the solute dynamics was discussed, assuming the equilibrium state of solvent particles. However, the validity of the assumption remains to be verified. In present chapter, I discuss the nonequilibrium effect of solvent particles, constraining the trajectory of a moving solute. I calculate the nonequilibrium density distribution of the solvent particles when a large sphere is inserted into the cylindrical vessel with a constant velocity. In addition, I will discuss the relationship with the number of solvent particles inside the vessel and the grand potential functional.

4.1 Introduction

The equilibrium effect of solvent particles on biomolecules (solutes) has been formulated on the basis on the equilibrium statistical mechanics. One of the theories is the integral equation theory (IET) [11], with which we can study the system consisting of spherical solvent particles. In the system consisting of non-spherical spherical solvent particles, the reference interaction site model (RISM) [53] has been used. These methods are formulated by considering the correlation between solvent particles in many-body systems. Applying these theories to biological systems, the equilibrium effect of solvent particles on the biomolecules can be obtained. They lead to an interpretation of mechanism of biological functions, such as tripartite efflux systems [22,23], motor proteins [21], chaperons [17–19], and ion channel [51].

In the previous chapter, approximating density distributions of solvent particles in equilibrium density distributions, the effects on the equilibrium density distributions on the dynamics of the biomolecule was clarified. The validity of the approximation for biological phenomena has not been understood. It can be evaluated by studying nonequilibrium density distributions of solvent particles on the dynamics of the biomolecule. In this chapter, I discuss the discrepancy between

nonequilibrium and equilibrium density distributions of solvent particles.

The effect of nonequilibrium density distributions of solvent particles is expected to play a role when solvent particles flow the confined space around a solute. It is because solvent particles cannot relax to the equilibrium state quickly owing to confinement of the movement of the solvent particle. Examples of such confining spaces include the inside of the basketlike shape observed in the GroEL-GroES [5, 6] and dextran glucosidase [61]. When an unfolded protein is inserted into the cavity of GroEL, solvent particles are trapped at the space between the protein and the GroEL due to the confined area within the cavity. It leads to the restricted movement of trapped solvent particles. Thus, the relaxation time of solvent particles becomes long. If the relaxation time is long compared to the time for movement of large sphere, the solvent particles is at nonequilibrium state. The effect of the nonequilibrium density distribution of solvent particles on the protein is different from that of the equilibrium density distribution.

Such nonequilibrium density distribution can be obtained by the time-dependent density functional theory (TDDFT) [25–27]. TDDFT gives the time development of the density field of liquid particles using the interaction between particles. It has been used for the study of dynamics in systems such as liquids [62, 63], supercooled liquids [64], and solutions [65–72]. In particular, a lot of researchers have studied the solvent particle dynamics around the solute by TDDFT [26, 65–72].

TDDFT has never been applied to the biological system. In the previous studies of biological systems, little has been reported on the nonequilibrium effect of solvent particles in biological systems. Since the many-body correlation of solvent particles has been focused in biological systems, it makes the high computational cost in the simulation for treating the movements of each particles. Typical examples are molecular dynamics simulation and Monte Carlo simulation. Since TDDFT can include the many-body effects by an ensemble average quantity, it is easily expected to capture the characteristics of solvent effects in biological systems. In contrast, few reports are available on application of TDDFT to the two or higher dimension system. The system for the dynamics of solvent particle around a moving solute should be an axial symmetry or no symmetry. Since an axisymetric system is two dimension, the dynamics of solvent particle around a moving solute does not understand.

The purpose of this chapter is to clarify the nonequilibrium effect of solvent particles on a moving solute. For the purpose, I formulate the theory by incorporating the movement of biomolecules into TDDFT. I discuss about the discrepancy between nonequilibrium distribution and equilibrium distribution of solvent particles. In addition, to discuss the nonequilibrium effect, I calculate the number of solvent particles inside of the vessel and the grand potential functional.

4.2 Theory

4.2.1 Treatment of a Moving Solute Particle

I consider solvent particles around an arbitrary shaped solute particle, which moves along an arbitrary various path. The trajectory of the moving solute $\boldsymbol{r}_{\mathrm{solu}}(t)$ is given as an input parameter. The solute-solvent interaction is taken into account as the external field $\Phi_{\mathrm{ext}}(\boldsymbol{r}, t)$ defined by

$$\Phi_{\mathrm{ext}}(\boldsymbol{r}, t) = u\left(\boldsymbol{r} - \boldsymbol{r}_{\mathrm{solu}}(t)\right). \tag{4.1}$$

Here, $u\left(\boldsymbol{r} - \boldsymbol{r}_{\mathrm{solu}}(t)\right)$ is the interaction between the solute and a solvent particle located at $\boldsymbol{r}$. Note that the external field $\Phi_{\mathrm{ext}}(\boldsymbol{r}, t)$ depends on time t due to the solute movement. The shape of the solutes does not need to have a symmetry, such as spherical symmetry.

4.2.2 Time Dependent Density Functional Theory

The time dependent density functional theory (TDDFT) [25–27] gives the time development of number density of spherical solvent particles $\rho(\boldsymbol{r}, t)$, using the grand potential functional $\Omega[\rho(\boldsymbol{r}, t)]$ defined by density functional theory [Eq. (2.11)]. If the thermodynamics force is assumed by $\nabla\delta\beta\Omega[\rho(\boldsymbol{r}, t)]/\delta\rho(\boldsymbol{r}, t)$, the flux of the number density of solvent particles $\boldsymbol{J}(\boldsymbol{r}, t)$ can be written by

$$\boldsymbol{J}(\boldsymbol{r}, t) = -D_{\mathrm{S}}\left[\rho(\boldsymbol{r}, t)\nabla\frac{\delta\beta\Omega[\rho(\boldsymbol{r}, t)]}{\delta\rho(\boldsymbol{r}, t)}\right]. \tag{4.2}$$

Here, D_S is the diffusion coefficient of the solvent and $\beta = 1/k_B T$ is the inverse temperature, where k_B is Boltzmann's constant and T is the absolute temperature. Time development of number density of solvent particles is described as

$$\frac{\partial\rho(\boldsymbol{r}, t)}{\partial t} = -\nabla\cdot\boldsymbol{J}(\boldsymbol{r}, t) \tag{4.3}$$

$$= D_{\mathrm{S}}\nabla\cdot\left[\rho(\boldsymbol{r}, t)\nabla\frac{\delta\beta\Omega[\rho(\boldsymbol{r}, t)]}{\delta\rho(\boldsymbol{r}, t)}\right]. \tag{4.4}$$

Equation (4.4) is called TDDFT.

The validity of the assumption on the thermodynamics force has already been discussed by some researchers. Marconi and Tarazona had derived TDDFT by using the rules of the Ito stochastic calculus, starting from the Langevin stochastic equations of motion for the velocities of particles [25]. Yoshimori had derived TDDFT by using the projection operator method, starting from the Hamiltonian system [27].

TDDFT has been used to analyze the relaxation process from the nonequilibrium state until the equilibirium state. In theses studies, the external field $\Phi(\boldsymbol{r})$ does not depend on time t. It is proved in [26] that the grand potential functional

$\Omega[\rho(\boldsymbol{r},t),\Phi(\boldsymbol{r})]$ is convex. In the minimum value of $\Omega[\rho(\boldsymbol{r},t),\Phi(\boldsymbol{r})]$, $\rho(\boldsymbol{r},t)$ becomes the equilibrium density distribution. TDDFT gives the time-development density $\rho(\boldsymbol{r},t)$ until the equilibrium state along the gradient of the grand potential functional $\Omega[\rho(\boldsymbol{r},t),\Phi(\boldsymbol{r})]$.

In this study, the extended theory is formulated by incorporating the time-dependent external field $\Phi(\boldsymbol{r},t)$ into TDDFT. The time-dependent external field $\Phi(\boldsymbol{r},t)$ represents the movement of the solute particle. Becase $\Phi(\boldsymbol{r},t)$ depends on t, the density distribution dependency of $\Omega[\rho(\boldsymbol{r},t),\Phi(\boldsymbol{r},t)]$ also changes with the time. Since the density distribution at the minimum value of $\Omega[\rho(\boldsymbol{r},t),\Phi(\boldsymbol{r},t)]$ also changes with time, the density distribution becomes in the nonequilibrium state. Therefore, TDDFT gives the time-dependent density distribution in the nonequilibrium system.

4.2.3 Grand Potential Functional

The grand potential functional $\Omega[\rho(\boldsymbol{r},t)]$ is obtained by the Ramakrishnan-Yussouff (RY) approximation. The derivation of RY approximation has been explained in §2.3. In the RY approximation, the grand potential functional is rewritten by

$$\begin{aligned}\beta\Omega[\rho(\boldsymbol{r},t)] &= \beta\Omega_0 + \int \beta\Phi_{\mathrm{ext}}(\boldsymbol{r},t)\rho(\boldsymbol{r},t)\mathrm{d}\boldsymbol{r} \\ &\quad + \int \rho(\boldsymbol{r},t)\ln[\rho(\boldsymbol{r},t)/\rho_0]\mathrm{d}\boldsymbol{r} \\ &\quad - \int \Delta\rho(\boldsymbol{r},t)\mathrm{d}\boldsymbol{r} \\ &\quad - \frac{1}{2}\int c_0(|\boldsymbol{r}'-\boldsymbol{r}|)\Delta\rho(\boldsymbol{r},t)\Delta\rho(\boldsymbol{r}',t)\mathrm{d}\boldsymbol{r}\mathrm{d}\boldsymbol{r}'.\end{aligned} \tag{4.5}$$

Here, Ω_0 and $c_0(|\boldsymbol{r}'-\boldsymbol{r}|)$ are the grand potential and the direct correlation function between solvent particles in the reference homogeneous system, respectively. In addition, $\Delta\rho(\boldsymbol{r},t) \equiv \rho(\boldsymbol{r},t) - \rho_0$, where ρ_0 is the density in the reference homogeneous system. Given just $c_0(|\boldsymbol{r}'-\boldsymbol{r}|)$, the time evolution of number density of solvent particles is calculated by Eqs. (4.4) and (4.5). The correlation $c_0(|\boldsymbol{r}'-\boldsymbol{r}|)$ is obtained by several methods.

The direct correlation function in the reference homogeneous system $c_0(|\boldsymbol{r}'-\boldsymbol{r}|)$ is calculated by the radial integral equation theory. It is represented by the Ornstein-Zernike (OZ) equation

$$w_0(r) = \rho_0 \int c_0(|\boldsymbol{r}'-\boldsymbol{r}|)h_0(r')\mathrm{d}\boldsymbol{r}' \tag{4.6}$$

and the hypernetted chain (HNC) closure

$$c_0(r) = \exp\{-\beta u(r) + w_0(r)\} - w_0(r) - 1. \tag{4.7}$$

Here, $w_0(r) = h_0(r) - c_0(r)$, $r = |\boldsymbol{r}|$, and $h_0(r)$ are the indirect and total correlation functions between solvent particles in the homogeneous system, respectively. In addition, $u(r)$ is the interaction potential between solvent particles. To obtain $c_0(|\boldsymbol{r}' - \boldsymbol{r}|)$, we solve Eqs. (4.6) and (4.7) by an iterative numerical approach.

4.3 Application to Insertion Process

The present theory is applied to the insertion process of a large sphere into a cylindrical vessel, which is immersed in small sphere solvents (Fig. 4.1). The large-sphere, vessel, and small spheres are modeled by the hard-body potential. The diameter of the small-sphere and large-sphere are fixed at d_{S} and $5d_{\mathrm{S}}$, respectively. Height, inner diameter, and outer diameter of the vessel are denoted by d_{H}, d_{I}, and $(25.6d_{\mathrm{S}} - d_{\mathrm{I}})/2$, respectively. The vessel has rounded corners of the top and rounded fillets of the bottom, where their radii are d_{S}. The large sphere and the vessel are assumed infinite dilution and the number density of the small spheres ρ_0 is given by $\rho_0 d_{\mathrm{S}}^3 = 0.7317$, which is that of water at 298 K and 1 atm.

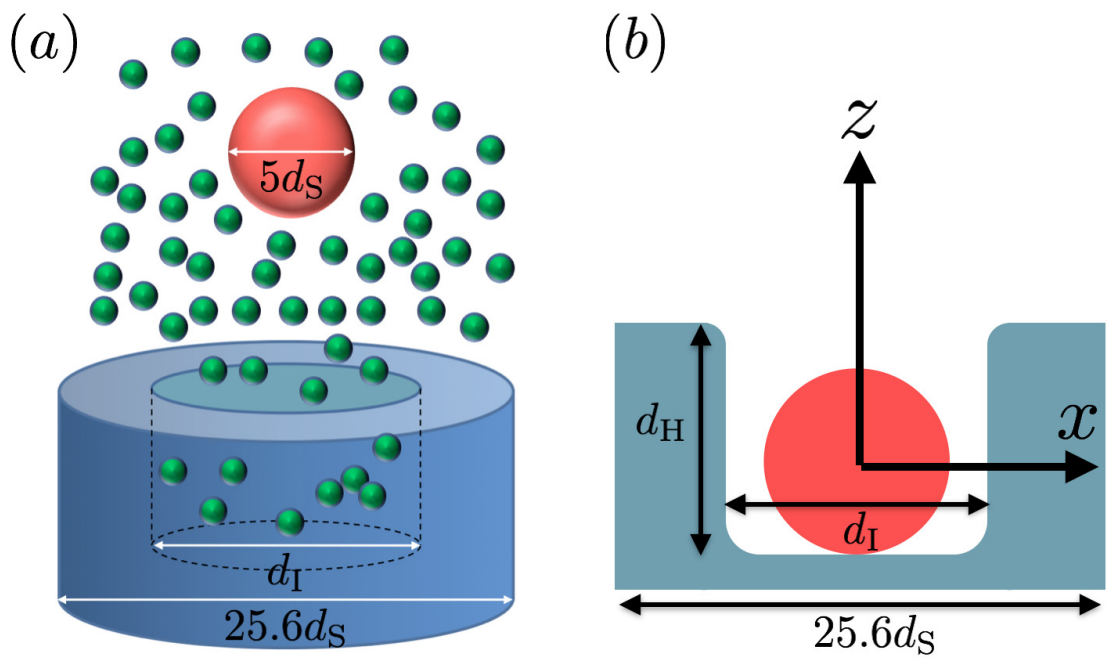

Figure 4.1: (a) Models of a large sphere, small spheres and a cylindrical vessel. The diameter of the small sphere and large sphere is set at d_{S} and $5d_{\mathrm{S}}$. The inner and outer diameter of the vessel are d_{I} and $25.6d_{\mathrm{S}}$. (b) The cross section of the vessel. Height, inner diameter and sidewall thickness of the vessel are denoted by d_{H}, d_{I} and $(25.6d_{\mathrm{S}} - d_{\mathrm{I}})/2$, respectively. The vessel has rounded corners of the top and rounded fillets of the bottom, where both of the radii are d_{S}. The thick solid lines represent the x-axis and z-axis, and the y-axis is perpendicular to the plane of the paper. The origin of the x-axis and y-axis is at the center of the vessel. The origin of the z-axis is at the center of the large sphere, which is in contact with the bottom of the vessel.

I consider the vessel-fixed Cartesian coordinate system (x, y, z) (Fig. 4.1). The origin of the x- and y-axis is the center of the vessel. At the origin of the z-axis, the center of the large sphere is in contact with the bottom of the vessel. The position (x, y, z) represents the center of the small sphere.

The large sphere is inserted along z-axis from the outside of the vessel into the vessel with a constant velocity V_{LS}. Thus, the center of the large sphere at time t is located at $\boldsymbol{r}_{\mathrm{LS}}(t) = (0, 0, z_{\mathrm{LS}}(t))$, where $z_{\mathrm{LS}}(t)$ can be written by

$$z_{\mathrm{LS}}(t) = z_{\mathrm{LS}}(0) - V_{\mathrm{LS}}t. \tag{4.8}$$

Here, $z_{\mathrm{LS}}(0) = 11.4d_{\mathrm{S}}$ is the initial position of large sphere. According to Eq (4.8), one can know time t from the the large-sphere position $z_{\mathrm{LS}}(t)$. In each calculation, the constant velocities are varied with $D_{\mathrm{S}}/2d_{\mathrm{S}}$, $D_{\mathrm{S}}/4d_{\mathrm{S}}$, $D_{\mathrm{S}}/8d_{\mathrm{S}}$, $D_{\mathrm{S}}/16d_{\mathrm{S}}$, $D_{\mathrm{S}}/32d_{\mathrm{S}}$, and $D_{\mathrm{S}}/64d_{\mathrm{S}}$. Here, D_{S} is the diffusion coefficient of the solvent in Eq. (4.4).

By the above, the external potential $\Phi_{\mathrm{ext}}(\boldsymbol{r}, t)$ can be written as

$$\Phi_{\mathrm{ext}}(\boldsymbol{r}, t) = u_{\mathrm{V,S}}(\boldsymbol{r}) + u_{\mathrm{L,S}}\left(|\boldsymbol{r} - \boldsymbol{r}_{\mathrm{LS}}(t)|\right), \tag{4.9}$$

where $u_{\mathrm{V,S}}(\boldsymbol{r})$ is the interaction between a cylindrical vessel and a small sphere and $u_{\mathrm{L,S}}\left(|\boldsymbol{r} - \boldsymbol{r}_{\mathrm{LS}}(t)|\right)$ is the interaction between a large sphere and a small sphere. In addition, $u_{\mathrm{L,S}}\left(|\boldsymbol{r} - \boldsymbol{r}_{\mathrm{LS}}(t)|\right)$ is infinity in $|\boldsymbol{r} - \boldsymbol{r}_{\mathrm{LS}}(t)| < 3d_{\mathrm{S}}$ and otherwise it is zero. Moreover, $u_{\mathrm{V,S}}(\boldsymbol{r})$ is infinity when the center of small sphere is overlapped with the vessel and otherwise it is zero. The calculation is performed until $z_{\mathrm{LS}}(t)$ is equal to d_{S}.

There are two steps to calculate the number density of solvent particles numerically. At the first step, I solve the combination of Eqs. (4.6) and (4.7) by the Newton-Raphson method. At the second step, using the direct correlation function obtained from the first step, I calculate Eq. (4.4) by the Euler method. In the second calculation, the grid resolution (N_{x}, N_{y}, and N_{z}) is $512 \times 512 \times 512$ and the grid spacing (Δx, Δy, and Δz) is set at $0.05d_{\mathrm{S}}$. The time step is $\Delta t = 1.0 \times 10^{-5} D_{\mathrm{S}}/d_{\mathrm{S}}^2$. I use a 2nd order central difference for discretization of the space. In this calculation, I use the fast Fourier transform in the cuFFT package and perform parallel computing in the other calculation part. Because of the discretization of time and hard-core model, number density of solvent particles should be treated specially around the large sphere. The detail of the special treatment is described in Appendix C.

There are three boundary conditions for the calculation. First, the periodic boundary condition for the x- and y-directions is assumed. Secondly, the boundary condition at $z = 17.2d_{\mathrm{S}}$ is given by $\rho(\boldsymbol{r}, t) = \rho_0$. It means that the particle bath is set at at $z \geq 17.2d_{\mathrm{S}}$. Thirdly, when the solvent particle comes in contact with the wall of the vessel or the large sphere, $J(\boldsymbol{r}, t) \cdot n = 0$ is also assumed, where n is the unit vector perpendicular to the wall of vessel or the large sphere. It means that a small sphere does not come in the vessel and the large sphere.

The initial density distribution of the solvent particles $\rho(\boldsymbol{r}, t = 0)$ is set at that in the equilibrium state, where the center of the large sphere is fixed at

$\boldsymbol{r}_{\mathrm{LS}}(t) = (0, 0, z_{\mathrm{LS}}(0))$. The equilibrium density distribution is obtained by the density functional theory,

$$\left.\frac{\delta\Omega[\rho(\boldsymbol{r})]}{\delta\rho(\boldsymbol{r})}\right|_{\rho(\boldsymbol{r})=\rho(\boldsymbol{r},t=0)} = 0. \tag{4.10}$$

Insertion of Eq (4.5) into Eq (4.10) yields

$$\rho(\boldsymbol{r}, t=0) = \rho_0 \exp\left\{-\beta\Phi_{\mathrm{ext}}(\boldsymbol{r}, t=0) + \int c_{0,\mathrm{SS}}(|\boldsymbol{r}' - \boldsymbol{r}|)\Delta\rho(\boldsymbol{r}, t=0)\mathrm{d}\boldsymbol{r}\right\}, \tag{4.11}$$

where $\Phi_{\mathrm{ext}}(\boldsymbol{r}, t = 0)$ is the solute-solvent interaction when the large-sphere is located on $\boldsymbol{r}_{\mathrm{LS}}(t) = (0, 0, z_{\mathrm{LS}}(0))$. The solution of Eq. (4.11) is calculated by the Newton-Raphson method numerically.

4.4 Density Distribution and Number of Solvent Particles in the Vessel

In this section, the relationship with the velocity of the large sphere and the nonequilibrium density distribution of solvent particles will be shown. The number of solvent particles inside the vessel is also discussed. I set height d_{H} and inner diameter d_{I} of the vessel at $6d_{\mathrm{S}}$ and $7d_{\mathrm{S}}$, respectively.

4.4.1 Results

Figure 4.2 shows the spatial distributions of the number density of solvent particles at the center position of the large sphere (a) $z_{\mathrm{LS}}(t) = 6.2d_{\mathrm{S}}$, (b) $z_{\mathrm{LS}}(t) = 3.7d_{\mathrm{S}}$, and (c) $z_{\mathrm{LS}}(t) = 1.2d_{\mathrm{S}}$. There are a lot of local maxima and minima near the large sphere and the vessel. The interval between these local maxima is about d_{S} owing to the excluded volumes of solvent particles. The values of the local maxima are large when the large sphere is inside of the vessel [Figs. 4.2(b) and (c)].

The difference in the number density from that in the equilibrium state $\delta\rho(\boldsymbol{r}, t) = \rho(\boldsymbol{r}, t) - \rho_{\mathrm{eq}}^{z_{\mathrm{LS}}(t)}(\boldsymbol{r})$ is calculated (Fig. 4.3). Here, $\rho_{\mathrm{eq}}^{z_{\mathrm{LS}}(t)}(\boldsymbol{r})$ is number density of solvent particles in the equilibrium state when the center of the large sphere is set at $z_{\mathrm{LS}}(t)$. It is obtained by the density functional theory [Eq. (4.11)]. Although $\delta\rho(\boldsymbol{r}, t)$ is almost negative at $z > z_{\mathrm{LS}}(t)$, large positive values are obtained in the region $z < z_{\mathrm{LS}}(t)$. In particular, inside of the vessel, we obtain a high peak of $\delta\rho(\boldsymbol{r}, t)$, whose magnitude increases as the large sphere approaches to the bottom of the vessel.

Since the discrepancy between the nonequilibrium and equilibrium distribution is large in the vessel cavity, I focus on the number of solvent particles inside of the vessel $N_{\mathrm{v}}(z_{\mathrm{LS}})$ (Fig. 4.4). It is defined by

$$N_{\mathrm{v}}(z_{\mathrm{LS}}) = \int\int\int_{V_{\mathrm{v}}} \mathrm{d}x\mathrm{d}y\mathrm{d}z\ \rho(\boldsymbol{r}, t). \tag{4.12}$$

Here, V_{v} represents the space inside of the vessel ($-2d_{\mathrm{S}} \leq z \leq 3.5d_{\mathrm{S}}$). $N_{\mathrm{v}}(z_{\mathrm{LS}})$ increases with the velocity of the large sphere. In particular, $N_{\mathrm{v}}(z_{\mathrm{LS}})$ at $z_{\mathrm{LS}}(t) = d_{\mathrm{S}}$ is 32.5 % larger that for the velocity of $D_{\mathrm{S}}/2d_{\mathrm{S}}$ than for the equilibrium state.

The $z_{\mathrm{LS}}(t)$-dependence of N_{v} differs in $z_{\mathrm{LS}}(t) > 6d_{\mathrm{S}}$, $3d_{\mathrm{S}} < z_{\mathrm{LS}}(t) < 6d_{\mathrm{S}}$, and $z_{\mathrm{LS}}(t) < 3d_{\mathrm{S}}$. In $z_{\mathrm{LS}}(t) > 6d_{\mathrm{S}}$, $N_{\mathrm{v}}(z_{\mathrm{LS}})$ increases with a decrease in $z_{\mathrm{LS}}(t)$. In $3d_{\mathrm{S}} < z_{\mathrm{LS}}(t) < 6d_{\mathrm{S}}$, $N_{\mathrm{v}}(z_{\mathrm{LS}})$ decreases with a decrease in $z_{\mathrm{LS}}(t)$. In $z_{\mathrm{LS(t)}} < 3d_{\mathrm{S}}$, while $N_{\mathrm{v}}(z_{\mathrm{LS}})$ decreases with a decrease in $z_{\mathrm{LS}}(t)$ for $V_{\mathrm{LS}} < D_{\mathrm{S}}/4d_{\mathrm{S}}$, $N_{\mathrm{v}}(z_{\mathrm{LS}})$ increases for $V_{\mathrm{LS}} \geq D_{\mathrm{S}}/4d_{\mathrm{S}}$. $N_{\mathrm{v}}(z_{\mathrm{LS}})$ increases as the large sphere moves faster, indicating that trapping solvent particles is enhanced due to the reduced probability of the escape from a vessel.

In order to analyze the number N_{v} in detail, $N_{\mathrm{v}}(z_{\mathrm{LS}})$ is divided into the number of solvent particles in the lower and upper parts of the vessel. The number of solvent particles in the lower part of the vessel N_{lower} is defined by

$$N_{\mathrm{lower}}(z_{\mathrm{LS}}) = \int\int\int_{V_{\mathrm{lower}}} \mathrm{d}x\mathrm{d}y\mathrm{d}z\ \rho(\boldsymbol{r}, t), \tag{4.13}$$

where V_{lower} is the space in the lower part of the vessel ($-2.0d_{\mathrm{S}} \leq z < 2.5d_{\mathrm{S}}$). And then, the number of solvent particles in the upper part of the vessel $N_{\mathrm{upper}}(z_{\mathrm{LS}})$ is defined by

$$N_{\mathrm{upper}}(z_{\mathrm{LS}}) = \int\int\int_{V_{\mathrm{upper}}} \mathrm{d}x\mathrm{d}y\mathrm{d}z\ \rho(\boldsymbol{r}, t), \tag{4.14}$$

where V_{upper} represents the space in the upper part inside the vessel ($2.5d_{\mathrm{S}} \leq z \leq 3.5d_{\mathrm{S}}$). $N_{\mathrm{upper}}(z_{\mathrm{LS}})$ satisfies in $N_{\mathrm{v}}(z_{\mathrm{LS}}) = N_{\mathrm{upper}}(z_{\mathrm{LS}}) + N_{\mathrm{lower}}(z_{\mathrm{LS}})$.

The number of solvent particles in the lower part of the vessel $N_{\mathrm{lower}}(z_{\mathrm{LS}})$ has the velocity dependence (Fig. 4.5). In $z_{\mathrm{LS}}(t) > 6d_{\mathrm{S}}$, $N_{\mathrm{lower}}(z_{\mathrm{LS}})$ increases with a decrease in z_{LS} and has a similar behavior to $N_{\mathrm{v}}(z_{\mathrm{LS}})$. In $3d_{\mathrm{S}} < z_{\mathrm{LS}}(t) < 6d_{\mathrm{S}}$, $N_{\mathrm{lower}}(z_{\mathrm{LS}})$ decreases with a decrease in $z_{\mathrm{LS}}(t)$. In $d_{\mathrm{S}} < z_{\mathrm{LS}}(t) < 3d_{\mathrm{S}}$, $N_{\mathrm{lower}}(z_{\mathrm{LS}})$ does not change much with $z_{\mathrm{LS}}(t)$ at $V_{\mathrm{LS}} = D_{\mathrm{S}}/2d_{\mathrm{S}}$ and $N_{\mathrm{lower}}(z_{\mathrm{LS}})$ decreases with a decrease in $z_{\mathrm{LS}}(t)$ for $V_{\mathrm{LS}} \leq D_{\mathrm{S}}/4d_{\mathrm{S}}$. As the large sphere moves faster, the N_{lower} remains to larger numbers compared with the equilibrium profile. It suggests that the trapping of solvent particles is more effective for the fast moving sphere, which is consistent with the result shown in Fig. 4.4.

For the particles on the top of a vessel, $N_{\mathrm{upper}}(z_{\mathrm{LS}})$ does not vary with the speed of a large sphere. As shown in Fig. 4.6, $N_{\mathrm{upper}}(z_{\mathrm{LS}})$ below $6d_{\mathrm{S}}$ in $z_{\mathrm{LS}}(t)$ at any speeds most matches with the profile at equilibrium. This result is consistent with the fact that the solvent particles are scraped by the large sphere in the lower part of a vessel. In addition, the local minimum at $z_{\mathrm{LS}}(t) = 3.5d_{\mathrm{S}}$ is present. It is because of the excluded volume for the solvent particles due to the large sphere. This local minimum will be discussed later.

An increase and decrease of $N_{\mathrm{v}}(z_{\mathrm{LS}})$ in $d_{\mathrm{S}} < z_{\mathrm{LS}}(t) < 3d_{\mathrm{S}}$ are caused by an increase in $N_{\mathrm{upper}}(z_{\mathrm{LS}})$ and the velocity dependence of $N_{\mathrm{lower}}(z_{\mathrm{LS}})$. $N_{\mathrm{upper}}(z_{\mathrm{LS}})$ increases with a decrease in $z_{\mathrm{LS}}(t)$ for $z_{\mathrm{LS}} < 3.5d_{\mathrm{S}}$, while $N_{\mathrm{lower}}(z_{\mathrm{LS}})$ decreases with a decrease in $z_{\mathrm{LS}}(t)$ at $V_{\mathrm{LS}} \leq D_{\mathrm{S}}/8d_{\mathrm{S}}$. When $V_{\mathrm{LS}} \leq D_{\mathrm{S}}/8d_{\mathrm{S}}$, $N_{\mathrm{v}}(z_{\mathrm{LS}})$ decreases

with a decrease in $z_{\mathrm{LS}}(t)$ because the decrease in $N_{\mathrm{lower}}(z_{\mathrm{LS}})$ is larger than the increase in $N_{\mathrm{upper}}(z_{\mathrm{LS}})$. In contrast, at $V_{\mathrm{LS}} = D_{\mathrm{S}}/4d_{\mathrm{S}}$ and $V_{\mathrm{LS}} = D_{\mathrm{S}}/2d_{\mathrm{S}}$, $N_{\mathrm{v}}(z_{\mathrm{LS}})$ increases with a decrease in $z_{\mathrm{LS}}(t)$ from $3d_{\mathrm{S}}$ to d_{S}. It is because the change of $N_{\mathrm{lower}}(z_{\mathrm{LS}})$ from $z_{\mathrm{LS}}(t) = 3d_{\mathrm{S}}$ to $z_{\mathrm{LS}}(t) = d_{\mathrm{S}}$ is small compared with the increase in $N_{\mathrm{upper}}(z_{\mathrm{LS}})$ at the high velocity.

By the value of the velocity, $N_{\mathrm{v}}(z_{\mathrm{LS}})$ in $d_{\mathrm{S}} < z_{\mathrm{LS}}(t) < 3d_{\mathrm{S}}$ has the two behaviors: one of a behavior is a decrease at $V_{\mathrm{LS}} \leq D_{\mathrm{S}}/8d_{\mathrm{S}}$ and the other one is an increase at $V_{\mathrm{LS}} = D_{\mathrm{S}}/4d_{\mathrm{S}}$ and $V_{\mathrm{LS}} = D_{\mathrm{S}}/2d_{\mathrm{S}}$. Therefore, in $d_{\mathrm{S}} < z_{\mathrm{LS}} < 3d_{\mathrm{S}}$, solvent particles escape from the vessel cavity at the low velocity of the large sphere ($V_{\mathrm{LS}} \leq D_{\mathrm{S}}/8d_{\mathrm{S}}$). In contrast, at the high velocity of the large sphere ($V_{\mathrm{LS}} = D_{\mathrm{S}}/4d_{\mathrm{S}}$ and $V_{\mathrm{LS}} = D_{\mathrm{S}}/2d_{\mathrm{S}}$), solvent particles flow into the vessel cavity in $d_{\mathrm{S}} < z_{\mathrm{LS}} < 3d_{\mathrm{S}}$. Certainly, the flux of solvent particles is negative at the entrance of the vessel ($z = 3.5d_{\mathrm{S}}$) at the high velocity.

4.4.2 Discussions

In this section, z_{LS}- and V_{LS}-dependences of N_{V} are discussed separately in three regions by the position of the large sphere. The regions are separated by $z_{\mathrm{LS}} = 6d_{\mathrm{S}}$ and $z_{\mathrm{LS}} = 3d_{\mathrm{S}}$. In $z_{\mathrm{LS}} = 6d_{\mathrm{S}}$, the front of the large sphere is located at the top of the vessel. In $z_{\mathrm{LS}} = 3d_{\mathrm{S}}$, the center of the large sphere is located at the inside of the vessel. In $z_{\mathrm{LS}} = 3d_{\mathrm{S}}$, the inner diameter of the vessel is $7.2d_{\mathrm{S}}$ for the rounded corner of the top of the vessel; it is $9d_{\mathrm{S}}$ in the top of the vessel ($z_{\mathrm{LS}} = 3.5d_{\mathrm{S}}$) and $7d_{\mathrm{S}}$ in the end of the rounded corner ($z_{\mathrm{LS}} = 2.5d_{\mathrm{S}}$). Three regions are denoted as follows:

region A $z_{\mathrm{LS}}(t) > 6d_{\mathrm{S}}$

region B $3d_{\mathrm{S}} < z_{\mathrm{LS}}(t) < 6d_{\mathrm{S}}$

region C $d_{\mathrm{S}} < z_{\mathrm{LS}}(t) < 3d_{\mathrm{S}}$

An increase of $N_{\mathrm{v}}(z_{\mathrm{LS}})$ with a decrease in z_{LS} for *region A* is discussed. If the velocity of the large sphere is large, solvent particles are trapped in the front of the large sphere due to less time for escaping. The trapped solvent particles are carried into the vessel with the large sphere (Fig. 4.7). The number of the trapped solvent particles increases with the velocity of the large sphere and becomes zero in the equilibrium state. For the solvent particles moving with the large sphere, since the flux of solvent particles along the insertion direction increases with a decrease in z_{LS}, N_{V} increases for *region A*.

A decrease in $N_{\mathrm{v}}(z_{\mathrm{LS}})$ with a decrease in z_{LS} for *region B* is discussed. In $z_{\mathrm{LS}} = 6d_{\mathrm{S}}$, the front of the large sphere is located in the top of the vessel. As the large sphere moves to the bottom of the vessel, the excluded volume increases. Due to the large excluded volume of the large sphere, the available volume for solvent particles becomes small. Since the available volume for solvent particles decreases with a decrease of $z_{\mathrm{LS}}(t)$, $N_{\mathrm{v}}(z_{\mathrm{LS}})$ decreases for *region B*.

The calculated result shows that the behavior of $N_{\mathrm{v}}(z_{\mathrm{LS}})$ for *region C* are caused by an increase in $N_{\mathrm{upper}}(z_{\mathrm{LS}})$ and the velocity dependence of $N_{\mathrm{lower}}(z_{\mathrm{LS}})$. An increase of $N_{\mathrm{upper}}(z_{\mathrm{LS}})$ and the velocity dependence of $N_{\mathrm{lower}}(z_{\mathrm{LS}})$ are discussed in the following two paragraphs.

First, an increase in $N_{\mathrm{upper}}(z_{\mathrm{LS}})$ for *region C* is explained by the excluded volume due to the large sphere. The position of the large sphere $z_{\mathrm{LS}}(t)$ decreases with the time t. In $z_{\mathrm{LS}}(t) = 3.5d_{\mathrm{LS}}$, the center of the large sphere passes through the upper area. Thus, the excluded volume in V_{upper} decreases with a decrease in $z_{\mathrm{LS}}(t)$ for $z_{\mathrm{LS}}(t) \leq 3.5d_{\mathrm{S}}$. Therefore, $N_{\mathrm{upper}}(z_{\mathrm{LS}})$ increases because of an increase in the available volume with a decrease in z_{LS}.

Next, the velocity dependence of $N_{\mathrm{lower}}(z_{\mathrm{LS}})$ can be interpreted by an increase in the trapped solvent particles in the vessel cavity. Since the front of the large sphere is located at the top surface of V_{lower} in $z_{\mathrm{LS}}(t) = 5d_{\mathrm{S}}$, the excluded volume in V_{lower} increases with a decrease in $z_{\mathrm{LS}}(t)$ for $d_{\mathrm{S}} < z_{\mathrm{LS}}(t) < 5d_{\mathrm{S}}$. At the low velocity of large sphere, the number $N_{\mathrm{lower}}(z_{\mathrm{LS}})$ decreases with a decrease in $z_{\mathrm{LS}}(t)$ by the solvent number due to an increase in the excluded volumes. When the large sphere moves more quickly than solvent particles, solvent particles can not escape from the vessel in spite of a decrease of the available volume. Thus, a decrease of $N_{\mathrm{lower}}(z_{\mathrm{LS}})$ with a decrease in $z_{\mathrm{LS}}(t)$ at the high velocity is smaller than that at the low velocity. By the above reason, the velocity dependence of $N_{\mathrm{lower}}(z_{\mathrm{LS}})$ can be interpreted by trapped solvent particles.

4.5 Grand Potential Functional

To discuss the effect of solvent particles on a moving solute particle, I calculate the difference of grand potential functional (DGPF) in the state at time t from initial state $\Delta\Omega[\rho(\boldsymbol{r},t)] \equiv \Omega[\rho(\boldsymbol{r},t)] - \Omega[\rho(\boldsymbol{r},t=0)]$ from Eq. (4.5). Here, $\rho(\boldsymbol{r},t=0)$ is number density of solvent particle in initial state.

In the equilibrium state, the configuration of the solute-vessel pair changes to the configuration in low grand potential of solvent particles from the configuration in high grand potential. Similarly, in the configuration, the low grand potential functional $\Omega[\rho(\boldsymbol{r},t)]$ is expected to be large probability that the large sphere can be inserted easily.

The DGPF $\Delta\Omega[\rho(\boldsymbol{r},t)]$ is given by the work from the initial state to the state at time t. To explain the relationship, I consider following three states.

1. initial state with Hamiltonian $\mathcal{H}$
   external potential $\Phi_{\mathrm{ext}}(\boldsymbol{r},t=0)$, virtual external potential $u(\boldsymbol{r}) = 0$,
   and number density $\rho(\boldsymbol{r},t=0)$

2. equilibrium state with $\mathcal{H} + \int \hat{\rho}(\boldsymbol{r})u(\boldsymbol{r})\mathrm{d}\boldsymbol{r}$
   external potential $\Phi_{\mathrm{ext}}(\boldsymbol{r},t)$, virtual external potential $u(\boldsymbol{r})$,
   and number density $\rho(\boldsymbol{r},t)$

3. nonequilibrium state with the Hamiltonian $\mathcal{H}$
   external potential $\Phi_{\rm ext}(\boldsymbol{r},t)$, virtual external potential $u(\boldsymbol{r})=0$,
   and number density $\rho(\boldsymbol{r},t)$

where $\mathcal{H}$ is defined by Eq. (2.1) and $\hat{\rho}(\boldsymbol{r})$ is the microscopic density. Using the density functional theory, I conclude that the DGPF $\Delta\Omega[\rho(\boldsymbol{r},t)]$ is equal to the sum of the minimum work from state 1 to 2 and the work from state 2 to 3. The proof of the relationship is started from

$$W=\int\int\rho(\boldsymbol{r})u(\boldsymbol{r},\lambda(t))\mathrm{d}\boldsymbol{r}\mathrm{d}\lambda(t), \tag{4.15}$$

where W is the work, $\lambda(t)$ is the degree of change of the virtual external potential $u(\boldsymbol{r},\lambda(t))$. The details of the deviation are shown in Appendix D.

4.5.1 Result for the Difference of the Grand Potential Functional

Figure 4.8 shows the DGPF $\Delta\Omega[\rho(\boldsymbol{r},t)]$. The DGPF $\Delta\Omega[\rho(\boldsymbol{r},t)]$ has some local minima and maxima with respect to $z_{\rm LS}(t)$. The position at the minima and maxima is the same for all the velocities of the large sphere. The value of $\Delta\Omega[\rho(\boldsymbol{r},t)]$ increases with the velocity of the large sphere. The discrepancy of $\Delta\Omega[\rho(\boldsymbol{r},t)]$ between the nonequilibrium and equilibrium state becomes large as the large sphere approaches to the bottom of the vessel. In addition, it dramatically increases at $z_{LS}(t)=3d_{\rm S}$.

4.5.2 Nonequilibrium part of Difference of Grand Potential Functional

I divide the DGPF $\Delta\Omega[\rho(\boldsymbol{r},t)]$ into an equilibrium part and a nonequilibrium part. The equilibrium part is defined by

$$\Delta\Omega^{\rm eq}[\rho_{\rm eq}^{z_{\rm LS}(t)}(\boldsymbol{r})]\equiv\Omega[\rho_{\rm eq}^{z_{\rm LS}(t)}(\boldsymbol{r})]-\Omega[\rho(\boldsymbol{r},t=0)]. \tag{4.16}$$

Here, $\rho_{\rm eq}^{z_{\rm LS}(t)}(\boldsymbol{r})$ is the number density distribution of solvent particles in equilibrium state when the large sphere is located at $z_{\rm LS}(t)$. $\rho(\boldsymbol{r},t=0)$ is the initial number density distribution in the equilibrium state. The nonequilibrium part is defined by $\Delta\Omega^{\rm neq}[\rho(\boldsymbol{r},t)]\equiv\Delta\Omega[\rho(\boldsymbol{r},t)]-\Delta\Omega^{\rm eq}[\rho_{\rm eq}^{z_{\rm LS}(t)}(\boldsymbol{r})]$. Thus, it is satisfied the relationship $\Delta\Omega[\rho(\boldsymbol{r},t)]=\Delta\Omega^{\rm eq}[\rho_{\rm eq}^{z_{\rm LS}(t)}(\boldsymbol{r})]+\Delta\Omega^{\rm neq}[\rho(\boldsymbol{r},t)]$. The nonequilibrium part $\Delta\Omega^{\rm neq}[\rho(\boldsymbol{r},t)]$ can be rewritten as

$$\Delta\Omega^{\rm neq}[\rho(\boldsymbol{r},t)]=\Omega[\rho(\boldsymbol{r},t)]-\Omega[\rho_{\rm eq}^{z_{\rm LS}(t)}(\boldsymbol{r})], \tag{4.17}$$

where $\rho(\boldsymbol{r},t)$ is nonequilibrium number density which is calculated by TDDFT [Eq. (4.4)]. The equilibrium part is shown in yellow filled circle of Fig. 4.8.

The nonequilibrium part of the DGPF is shown in Fig. 4.9. The nonequilibrium part increases with the velocity of the large sphere V_{LS}. In addition, it increases with the large sphere position $z_{\mathrm{LS}}(t)$ monotonically. According to yellow filled circle of Fig. 4.8, in contrast, the equilibrium part has the oscillation with respect to $z_{\mathrm{LS}}(t)$. Because of the monotonic increase of the nonequilibrium part, one can find that the oscillation of the DGPF $\Delta\Omega[\rho(\boldsymbol{r},t)]$ with respect to $z_{\mathrm{LS}}(t)$ is caused by the equilibrium part.

4.5.3 Dependence of the DGPF on Height of the Vessel

To clarify the origin of the dramatic increase in the DGPF $\Delta\Omega[\rho(\boldsymbol{r},t)]$, height of the vessel d_{H} is changed into $7d_{\mathrm{S}}$ from $6d_{\mathrm{S}}$. Figures 4.10 and 4.11 show the number of solvent particle inside the vessel $N_{\mathrm{v}}(z_{\mathrm{LS}})$ and the DGPF $\Delta\Omega[\rho(\boldsymbol{r},t)]$ for $d_{\mathrm{H}} = 7d_{\mathrm{S}}$. The values of $N_{\mathrm{v}}(z_{\mathrm{LS}})$ and $\Delta\Omega[\rho(\boldsymbol{r},t)]$ increase with the velocity of the large sphere. The number $N_{\mathrm{v}}(z_{\mathrm{LS}})$ has a large V_{LS}-dependence at $z_{\mathrm{LS}}(t) > 4d_{\mathrm{S}}$. The DGPF $\Delta\Omega[\rho(\boldsymbol{r},t)]$ also dramatically increases with V_{LS} at $z_{\mathrm{LS}}(t) = 4.0d_{\mathrm{S}}$. The position in which $N_{\mathrm{v}}(z_{\mathrm{LS}})$ largely depends on the velocity is the same at the position where $\Delta\Omega[\rho(\boldsymbol{r},t)]$ dramatically increases.

Both of $N_{\mathrm{v}}(z_{\mathrm{LS}})$ and $\Delta\Omega[\rho(\boldsymbol{r},t)]$ has a similar d_{H}-dependence. The value of $\Delta\Omega[\rho(\boldsymbol{r},t)]$ increases dramatically at $z_{\mathrm{LS}}(t) = 3.0d_{\mathrm{S}}$ for $d_{\mathrm{H}} = 6d_{\mathrm{S}}$ and at $z_{\mathrm{LS}}(t) = 4.0d_{\mathrm{S}}$ for $d_{\mathrm{H}} = 7d_{\mathrm{S}}$. In the same way, $N_{\mathrm{v}}(z_{\mathrm{LS}})$ has a large V_{LS}-dependence at $z_{\mathrm{LS}}(t) = 3.0d_{\mathrm{S}}$ for $d_{\mathrm{H}} = 6d_{\mathrm{S}}$ and at $z_{\mathrm{LS}}(t) = 4.0d_{\mathrm{S}}$ for $d_{\mathrm{H}} = 7d_{\mathrm{S}}$. Therefore, both of large V_{LS}-dependence in $N_{\mathrm{v}}(z_{\mathrm{LS}})$ and dramatic increase in $\Delta\Omega[\rho(\boldsymbol{r},t)]$ start when the center of the large sphere is located at the entrance of the vessel cavity. Thus, the origin of the dramatic increase in $\Delta\Omega[\rho(\boldsymbol{r},t)]$ is related to the large sphere position at the entrance of the vessel cavity.

4.5.4 Dependence of the DGPF on Inner Diameter of the Vessel

The large V_{LS}-dependence in $N_{\mathrm{v}}(z_{\mathrm{LS}})$ and dramatic increase of $\Delta\Omega[\rho(\boldsymbol{r},t)]$ start when the center of the large-sphere is located at the entrance of the vessel cavity. When the center of the large-sphere is at the entrance of the vessel cavity, the space between the large sphere and the sidewall of the vessel is small (d_{S}). To clarify the effect of the gap from the surface of a large sphere to sidewalls away for trapping of solvent particles in a vessel, DPGF is examined in various inner diameters of a vessel d_{I} ($9d_{\mathrm{S}}$ and $11d_{\mathrm{S}}$).

Figure. 4.12 shows the d_{I}-dependence of the DGPF $\Delta\Omega[\rho(\boldsymbol{r},t)]$. The profile of the DGPF for $d_{\mathrm{S}} \leq z_{\mathrm{LS}} < 3d_{\mathrm{S}}$ is considered because the increase in the DGPF with V_{LS} at $d_{\mathrm{I}} = 7d_{\mathrm{S}}$ is more significant in this bottom region of a vessel than in the other regions. In this region, when solvent particles are in the equilibrium state, $\Delta\Omega[\rho(\boldsymbol{r},t)]$ for $d_{\mathrm{I}} = 9d_{\mathrm{S}}$ is smaller than that for $d_{\mathrm{I}} = 11d_{\mathrm{S}}$ [Fig. 4.12-(a)]. As V_{LS} increases from zero, the DGPF for both values of d_{I} exhibits increases, which are more significant at $d_{\mathrm{I}} = 9d_{\mathrm{S}}$ than at $d_{\mathrm{I}} = 11d_{\mathrm{S}}$[Fig. 4.12-(b)]. According to those

results, the small gap from the surface of a large sphere to sidewalls enhances the magnitude of the DGPF for large values of V_{LS}.

4.5.5 Discussions

From the following results, one find that the DGPF $\Delta\Omega[\rho(\boldsymbol{r},\boldsymbol{t})]$ is correlated with the number of solvent particles inside of the vessel $N_{\mathrm{v}}(z_{\mathrm{LS}})$. Both of $\Delta\Omega[\rho(\boldsymbol{r},\boldsymbol{t})]$ and $N_{\mathrm{v}}(t)$ increases with the velocity of the large sphere V_{LS} in all the position of the large sphere $z_{\mathrm{LS}}(t)$. Both of the discrepancy of $\Delta\Omega[\rho(\boldsymbol{r},\boldsymbol{t})]$ and $N_{\mathrm{v}}(t)$ between the nonequilibrium and equilibrium state increases with a decrease of $z_{\mathrm{LS}}(t)$ in all V_{LS}. The value of $\Delta\Omega[\rho(\boldsymbol{r},t)]$ increases dramatically with V_{LS} at $z_{\mathrm{LS}}(t) = 3.0d_{\mathrm{S}}$ for $d_{\mathrm{H}} = 6d_{\mathrm{S}}$ and at $z_{\mathrm{LS}}(t) = 4.0d_{\mathrm{S}}$ for $d_{\mathrm{H}} = 7d_{\mathrm{S}}$. At the same $z_{\mathrm{LS}}(t)$ and d_{I}, $N_{\mathrm{v}}(t)$ increases dramatically with V_{LS}.

The DGPF is interpreted by the correlation with the number of solvent particles inside of the vessel $N_{\mathrm{v}}(t)$. Solvent particles inside the vessel should push back the large sphere. Thus, when the number of solvent particles is large inside the vessel, the large sphere is hard to be inserted into the vessel. The large number of solvent particles inside the vessel is correlated with the high DGPF. Therefore, in the high DGPF, the large sphere is hard to be inserted into the vessel. By the above, I propose that the DGPF represents the difficulty of the large-sphere insertion into the vessel.

To discuss nonequilibrium effects, significant increases in the DPGF (Fig. 4.8) are considered. The DPGF increases to $10k_{\mathrm{B}}T$ at $2d_{\mathrm{S}} < z_{\mathrm{LS}} < 3d_{\mathrm{S}}$ with $V_{\mathrm{LS}} \geq D_{\mathrm{S}}/(8d_{\mathrm{S}})$ and $d_{\mathrm{I}} = 7d_{\mathrm{S}}$, while not increasing at $d_{\mathrm{I}} = 9d_{\mathrm{S}}$ or $11d_{\mathrm{S}}$ (Fig. 4.12). The d_{I}-dependence of the DPGF is explained by a small gap between the vessel side wall and large sphere δ, where $\delta = d_{\mathrm{S}}$ at $d_{\mathrm{I}} = 7d_{\mathrm{S}}$ and $\delta > d_{\mathrm{S}}$ at $d_{\mathrm{I}} = 9d_{\mathrm{S}}$ and $11d_{\mathrm{S}}$. In addition, one can find $\delta = d_{\mathrm{S}}$ for $z_{\mathrm{LS}} < 3d_{\mathrm{S}}$ at $d_{\mathrm{H}} = 6d_{\mathrm{S}}$, by the geometric consideration for the vessel and large sphere, while $\delta = d_{\mathrm{S}}$ at $z_{\mathrm{LS}} < 4d_{\mathrm{S}}$ at $d_{\mathrm{H}} = 7d_{\mathrm{S}}$.

4.6 Summary

I have formulated a theoretical method for studying the dynamics of solvent particle around a moving solute particle. I have added the movement of solute particle to time dependent density functional theory (TDDFT) by changing the solvent-solute interaction with time. Applying the theory to the insertion of a large sphere into a cylindrical vessel immersed in solvent particles, the nonequilibrium density distribution of solvent particles around the moving solute particle and the vessel has been obtained.

The nonequilibrium state is characterized by the large number of solvent particles inside of the vessel. In particular, the number of solvent particles deviates from the equilibrium value in the bottom of the vessel largely. The discrepancy from the equilibrium value increases with the velocity of the large sphere. It increases as

the large sphere approaches to the vessel. In particular, the discrepancy increases dramatically when the large sphere is located at the entrance of the vessel cavity.

The behavior of the number of solvent particles inside the vessel $N_{\mathrm{v}}(z_{\mathrm{LS}})$ depends on the position of the large sphere $z_{\mathrm{LS}}(t)$ for $d_{\mathrm{I}} = 7d_{\mathrm{LS}}$, where d_{I} is the inner diameter of the vessel. When the large sphere is located outside the vessel, ($z_{\mathrm{LS}}(t) > 6d_{\mathrm{S}}$ for $d_{\mathrm{H}} = 6d_{\mathrm{S}}$ and $z_{\mathrm{LS}}(t) > 7d_{\mathrm{S}}$ for $d_{\mathrm{H}} = 7d_{\mathrm{S}}$), $N_{\mathrm{v}}(t)$ increases with a decrease of $z_{\mathrm{LS}}(t)$. It can be interpreted by the transport of solvent particles for the large sphere. When the front of the large sphere is inside of the vessel, ($3d_{\mathrm{S}} < z_{\mathrm{LS}}(t) < 6d_{\mathrm{S}}$ for $d_{\mathrm{H}} = 6d_{\mathrm{S}}$ and $4d_{\mathrm{S}} < z_{\mathrm{LS}}(t) < 7d_{\mathrm{S}}$ for $d_{\mathrm{H}} = 7d_{\mathrm{S}}$), $N_{\mathrm{v}}(t)$ decreases. It can be explained by the excluded volume of the large sphere.

When the center of the large sphere is inside the vessel, ($d_{\mathrm{S}} < z_{\mathrm{LS}}(t) < 3d_{\mathrm{S}}$ for $d_{\mathrm{H}} = 6d_{\mathrm{S}}$ and $d_{\mathrm{S}} < z_{\mathrm{LS}}(t) < 4d_{\mathrm{S}}$ for $d_{\mathrm{H}} = 7d_{\mathrm{S}}$), the z_{LS}-dependence of N_{v} largely depends on the velocity of the large sphere. At the low velocity, N_{v} decreases. It is explained by the excluded volume of the large sphere. At the high velocity, N_{v} increases. It is explained by the trapped solvent particles for the slow diffusion of solvent particles compared with the velocity of large sphere.

I have calculated the difference of the grand potential functional (DGPF) between the state at time t and the initial state. The calculated DGPF has some local minima and maxima with respect to the position of large sphere. This oscillation is caused by the equilibrium part of the DGPF. The DGPF increases with the velocity of the large sphere. It dramatically increases with the velocity when the large sphere is located at the entrance of the vessel ($z_{\mathrm{LS}}(t) = d_{\mathrm{S}}$ for $d_{\mathrm{H}} = 6d_{\mathrm{S}}$ and $z_{\mathrm{LS}}(t) = 4d_{\mathrm{S}}$ for $d_{\mathrm{H}} = 7d_{\mathrm{S}}$). The velocity dependence of the DGPF is caused by the nonequilibrium part. The nonequilibrium part of the DGPF increases with a decrease in a distance between the large sphere and the bottom of the vessel and a decrease in inner diameter of the vessel. Moreover, the DGPF is correlated with the number of solvent particles inside the vessel.

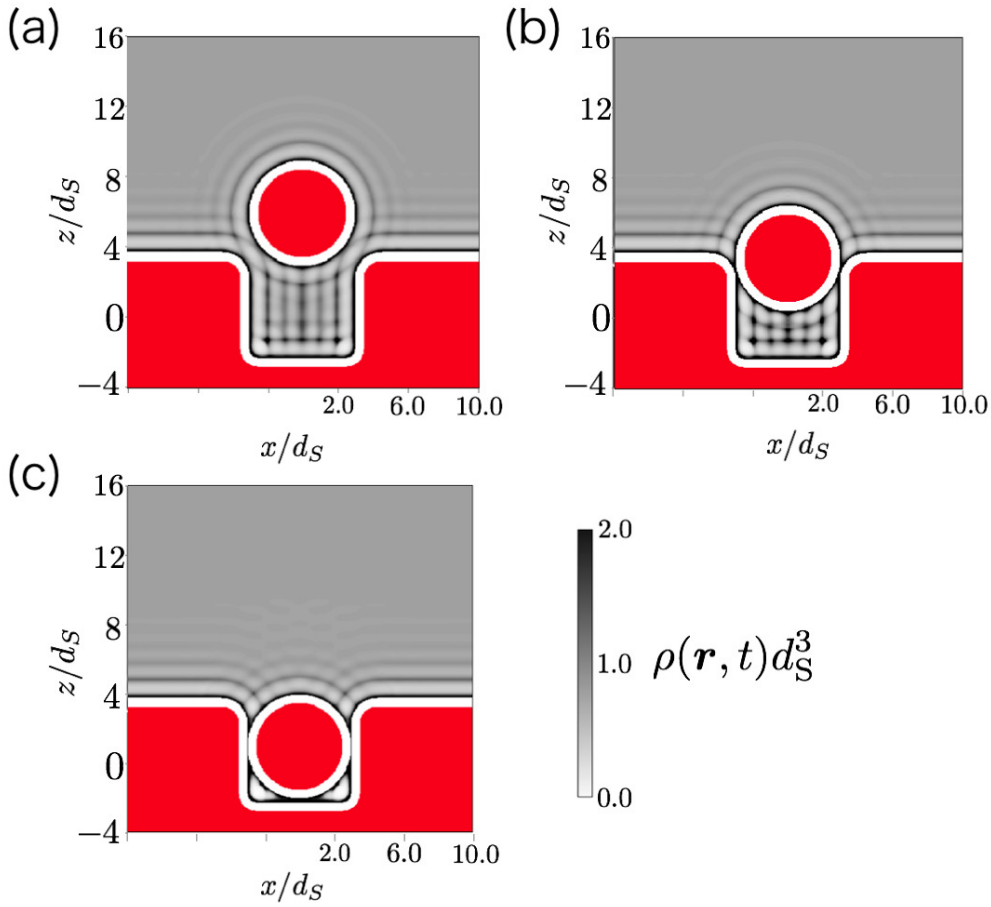

Figure 4.2: Spatial distributions of number density of solvent particles $\rho(\boldsymbol{r}, t)$ in the case of the large-sphere insertion into the vessel with a constant velocity $D_{\mathrm{S}}/2d_{\mathrm{S}}$. Here, d_{S} and D_{S} are the diameter and diffusion coefficient of the solvent particle, respectively. In the three counter maps, the center position of the large sphere $z_{\mathrm{LS}}(t)$ is given by (a) $6.2d_{\mathrm{S}}$, (b) $3.7d_{\mathrm{S}}$ and (c) $1.2d_{\mathrm{S}}$. Darker colors indicate higher number density. Values of $\rho(\boldsymbol{r}, t)d_{\mathrm{S}}^3$ larger than 2 are represented by the same color, indicating that the maximal value is larger than 2. The red area represents the large sphere and the vessel. The x-axis and z-axis are shown in Fig. 4.1.

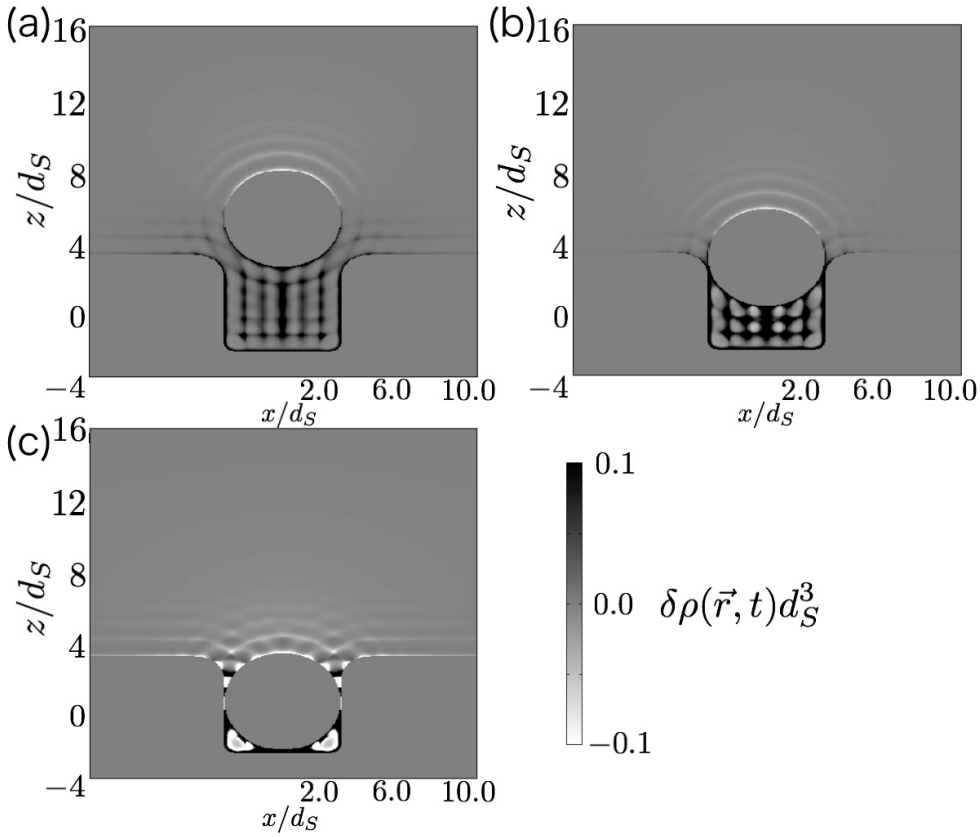

Figure 4.3: Differences in number density of solvent particles from that in the equilibrium state $\delta\rho(\boldsymbol{r},t) = \rho(\boldsymbol{r},t) - \rho_{\rm eq}^{z_{\rm LS}(t)}(\boldsymbol{r})$ in the case of the large-sphere insertion into the vessel at a constant velocity $D_{\rm S}/2d_{\rm S}$. Here, $\rho_{\rm eq}^{z_{\rm LS}(t)}(\boldsymbol{r})$ is number density of solvent particles in the equilibrium state when the center of the large sphere is set at $z_{\rm LS}(t)$. In the three counter maps, $z_{\rm LS}(t)$ is given by (a) $6.2d_{\rm S}$, (b) $3.7d_{\rm S}$, and (c) $1.2d_{\rm S}$. The difference $\delta\rho(\boldsymbol{r},t)$ becomes increasingly negative as the color approaches white and increasingly positive as the color approaches black. Values of $\delta\rho(\boldsymbol{r},t)d_{\rm S}^3$ larger than 0.1 are represented by the same color, indicating that the maximal value is larger than 0.1. Values of $\delta\rho(\boldsymbol{r},t)d_{\rm S}^3$ smaller than -0.1 are represented by the same color, indicating that the minimal value is smaller than -0.1. The symbols $D_{\rm S}$, $d_{\rm S}$, and $z_{\rm LS}$ and the axes are the same in Fig. 4.2.

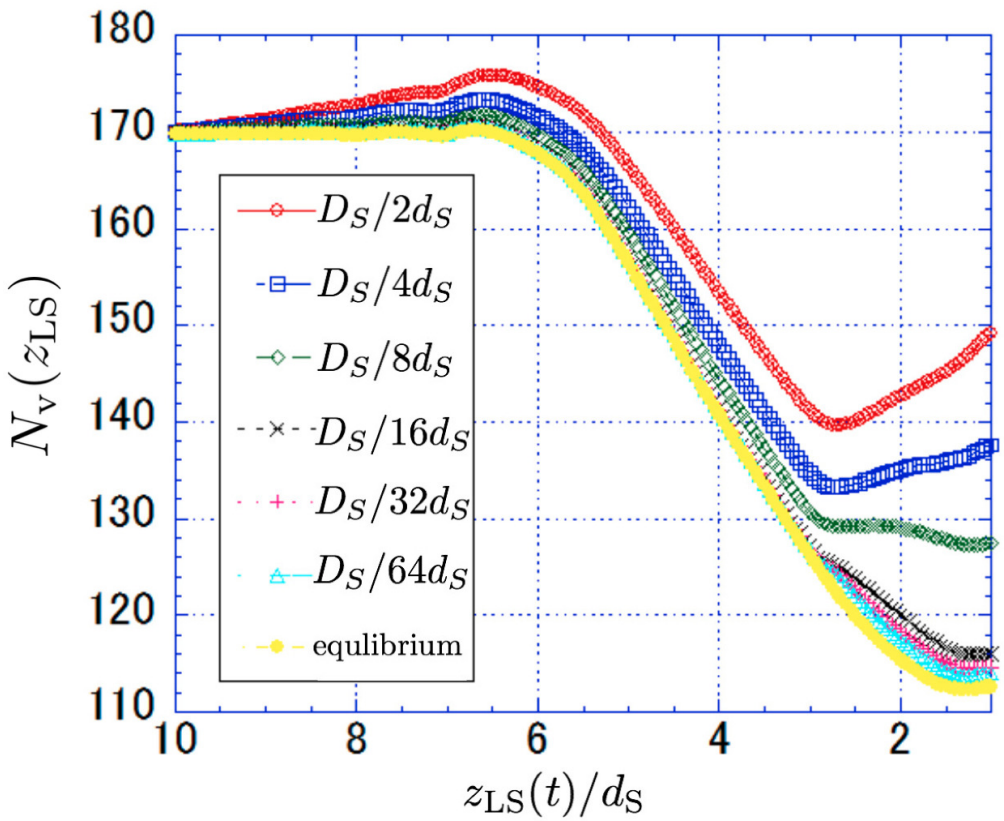

Figure 4.4: Total number of solvent particles inside of the vessel ($-2d_{\rm S} < z < 3.5d_{\rm S}$) $N_{\rm v}(z_{\rm LS})$ as the function of the center position of the large sphere $z_{\rm LS}(t)$. Here, $d_{\rm S}$ is the diameter of a solvent particle, $N_{\rm v}(z_{\rm LS})$ is defined by Eq. (4.12), and $z_{\rm LS}(t)$ satisfies in $z_{\rm LS}(t) = z_{\rm LS}(0) - V_{\rm LS}t$. The velocities of the large sphere $V_{\rm LS}$ are given by $D_{\rm S}/2d_{\rm S}$ (red open circle), $D_{\rm S}/4d_{\rm S}$ (blue open square), $D_{\rm S}/8d_{\rm S}$ (green open diamond), $D_{\rm S}/32d_{\rm S}$ (black cross symbol), $D_{\rm S}/48d_{\rm S}$ (pink plus symbol), and $D_{\rm S}/64d_{\rm S}$ (light blue open triangle). The yellow filled circle represents the total number in the equilibrium state. Here, $d_{\rm S}$ and $D_{\rm S}$ are the diameter and diffusion coefficient of a solvent particle, respectively. The value of $z_{\rm LS}(t)$ is that on the z-axis in Fig. 4.1.

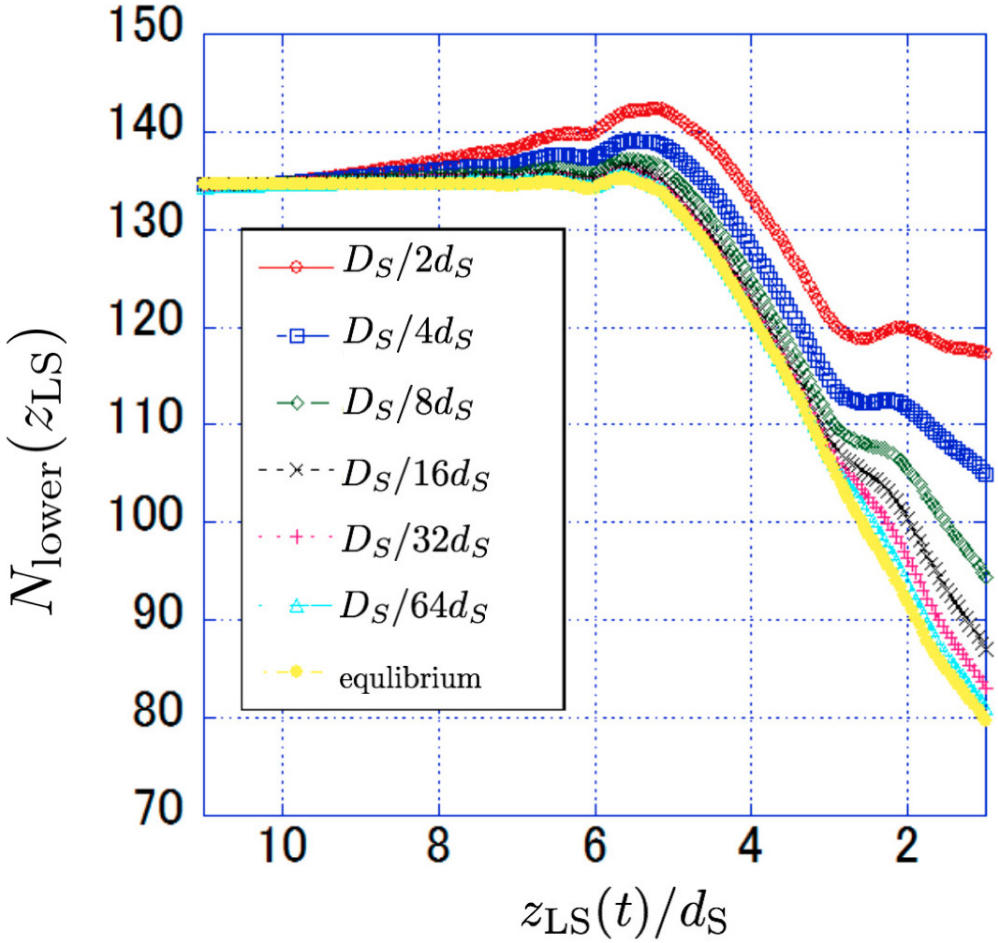

Figure 4.5: Number of solvent particles in the lower part of the vessel ($-2d_{\rm S} < z < 2.5d_{\rm S}$) $N_{\rm lower}(z_{\rm LS})$ as a function of the center position of the large sphere $z_{\rm LS}(t)$. Here, $d_{\rm S}$ is the diameter of a solvent particle, $N_{\rm lower}(z_{\rm LS})$ is defined by Eq. (4.12), $z_{\rm LS}(t)$ satisfies in $z_{\rm LS}(t) = z_{\rm LS}(0) - V_{\rm LS}t$, and $V_{\rm LS}$ is the velocities of the large sphere. The colors of the curves are the same as those in Fig. 4.4. The value of $z_{\rm LS}$ is that on the z-axis in Fig. 4.1.

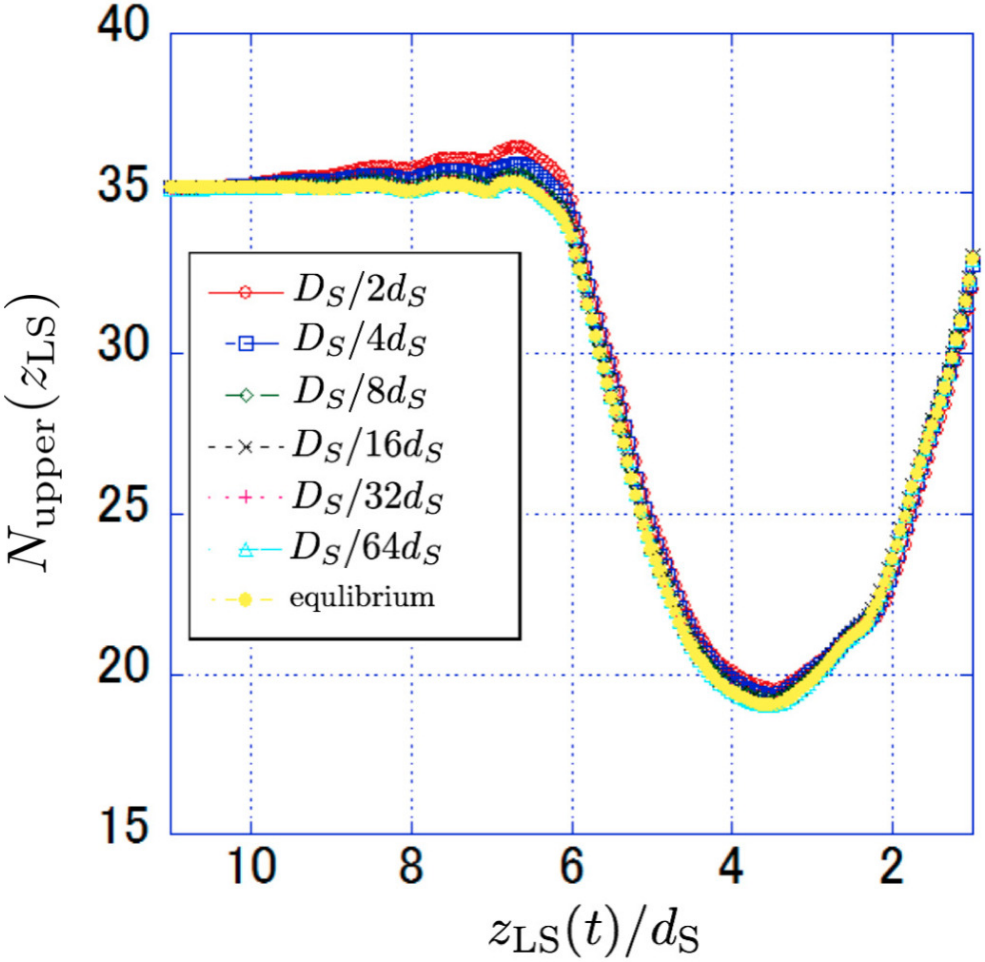

Figure 4.6: Number of solvent particles in the upper part of the vessel ($2.5d_{\rm S} < z < 3.5d_{\rm S}$) $N_{\rm upper}(z_{\rm LS})$ as a function of the center position of the large sphere $z_{\rm LS}(t)$. Here, $d_{\rm S}$ is the diameter of a solvent particle, $N_{\rm upper}(z_{\rm LS})$ is defined by Eq. (4.14), $z_{\rm LS}(t)$ satisfies in $z_{\rm LS}(t) = z_{\rm LS}(0) - V_{\rm LS}t$, and $V_{\rm LS}$ is the velocities of the large sphere. The colors of the curves are the same as those in Fig. 4.4. The value of $z_{\rm LS}(t)$ is that on the z-axis in Fig. 4.1.

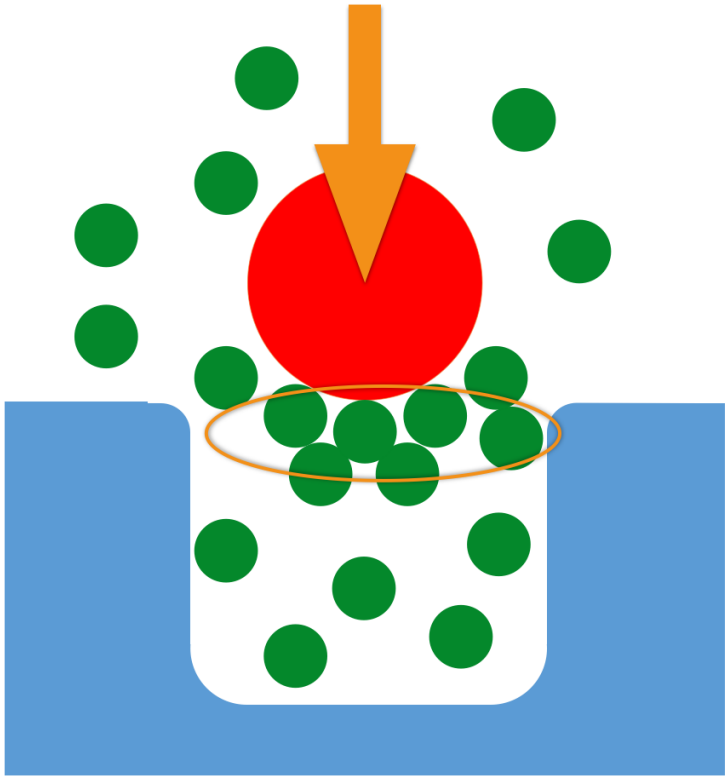

Figure 4.7: A drive of solvent particles by the large sphere. The yellow arrow represents the direction of the movement of the large sphere. The yellow circle represents the area where drove solvent particles are located.

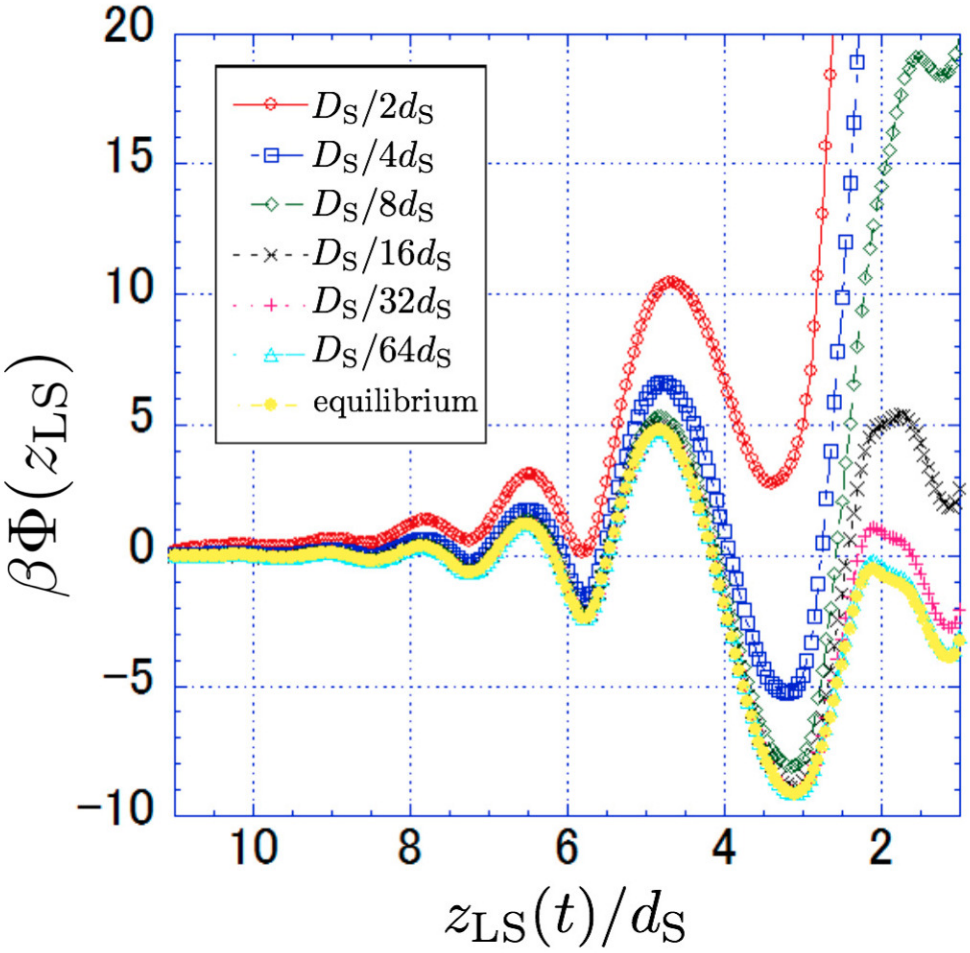

Figure 4.8: The difference of grand potential functional in the state at time t from the initial state $\Phi(z_{\rm LS})$. $\Phi(z_{\rm LS})$ is defined by $\Phi(z_{\rm LS}) \equiv \Delta\Omega[\rho(\boldsymbol{r},t)] \equiv \Omega[\rho(\boldsymbol{r},t)] - \Omega[\rho(\boldsymbol{r},t=0)]$. $z_{\rm LS}(t)$ is the position of large sphere, which moves from $z_{\rm LS}(0)$ (intial sate) to $z_{\rm LS}(t)$ with the constant velocity $V_{\rm LS}$. $V_{\rm LS}$ are given by $D_{\rm S}/2d_{\rm S}$ (red open circle), $D_{\rm S}/4d_{\rm S}$ (blue open square), $D_{\rm S}/8d_{\rm S}$ (green open diamond), $D_{\rm S}/32d_{\rm S}$ (black cross symbol), $D_{\rm S}/48d_{\rm S}$ (pink plus symbol), and $D_{\rm S}/64d_{\rm S}$ (light blue open triangle). The yellow filled circle represents the total number in the equilibrium state. Here, $d_{\rm S}$ and $D_{\rm S}$ are the diameter and diffusion coefficient of a solvent particle, respectively. The value of $z_{\rm LS}(t)$ is that on the z-axis in Fig. 4.1. The initial number density of solvent particles is set at the equilibrium density distribution.

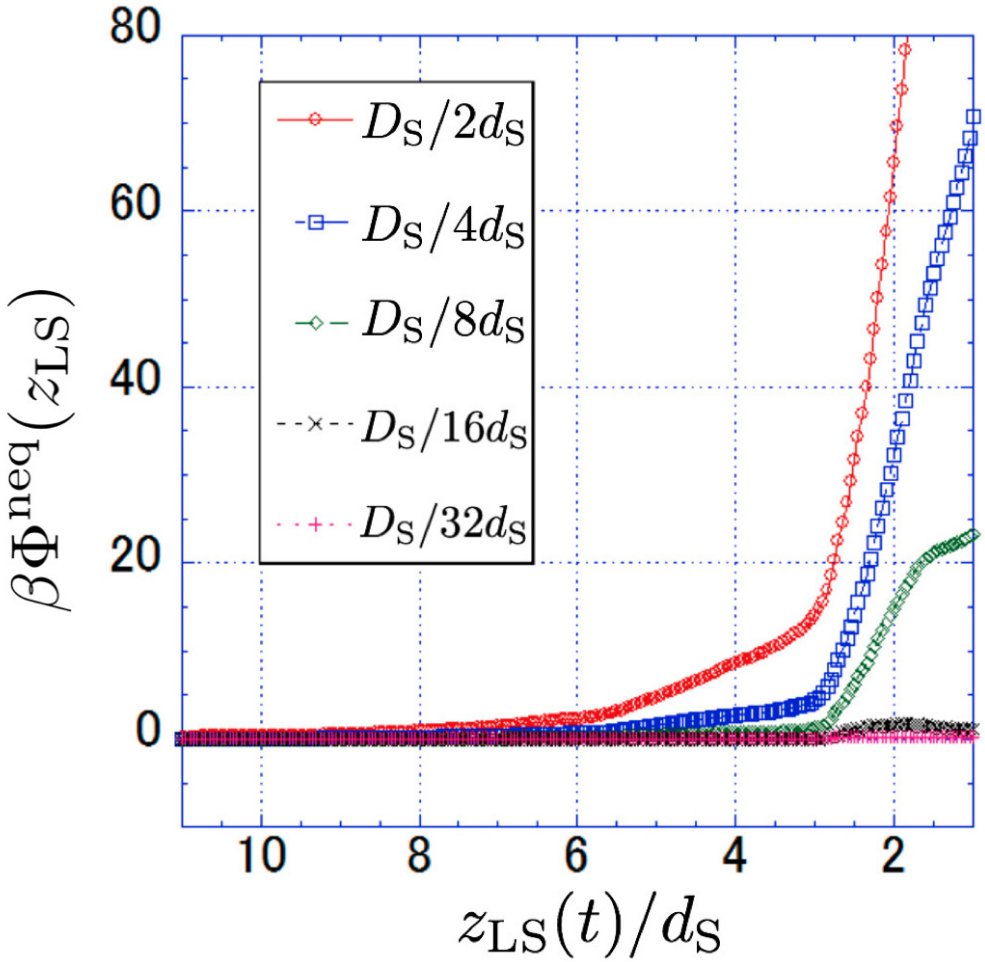

Figure 4.9: The nonequilibrium part of difference of grand potential functional $\Phi^{\mathrm{neq}}(z_{\mathrm{LS}})$. $\Phi^{\mathrm{neq}}(z_{\mathrm{LS}})$ is defined by $\Phi^{\mathrm{neq}}(z_{\mathrm{LS}}) \equiv \Delta\Omega^{\mathrm{neq}}[\rho(\boldsymbol{r},t)] = \Omega[\rho(\boldsymbol{r},t)] - \Omega[\rho_{\mathrm{eq}}^{z_{\mathrm{LS}}(t)}(\boldsymbol{r})]$. Here, $\rho(\boldsymbol{r},t)$ is the nonequilibrium number density distribution of solvent particles at time t and is calculated by TDDFT [Eq. (4.4)]. In addition, $\rho_{\mathrm{eq}}^{z_{\mathrm{LS}}(t)}(\boldsymbol{r})$ is the equilibrium number density distribution when the large sphere is located at $z_{\mathrm{LS}}(t)$. It is calculated by DFT [Eq. (4.11)]. The colors of the curves are the same as those in Fig. 4.4. Here, d_{S} and D_{S} are the diameter and diffusion coefficient of a solvent particle, respectively. The value of $z_{\mathrm{LS}}(t)$ is that on the z-axis in Fig. 4.1.

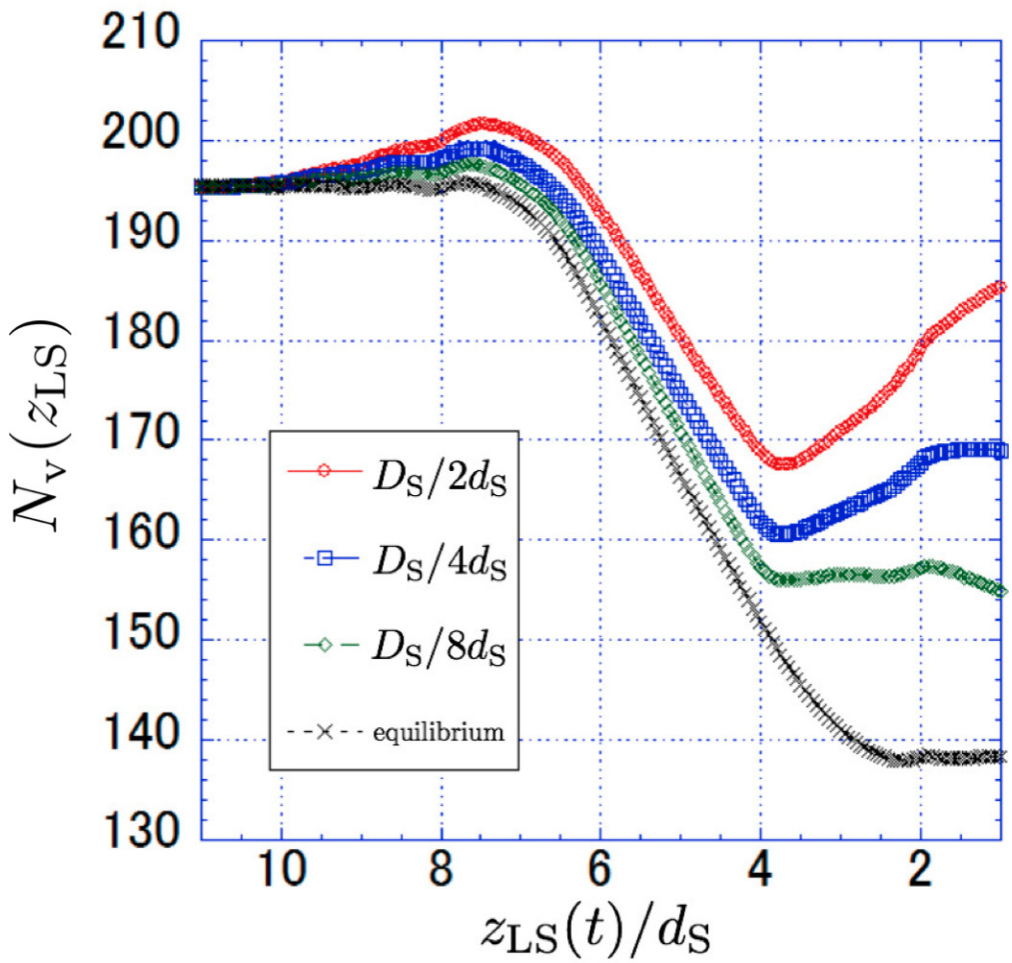

Figure 4.10: The number of solvent particle inside the vessel $N_{\rm v}(z_{\rm LS})$ for $d_{\rm H} = 7d_{\rm S}$. Here, $N_{\rm v}(z_{\rm LS})$ is obtained by the integration of the number density in the space of $-2d_{\rm S} \leq z \leq 4.5d_{\rm S}$. $z_{\rm LS}(t)$ is the position of large sphere, which moves from $z_{\rm LS}(0)$ (intial sate) to $z_{\rm LS}(t)$ with the constant velocity $V_{\rm LS}$. The velocity of the large sphere $V_{\rm LS}$ is given by $D_{\rm S}/2d_{\rm S}$ (red open circle), $D_{\rm S}/4d_{\rm S}$ (blue open square), $D_{\rm S}/8d_{\rm S}$ (green open diamond). The black cross symbol represents the value in equilibrium. Here, $d_{\rm S}$ and $D_{\rm S}$ are the diameter and diffusion coefficient of a solvent particle, respectively. The value of $z_{\rm LS}(t)$ is that on the z-axis in Fig. 4.1.

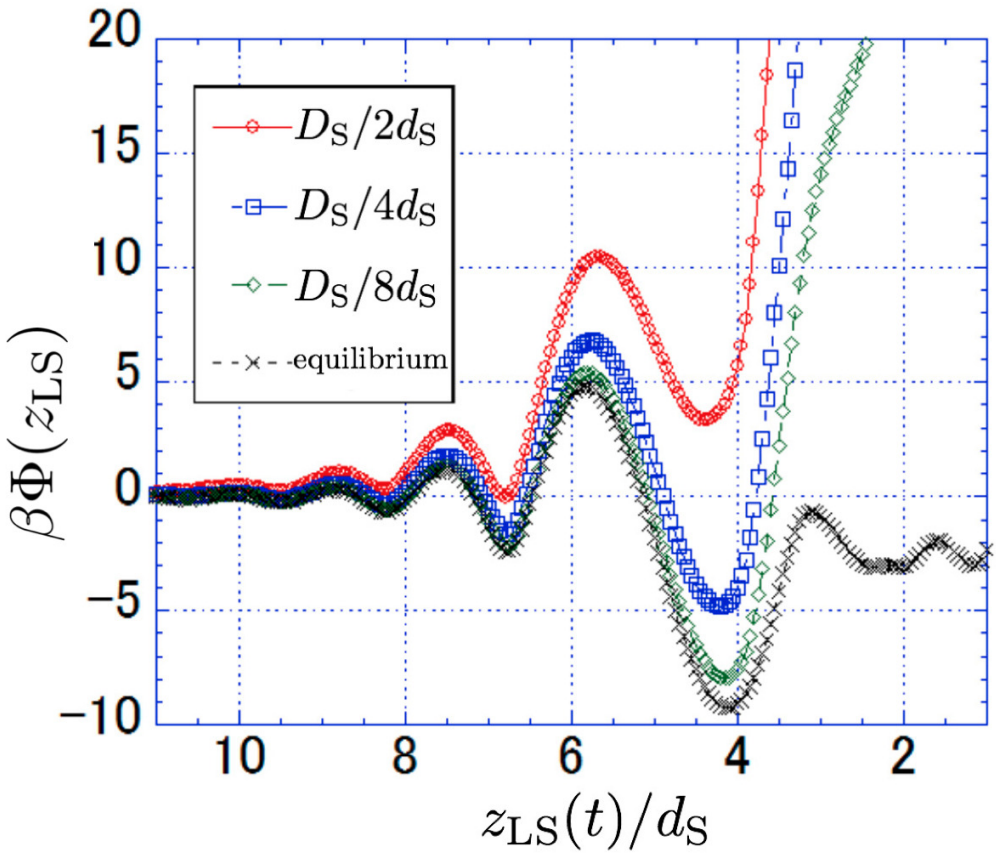

Figure 4.11: The difference of the grand potential functional $\Phi(z_{\rm LS})$ for $d_{\rm H} = 7d_{\rm S}$. Here, $\Phi(z_{\rm LS})$ is defined by $\Phi(z_{\rm LS}) \equiv \Delta\Omega[\rho(\boldsymbol{r},t)] \equiv \Omega[\rho(\boldsymbol{r},t)] - \Omega[\rho(\boldsymbol{r},t=0)]$. $z_{\rm LS}(t)$ is the position of large sphere, which moves from $z_{\rm LS}(0)$ (intial sate) to $z_{\rm LS}(t)$ with the constant velocity $V_{\rm LS}$. The velocity of the large sphere $V_{\rm LS}$ is given by $D_{\rm S}/2d_{\rm S}$ (red open circle), $D_{\rm S}/4d_{\rm S}$ (blue open square), $D_{\rm S}/8d_{\rm S}$ (green open diamond). The black cross symbol represents the value in equilibrium. Here, $d_{\rm S}$ and $D_{\rm S}$ are the diameter and diffusion coefficient of a solvent particle, respectively. The value of $z_{\rm LS}(t)$ is that on the z-axis in Fig. 4.1.

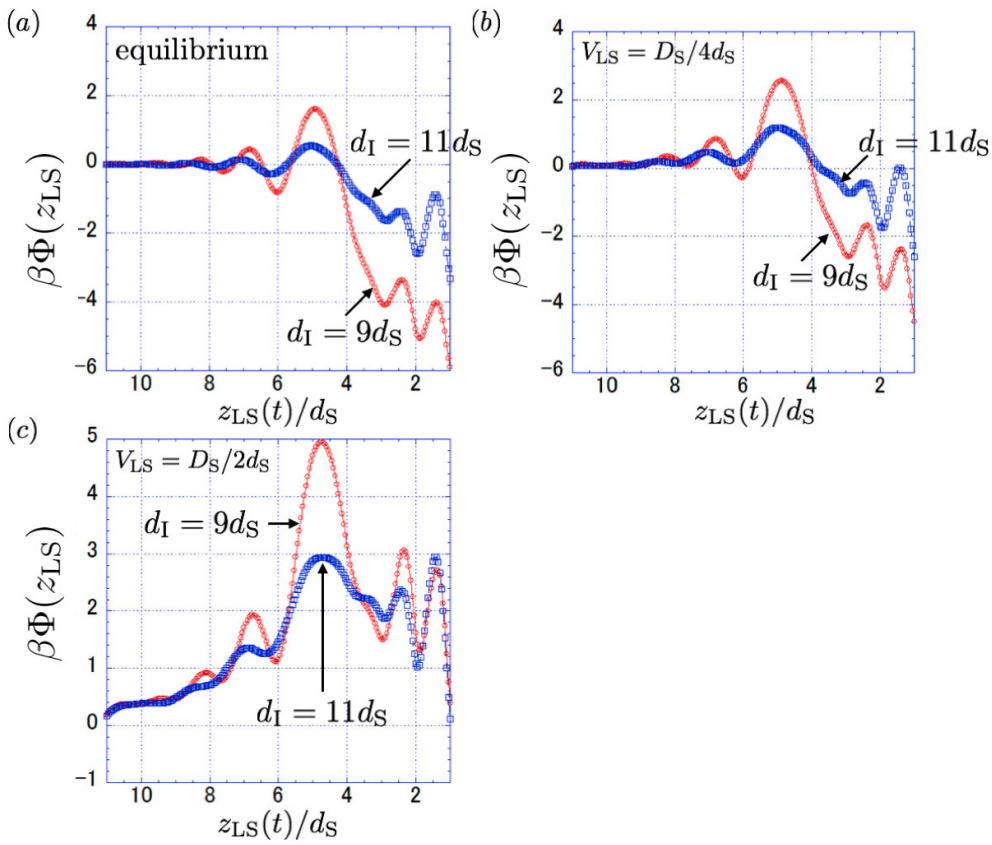

Figure 4.12: The difference of grand potential functional $\Phi(z_{\rm LS}) \equiv \Delta\Omega[\rho(\boldsymbol{r}, t)]$ for $d_{\rm I} = 9d_{\rm S}$ (red curve) and $d_{\rm I} = 11d_{\rm S}$ (blue curve): (a) equilibrium case, (b) $V_{\rm LS} = D_{\rm S}/4d_{\rm S}$, and (c) $V_{\rm LS} = D_{\rm S}/2d_{\rm S}$. Here, $d_{\rm S}$ and $D_{\rm S}$ are the diameter and diffusion coefficient of a solvent particle, respectively. The colors of the curves are the same as those in Fig. 4.4. The value of $z_{\rm LS}(t)$ is that on the z-axis in Fig. 4.1.

Chapter 5

Summary

In this thesis, two studies have been carried out to clarify the relationship between the dynamics of solute particle and the density distribution of solvent particle. First, I have studied the solute particle dynamics affected by the equilibrium density distribution of solvent particles. Secondly, I have studied the time development of solvent density distribution with given trajectories of a moving solute. The model in these studies is for the solute insertion process into a cylindrical vessel immersed in solvent particles.

(1) *The solute dynamics*
I have studied the solute insertion dynamics into the cylindrical vessel, assuming the equilibrium density distribution of solvent particles. To clarify the relationship between the dynamics of a solute and the equilibrium density distribution of solvent particles, the theoretical method has been formulated by using Fokker-Planck (FP) equation with the potential of mean force (PMF). The PMF represents the equilibrium effect of solvent particles. The calculated probability density of the large sphere is high in the center of the vessel cavity in the short time. After this time, the high probability is speared to the bottom and sidewall of the vessel. I have estimated the time when the large sphere is located in the center of the vessel cavity. It is obtained from the time when the position of highest probability density transits from the center of the vessel cavity to the bottom of the vessel cavity.

(2) *The solvent dynamics*
I have studied the dynamics of solvent particles with given a trajectory of a solute particle insertion into a cylindrical vessel with a constant velocity. To clarify the relationship between the velocity of a moving solute and time development of density distribution of solvent particle, the theoretical method has been formulated by using the time dependent density functional theory (TDDFT) which is incorporated with the movement of a solute particle. By using TDDFT, I have calculated the time development of the number density distribution of solvent particles numerically. The difference of the number density distribution between

nonequilibrium and equilibrium states is large inside the vessel. The number of solvent particles inside the vessel increases with the velocity of the large sphere. It has the large velocity-dependence when the center of large sphere is at the entrance of vessel. With the low velocity of the large sphere, the number of solvent particles decreases with the decrease of the distance between the solute and vessel. In contrast, at the high velocity, it increases with the decrease of the distance.

I also have calculated the difference of the grand potential functional (DGPF) between the state at time t and that at $t = 0$. The calculated DGPF increases with the velocity of the large sphere and a decrease in the inner diameter of the vessel. It has some local maxima and minima with respect to the large-sphere position. The positions of the local maxima and minima in nonequilibrium state are same as those in the equilibrium state.
The value of the DGPF at a position of the large sphere $z_{\mathrm{LS}}(t)$ for $d_{\mathrm{I}} = 6d_{\mathrm{S}}$ is roughly equal to that in the position $z_{\mathrm{LS}}(t) - d_{\mathrm{S}}$ for $d_{\mathrm{I}} = 7d_{\mathrm{S}}$.
The DGPF has the similar velocity, large-sphere position, and vessel-height dependence to those of the number of solvent particles inside of the vessel. Therefore, the DGPF is correlated to the number of solvent particles inside the vessel. When a lot of solvent particles is trapped at the inside of the vessel, the solute particle is hard to be inserted into the vessel due to the trapped solvent particle. By the above, I propose that the DGPF is correlated to the difficulty of the large-sphere insertion into the vessel. Besides, the DGPF is equivalent to the work from the initial state to the state at time t.

Appendix A

Ornstein Zernike Equation and Hyper-netted Chain Approximation

A.1 Ornstein Zernike Equation

The Ornstein Zernike (OZ) equation [10,32] is derived from the chain rule exactly, which is written as

$$\int \frac{\delta\beta u(\boldsymbol{r})}{\delta\rho(\boldsymbol{r}'')}\frac{\delta\rho(\boldsymbol{r}'')}{\delta\beta u(\boldsymbol{r}')}\mathrm{d}\boldsymbol{r}'' = \delta(\boldsymbol{r}-\boldsymbol{r}'). \tag{A.1}$$

Here, $\rho(\boldsymbol{r})$ is the number density and $u(\boldsymbol{r})$ is the virtual external field. In addition, $\beta = 1/(k_{\mathrm{B}}T)$ where k_{B} is Boltzmann's constant and T is the absolute temperature.

A functional derivative of $\beta u(\boldsymbol{r})$ is obtained from Eqs. (2.13) and (2.25) by

$$\frac{\delta\beta u(\boldsymbol{r})}{\delta\rho(\boldsymbol{r}')} = -\frac{\delta^2\Omega[\rho(\boldsymbol{r})]}{\delta\rho(\boldsymbol{r})\delta\rho(\boldsymbol{r}')} = -\frac{\delta(\boldsymbol{r}'-\boldsymbol{r})}{\rho(\boldsymbol{r})} + c(\boldsymbol{r},\boldsymbol{r}'). \tag{A.2}$$

Here, the relation $\delta\rho(\boldsymbol{r})/\delta\rho(\boldsymbol{r}') = \delta(\boldsymbol{r}-\boldsymbol{r}')$ is used. In addition, $c(\boldsymbol{r},\boldsymbol{r}')$ is the direct correlation function, which is defined by Eq. (2.24).

To obtain $\delta\rho(\boldsymbol{r}'')/\delta\beta u(\boldsymbol{r}')$, the starting point is

$$\rho(\boldsymbol{r}) \equiv \frac{1}{\Xi}\sum_{N=1}^{\infty}\frac{e^{N\beta\mu}}{N!h^{3N}}\int \hat{\rho}(\boldsymbol{r})\exp\left[-\beta\left\{\mathcal{H}(\boldsymbol{r}^N,\boldsymbol{p}^N) + \int \hat{\rho}(\boldsymbol{r}')u(\boldsymbol{r}')\mathrm{d}\boldsymbol{r}'\right\}\right]\mathrm{d}\boldsymbol{r}^N\mathrm{d}\boldsymbol{p}^N, \tag{A.3}$$

where

$$\Xi \equiv \sum_{N=1}^{\infty}\frac{e^{N\beta\mu}}{N!h^{3N}}\int \exp\left[-\beta\left\{\mathcal{H}(\boldsymbol{r}^N,\boldsymbol{p}^N) + \int \hat{\rho}(\boldsymbol{r}')u(\boldsymbol{r}')\mathrm{d}\boldsymbol{r}'\right\}\right]\mathrm{d}\boldsymbol{r}^N\mathrm{d}\boldsymbol{p}^N. \tag{A.4}$$

Here, $\mathcal{H}(\boldsymbol{r}^N,\boldsymbol{p}^N)$ is the Hamiltonian, where $\boldsymbol{r}^N$ and $\boldsymbol{p}^N$ are the $3N$ coordinates and $3N$ momenta of particles. In addition, h is Planck's constant, μ is the chemical

potential, and $\hat{\rho}(\boldsymbol{r}) \equiv \sum_{i=1}^{N} \delta(\boldsymbol{r} - \boldsymbol{r}_i)$. A functional derivative of $\rho(\boldsymbol{r})$ is given in straightforward way by

$$\frac{\delta\rho(\boldsymbol{r})}{\delta\beta u(\boldsymbol{r})} = -\rho(\boldsymbol{r})\rho(\boldsymbol{r}')h(\boldsymbol{r},\boldsymbol{r}') - \rho(\boldsymbol{r})\delta(\boldsymbol{r} - \boldsymbol{r}'), \tag{A.5}$$

where $h(\boldsymbol{r},\boldsymbol{r}') \equiv (\langle\hat{\rho}(\boldsymbol{r})\hat{\rho}(\boldsymbol{r}')\rangle - \langle\hat{\rho}(\boldsymbol{r})\rangle\langle\hat{\rho}(\boldsymbol{r})\rangle)/(\langle\hat{\rho}(\boldsymbol{r})\rangle\langle\hat{\rho}(\boldsymbol{r})\rangle)$ is the pair correlation function.

Insertion of Eqs. (A.2) and (A.5) into Eq. (A.1) yields the OZ equation, which is written by

$$h(\boldsymbol{r},\boldsymbol{r}') = c(\boldsymbol{r},\boldsymbol{r}') + \int c(\boldsymbol{r},\boldsymbol{r}'')\rho(\boldsymbol{r}'')h(\boldsymbol{r}'',\boldsymbol{r}')\mathrm{d}\boldsymbol{r}''. \tag{A.6}$$

Since the homogeneous system has the radial symmetry, the OZ equation in the homogeneous system can be written as

$$h(r) = c(r) + \rho_0 \int c(|\boldsymbol{r}' - \boldsymbol{r}|)h(r')\mathrm{d}\boldsymbol{r}'. \tag{A.7}$$

Here, ρ_0 is the average number density and $r = |\boldsymbol{r}|$.

A.2 Percus's Method

In the Percus's method, two systems are considered [10, 45]. One is the homogeneous systems. The other is the system in the presence of the external field corresponding to the interactions $\Phi_{\mathrm{ext}}(\boldsymbol{r}) = v(\boldsymbol{r})$. The system in the presence of $\Phi_{\mathrm{ext}}(\boldsymbol{r}) = v(\boldsymbol{r})$ means that the particle labeled $N+1$ is fixed at $\boldsymbol{r} = \boldsymbol{r}_{N+1}$. The sum of the interactions $V_N(\boldsymbol{r}^N)$ and the external field $\Phi_{\mathrm{ext},N}(\boldsymbol{r}^N)$ is

$$V_N(\boldsymbol{r}^N) + \Phi_{\mathrm{ext},N}(\boldsymbol{r}^N) = \sum_{j>i}^{N}\sum_{i=1}^{N} v(\boldsymbol{r}_{i,j}) + \sum_{i=1}^{N} v(\boldsymbol{r}_{i,N+1}) = V_{N+1}(\boldsymbol{r}^{N+1}), \tag{A.8}$$

where $\boldsymbol{r}_{i,j} = \boldsymbol{r}_i - \boldsymbol{r}_j$. Therefore, the system consisting of N particles in the presence of the external field, which corresponds to the interactions, is connected with the system consisting of $N+1$ particles in the absence of the external field.

The density distribution in the presence of external filed $\rho(\boldsymbol{r}|\phi)$ can be written

by

$$
\begin{aligned}
\rho(\boldsymbol{r}|\phi) &\equiv \left\langle \sum_{i=1}^{N} \delta(\boldsymbol{r}-\boldsymbol{r}_i) \right\rangle_{\phi} \\
&= \frac{1}{\Xi_\phi} \sum_{i=1}^{\infty} \frac{z^N}{(N-1)!} \int \exp\{-\beta(V_N + \Phi_{\mathrm{ext},N})\} \mathrm{d}\boldsymbol{r}^{N-1} \\
&= \frac{1}{\Xi_\phi} \sum_{i=1}^{\infty} \frac{z^N}{(N-1)!} \int \exp\{-\beta V_{N+1}\} \mathrm{d}\boldsymbol{r}^{N-1} \\
&= \frac{\Xi_0}{z\Xi_\phi \Xi_0} \sum_{i=1}^{\infty} \frac{z^N}{(N-2)!} \int \exp\{-\beta V_N\} \mathrm{d}\boldsymbol{r}^{N-2} \\
&= \frac{\Xi_0}{z\Xi_\phi} \left\langle \sum_{j\neq i}^{N} \sum_{i=1}^{N} \delta(\boldsymbol{r}-\boldsymbol{r}_i)\delta(\boldsymbol{r}-\boldsymbol{r}_j) \right\rangle_0 \\
&= \frac{\Xi_0}{z\Xi_\phi} \langle \hat{\rho}(\boldsymbol{r})\hat{\rho}(\boldsymbol{r}') \rangle_0 \,, \qquad \text{(A.9)}
\end{aligned}
$$

where $z \equiv e^{\beta\mu}/\lambda^3$, $\langle ... \rangle_\phi$ is the ensemble average in the presence of the external filed, and $\langle ... \rangle_0$ is the ensemble average in the homogeneous system. By this equation, the system in the presence of the external field is related to the homogeneous system. By the similar way, The grand partial function Ξ_ϕ is also related to the homogeneous system, $z\Xi_\phi = \langle \hat{\rho}(\boldsymbol{r}) \rangle_0 \Xi_0$.

Let us define the pair distribution function in the homogeneous system $g(\boldsymbol{r})$ and the single particle density in the homogeneous system ρ_0 by

$$
g(\boldsymbol{r}) = \frac{\langle \hat{\rho}(\boldsymbol{r})\hat{\rho}(\boldsymbol{r}') \rangle_0}{\langle \hat{\rho}(\boldsymbol{r}) \rangle_0 \langle \hat{\rho}(\boldsymbol{r}) \rangle_0} \qquad \text{(A.10)}
$$

and

$$
\rho_0 = \langle \hat{\rho}(\boldsymbol{r}) \rangle_0, \qquad \text{(A.11)}
$$

respectively. Using these definitions and $z\Xi_\phi = \langle \hat{\rho}(\boldsymbol{r}) \rangle_0 \Xi_0$, the single-particle number density in the presence of the external field [Eq. (A.9)] is related to $g(\boldsymbol{r})$,

$$
\rho(\boldsymbol{r}|\phi) = \rho_0 g(\boldsymbol{r}). \qquad \text{(A.12)}
$$

The idea that the system in the presence of $\Phi_{\mathrm{ext}}(\boldsymbol{r}) = v(\boldsymbol{r})$ is connected with the $N+1$ system is called Purcus's method.

A.3 Hyper-netted Chain (HNC) Approximation

The HNC approximation [34–36] can be derived by the combination of the DFT, RY approximation and Percus's method [10]. Insertion of Eqs. (A.12) and $\Phi_{\mathrm{ext}}(\boldsymbol{r}) =$

$v(\boldsymbol{r})$ into Eq. (2.26) derived by DFT and RY approximation yields the HNC approximation,

$$g(r) = \exp\left\{-\beta v(r) + \rho_0 \int c_{0,\mathrm{SS}}(|\boldsymbol{r}' - \boldsymbol{r}|)h(r')\mathrm{d}\boldsymbol{r}'\right\}. \tag{A.13}$$

The combination of OZ equation [Eq. (A.7)] and HNC approximation [Eq. (A.13)] gives the pair correlation function $h(r)$ and the direct correlation function $c_{0,\mathrm{SS}}(|\boldsymbol{r}' - \boldsymbol{r}|)$.

Appendix B

Morita-Hiroike Formula

The Morita-Hiroike formula is the expression of the chemical potential of an arbitrary shaped particle (e.g. protein). The chemical potential of an arbitrary shaped particle μ is defined by

$$\mu \equiv \Omega[\rho(\boldsymbol{r}), \Phi_{\mathrm{ext}}(\boldsymbol{r})] - \Omega_0, \tag{B.1}$$

where $\Omega[\rho(\boldsymbol{r}), \Phi_{\mathrm{ext}}(\boldsymbol{r})]$ is the grand potential functional which is defined by Eq. (2.11). In addition, Ω_0 is the grand potential functional in the homogeneous system, $\Phi_{\mathrm{ext}}(\boldsymbol{r})$ is the interaction between the arbitrary shaped particle and solvent particle, and $\rho(\boldsymbol{r})$ is the number density distribution around the arbitrary shaped particle.

Using the Ramakrishnan-Yussouff (RY) approximation [Eq. (2.25)], the chemical potential can be rewritten by

$$\begin{aligned}
\mu &\equiv \Omega[\rho(\boldsymbol{r}), \Phi_{\mathrm{ext}}(\boldsymbol{r})] - \Omega_0 \\
&= \int \rho(\boldsymbol{r}) \ln[\rho(\boldsymbol{r})/\rho_0] \mathrm{d}\boldsymbol{r} \\
&\quad + \int \beta \Phi_{\mathrm{ext}}(\boldsymbol{r}) \rho(\boldsymbol{r}) \mathrm{d}\boldsymbol{r} - \int \Delta\rho(\boldsymbol{r}) \mathrm{d}\boldsymbol{r} \\
&\quad - \frac{1}{2} \int \int c_{0,\mathrm{SS}}(|\boldsymbol{r}' - \boldsymbol{r}|) \Delta\rho(\boldsymbol{r}) \Delta\rho(\boldsymbol{r}') \mathrm{d}\boldsymbol{r} \mathrm{d}\boldsymbol{r}'.
\end{aligned} \tag{B.2}$$

Here, $\Delta\rho(\boldsymbol{r}) = \rho(\boldsymbol{r}) - \rho_0$, where ρ_0 is the average number density. In addition, $c_{0,\mathrm{SS}}(|\boldsymbol{r}' - \boldsymbol{r}|)$ is the direct correlation function in the homogeneous system. It is defined by Eq. (2.24).

Using the combination of the density functional theory and RY approximation [Eq. (2.26)]

$$\rho(\boldsymbol{r})/\rho_0 = \exp\left\{ -\beta \Phi_{\mathrm{ext}}(\boldsymbol{r}) + \int c_{0,\mathrm{SS}}(|\boldsymbol{r}' - \boldsymbol{r}|) \Delta\rho(\boldsymbol{r}) \mathrm{d}\boldsymbol{r}' \right\}, \tag{B.3}$$

the chemical potential can be rewritten by

$$\begin{aligned}
\mu &\equiv \Omega[\rho(\boldsymbol{r}), \Phi_{\rm ext}(\boldsymbol{r})] - \Omega_0 \\
&= \int\int c_{0,\rm SS}(|\boldsymbol{r}' - \boldsymbol{r}|)\rho(\boldsymbol{r})\Delta\rho(\boldsymbol{r}')\mathrm{d}\boldsymbol{r}\mathrm{d}\boldsymbol{r}' - \int \Delta\rho(\boldsymbol{r})\mathrm{d}\boldsymbol{r} \\
&\quad -\frac{1}{2}\int\int c_{0,\rm SS}(|\boldsymbol{r}' - \boldsymbol{r}|)\Delta\rho(\boldsymbol{r})\Delta\rho(\boldsymbol{r}')\mathrm{d}\boldsymbol{r}\mathrm{d}\boldsymbol{r}' \\
&= \rho_0\int\int c_{0,\rm SS}(|\boldsymbol{r}' - \boldsymbol{r}|)\Delta\rho(\boldsymbol{r}')\mathrm{d}\boldsymbol{r}\mathrm{d}\boldsymbol{r}' - \int \Delta\rho(\boldsymbol{r})\mathrm{d}\boldsymbol{r} \\
&\quad +\frac{1}{2}\int\int c_{0,\rm SS}(|\boldsymbol{r}' - \boldsymbol{r}|)\Delta\rho(\boldsymbol{r})\Delta\rho(\boldsymbol{r}')\mathrm{d}\boldsymbol{r}\mathrm{d}\boldsymbol{r}'. \qquad \text{(B.4)}
\end{aligned}$$

Moreover, let us consider the Percus's method. In appendix A.2, the external filed corresponding to the interactions $\Phi_{\rm ext}(\boldsymbol{r}) = v(\boldsymbol{r})$ is considered. In this chapter, the external filed $\Phi_{\rm ext}(\boldsymbol{r})$ represents the interaction between the arbitrary shaped particle and solvent particle, while it represents the interaction between solvent particles in appendix A.2. Therefore, one can find the relationship between the density distribution in the presence of the external field $\rho(\boldsymbol{r})$ and the pair distribution function between an arbitrary shaped particle and solvent particle $g_{\rm P,S}(\boldsymbol{r})$, which is written as

$$\rho(\boldsymbol{r}) = \rho_0 g_{\rm P,S}(\boldsymbol{r}). \qquad \text{(B.5)}$$

Since the pair correlation function between an arbitrary shaped particle and solvent particle is defined by $h_{\rm P,S}(\boldsymbol{r}) \equiv g_{\rm P,S}(\boldsymbol{r}) - 1$, one can obtain

$$\Delta\rho(\boldsymbol{r}) = \rho_0 h_{\rm P,S}(\boldsymbol{r}). \qquad \text{(B.6)}$$

By using this equation, the chemical potential can be rewritten by

$$\begin{aligned}
\mu &= \rho_0^2\int\int c_{0,\rm SS}(|\boldsymbol{r}' - \boldsymbol{r}|)h_{\rm P,S}(\boldsymbol{r}')\mathrm{d}\boldsymbol{r}\mathrm{d}\boldsymbol{r}' - \rho_0\int h_{\rm P,S}(\boldsymbol{r})\mathrm{d}\boldsymbol{r} \\
&\quad +\frac{\rho_0^2}{2}\int\int c_{0,\rm SS}(|\boldsymbol{r}' - \boldsymbol{r}|)h_{\rm P,S}(\boldsymbol{r})h_{\rm P,S}(\boldsymbol{r}')\mathrm{d}\boldsymbol{r}\mathrm{d}\boldsymbol{r}'. \qquad \text{(B.7)}
\end{aligned}$$

The Ornstein Zernike (OZ) equation for an arbitrary shaped particle and solvent particle is

$$h_{P,S}(\boldsymbol{r}) = c_{P,S}(\boldsymbol{r}) + \sum_{\gamma=\rm P,S}\rho_\gamma\int c_{\rm S,\gamma}(\boldsymbol{r}' - \boldsymbol{r})h_{\rm P,\gamma}(\boldsymbol{r}')\mathrm{d}\boldsymbol{r}', \qquad \text{(B.8)}$$

where, $c_{\rm P,S}(\boldsymbol{r})$ is the direct correlation function between an arbitrary shaped particle and solvent particle. Under the assumption of $\rho_S >> \rho_P$, one can obtain

$$h_{P,S}(\boldsymbol{r}) = c_{P,S}(\boldsymbol{r}) + \rho_{\rm S}\int c_{\rm S,S}(\boldsymbol{r}' - \boldsymbol{r})h_{\rm P,S}(\boldsymbol{r}')\mathrm{d}\boldsymbol{r}'. \qquad \text{(B.9)}$$

Here, ρ_S is the number density of solvent particles. In the dilution limit of the arbitrary shaped particle, one can find the relation $\rho_S = \rho_0$ and $c_{\rm S,S}(\boldsymbol{r}' - \boldsymbol{r}) =$

$c_{0,\mathrm{SS}}(\boldsymbol{r}' - \boldsymbol{r})$. By these equations, Eqs. (B.9), and (B.7), the chemical potential is written as

$$\mu = \rho_0 \int \left[\frac{1}{2} \{ h_{\mathrm{P,S}}(\boldsymbol{r}) \}^2 - \frac{1}{2} h_{\mathrm{P,S}}(\boldsymbol{r}) c_{\mathrm{P,S}}(\boldsymbol{r}) - c_{\mathrm{P,S}}(\boldsymbol{r}) \mathrm{d}\boldsymbol{r} \right]. \tag{B.10}$$

It is called Morita-Hiroike formula.

Appendix C

Special Treatment of Number Density of Solvent Particles for the Hard-body Model

Around the large sphere, the number density of solvent particles is treated specially in order to avoid the overlap between the large sphere and solvent particles due to the discretization of time. In our algorithm, the overlapped solvent particles are removed and the number of overlapped solvent particles is added to the surface of the bottom side of the large sphere (Fig. C.1).

First, the overlapped solvent particles are removed in two regions.

1. $|\boldsymbol{r} - \boldsymbol{r}_{\mathrm{LS}}(t+\Delta t)| \leq 3d_{\mathrm{S}}$
2. $(x - x_{\mathrm{LS}})^2 + (y - y_{\mathrm{LS}})^2 \leq 9d_{\mathrm{S}}^2$ and $z_{\mathrm{LS}}(t) < z < z_{\mathrm{LS}}(t+\Delta t)$

Here, $\boldsymbol{r}_{\mathrm{LS}}(t) = (x_{\mathrm{LS}}, y_{\mathrm{LS}}, z_{\mathrm{LS}}(t))$, Δt and d_{S} are the position of the large sphere, time interval, and diameter of the solvent particles, respectively. The region 1 is represented by the gray circle in Fig C.1-(a). The region 2 is represented by the gray square in Fig C.1-(b). In these regions, I set $\rho(\boldsymbol{r}, t)$ at zero.

Next, the overlapped solvent particles are added on the surface of the bottom side $z \leq z_{\mathrm{LS}}(t+\Delta t)$ of the large sphere. Thus, the number density $\rho(\boldsymbol{r}, t+\Delta t)$ is given by

$$\rho(\boldsymbol{r}, t+\Delta t) = \tilde{\rho}(\boldsymbol{r}, t+\Delta t) + \int_{z_{\mathrm{sur,LS}}(x,y,t)}^{z_{\mathrm{sur,LS}}(x,y,t+\Delta t)} \rho_{\mathrm{S}}(x, y, Z, t)\mathrm{d}Z, \tag{C.1}$$

where, $\tilde{\rho}(\boldsymbol{r}, t+\Delta t)$ is calculated by Eq. (4.4). In addition, $z_{\mathrm{sur,LS}}(x, y, t) = z_{\mathrm{LS}}(t) - \sqrt{9d_{\mathrm{S}}^2 - (x^2 + y^2)}$ is the position on the surface of the large sphere at the position (x, y) and time t. The present numerical algorithm is exact in one dimension, although we ignore three-dimensional effects.

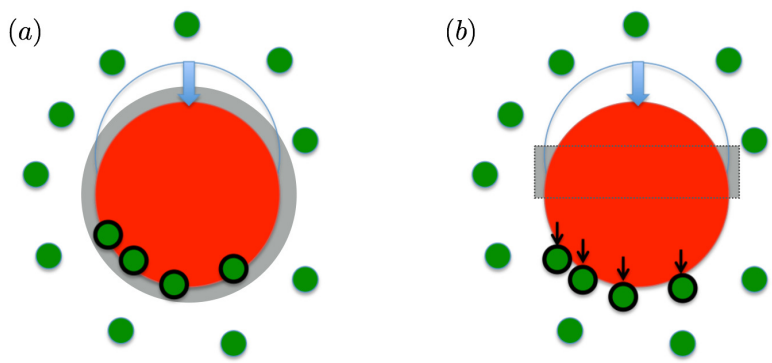

Figure C.1: The special treatment of the number density for the hard sphere model. It is described by the cross section. The blue dot circle represent the large sphere at time t. The red and green circles represent the large sphere at time $t + \Delta t$ and small-sphere, which is modeled in Fig. 3.1. If the solvent particles are overlapped as shown in (a), they are removed. The removed particles are added on the surface of the bottom side of the large sphere as shown in (b). The gray area in (a) is in the space $|\boldsymbol{r} - \boldsymbol{r}_{\mathrm{LS}}(t + \Delta t)| \leq 3d_{\mathrm{S}}$. The gray area in (b) is in the space which is satisfied with both of $(x - x_{\mathrm{LS}})^2 + (y - y_{\mathrm{LS}})^2 \leq 9d_{\mathrm{S}}^2$ and $z_{\mathrm{LS}}(t) < z < z_{\mathrm{LS}}(t + \Delta t)$. Here, $\boldsymbol{r}_{\mathrm{LS}}(t) = (x_{\mathrm{LS}}, y_{\mathrm{LS}}, z_{\mathrm{LS}}(t))$, Δt and d_{S} are the position of the large sphere, time interval, and diameter of the solvent particles, respectively.

Appendix D

Relationship with the Grand Potential Functional and Work

The grand potential functional $\Omega[\rho(\boldsymbol{r},t)]$ can be related to the work from the initial state to the state at time t. To explain the relation, I consider the virtual external potential $u(\boldsymbol{r})$. Following the three states are considered.

1. initial state with Hamiltonian $\mathcal{H}$
external potential $\Phi_{\mathrm{ext}}(\boldsymbol{r},t=0)$, virtual external potential $u(\boldsymbol{r})=0$,
and number density $\rho(\boldsymbol{r},t=0)$

2. equilibrium state with $\mathcal{H}+\int\hat{\rho}(\boldsymbol{r})u(\boldsymbol{r})\mathrm{d}\boldsymbol{r}$
external potential $\Phi_{\mathrm{ext}}(\boldsymbol{r},t)$, virtual external potential $u(\boldsymbol{r})$,
and number density $\rho(\boldsymbol{r},t)$

3. nonequilibrium state with the Hamiltonian $\mathcal{H}(t)$
external potential $\Phi_{\mathrm{ext}}(\boldsymbol{r},t)$, virtual external potential $u(\boldsymbol{r})=0$,
and number density $\rho(\boldsymbol{r},t)$

Here, $\hat{\rho}(\boldsymbol{r})$ is the microscopic number density and $\mathcal{H}$ is defined by Eq. (2.1). The starting point is the work from state A to B $W_{A\to B}$, which can be written as

$$W_{A\to B}=\int\int\langle\hat{\rho}(\boldsymbol{r})\rangle_t\frac{\partial u(\boldsymbol{r},\lambda(t))}{\partial\lambda}\mathrm{d}\boldsymbol{r}\mathrm{d}\lambda(t). \tag{D.1}$$

where λ is the degree of change from state A. to state B.. In addition, λ is in the range from 0 to 1. The sum of $W_{1\to 2}$ and $W_{2\to 3}$ is discussed.

Instead of the states 1. and 2., I consider the states whose Hamiltonian is equivalent to those of the states.

1'. initial state with Hamiltonian $\mathcal{H}$
external potential 0, virtual external potential $\Phi_{\mathrm{ext}}(\boldsymbol{r},t=0)$,
and number density $\rho(\boldsymbol{r},t=0)$

2'. equilibrium state with $\mathcal{H} + \int \hat{\rho}(\boldsymbol{r})u(\boldsymbol{r})\mathrm{d}\boldsymbol{r}$
external potential 0, virtual external potential $u(\boldsymbol{r}) + \Phi_{\mathrm{ext}}(\boldsymbol{r}, t)$,
and number density $\rho(\boldsymbol{r}, t)$

The equivalence can be certified by

$$\begin{aligned}
\mathcal{H}(\boldsymbol{r}^N, \boldsymbol{p}^N) &+ \int \hat{\rho}(\boldsymbol{r})u(\boldsymbol{r})\mathrm{d}\boldsymbol{r} \\
&= \sum_{i=1}^{N} \frac{\boldsymbol{p}_i^2}{2m} + \sum_{i>j}^{N}\sum_{j=1}^{N} v(\boldsymbol{r}_{i,j}) + \sum_{i=1}^{N} \Phi_{\mathrm{ext}}(\boldsymbol{r}_i) + \int \hat{\rho}(\boldsymbol{r})u(\boldsymbol{r})\mathrm{d}\boldsymbol{r} \\
&= \sum_{i=1}^{N} \frac{\boldsymbol{p}_i^2}{2m} + \sum_{i>j}^{N}\sum_{j=1}^{N} v(\boldsymbol{r}_{i,j}) + \int \hat{\rho}(\boldsymbol{r}) \left\{\Phi_{\mathrm{ext}}(\boldsymbol{r}) + u(\boldsymbol{r})\right\} \mathrm{d}\boldsymbol{r}.
\end{aligned} \tag{D.2}$$

Here, I use the definition of the microscopic density, $\hat{\rho}(\boldsymbol{r}) \equiv \sum_{i=1}^{n} \delta(\boldsymbol{r} - \boldsymbol{r}_i)$. Since the Hamiltonian of the system 1. and 2. is equivalent to those of the system $1'$. and $2'$., respectivelty, The work from the state $1'$. to $2'$. is equivalent to The work from the state 1. to 2.,

$$W_{1'\to 2'}^{\min} = W_{1\to 2}^{\min}. \tag{D.3}$$

In the process from the state $1'$. to $2'$., $u(\boldsymbol{r}, \lambda(t))$ and $\langle \hat{\rho}(\boldsymbol{r})\rangle_t$ depend on λ. Moreover, the quasi-static process is assumed. Thus, it can be assumed that $\langle \hat{\rho}(\boldsymbol{r})\rangle_t$ replaces $\rho_{\mathrm{eq}}(\boldsymbol{r}, \lambda)$, where $\rho_{\mathrm{eq}}(\boldsymbol{r}, \lambda)$ is the number density in the grand canonical ensemble average with $\mathcal{H} + \int \hat{\rho}(\boldsymbol{r})u(\boldsymbol{r}, \lambda)\mathrm{d}\boldsymbol{r}$. The work from the state $1'$. to $2'$. represents the minimum work $W_{1'\to 2'}^{\min}$, which is written by

$$W_{1'\to 2'}^{\min} = \int\int \rho_{\mathrm{eq}}(\boldsymbol{r}, \lambda)\frac{\partial u(\boldsymbol{r}, \lambda)}{\partial \lambda}\mathrm{d}\boldsymbol{r}\mathrm{d}\lambda. \tag{D.4}$$

One can confirm that the work $W_{1\to 2}^{\min}$ is the quantity of state. Besides, λ has the relationships $u(\boldsymbol{r}, \lambda = 0) = \Phi_{\mathrm{ext}}(\boldsymbol{r}, t = 0)$, $u(\boldsymbol{r}, \lambda = 1) = u(\boldsymbol{r}) + \Phi_{\mathrm{ext}}(\boldsymbol{r}, t)$, $\rho_{\mathrm{eq}}(\boldsymbol{r}, \lambda = 0) = \rho(\boldsymbol{r}, t = 0)$, and $\rho_{\mathrm{eq}}(\boldsymbol{r}, \lambda = 1) = \rho(\boldsymbol{r}, t)$.

The minimum work $W_{1'\to 2'}^{\min}$ can be calculated from partial integration by

$$\begin{aligned}
W_{1'\to 2'}^{\min} &= \int\int \rho_{\mathrm{eq}}(\boldsymbol{r}, \lambda)\frac{\partial u(\boldsymbol{r}, \lambda)}{\partial \lambda}\mathrm{d}\boldsymbol{r}\mathrm{d}\lambda \\
&= \left[\int \rho_{\mathrm{eq}}(\boldsymbol{r}, \lambda)u(\boldsymbol{r}, \lambda)\mathrm{d}\boldsymbol{r}\right]_{\lambda=0}^{1} - \int\int \frac{\partial \rho_{\mathrm{eq}}(\boldsymbol{r}, \lambda)}{\partial \lambda}u(\boldsymbol{r}, \lambda)\mathrm{d}\boldsymbol{r}\mathrm{d}\lambda \\
&= \int \rho(\boldsymbol{r}, t)u(\boldsymbol{r})\mathrm{d}\boldsymbol{r} + \int \rho(\boldsymbol{r}, t)\Phi_{\mathrm{ext}}(\boldsymbol{r}, t)\mathrm{d}\boldsymbol{r} - \int \rho(\boldsymbol{r}, t = 0)\Phi_{\mathrm{ext}}(\boldsymbol{r}, t = 0)\mathrm{d}\boldsymbol{r} \\
&\qquad - \int\int \frac{\partial \rho_{\mathrm{eq}}(\boldsymbol{r}, \lambda)}{\partial \lambda}u(\boldsymbol{r}, \lambda)\mathrm{d}\boldsymbol{r}\mathrm{d}\lambda.
\end{aligned} \tag{D.5}$$

Using the result of DFT in Eq (2.13), one can obtain the expression of $W^{\min}_{1'\to 2'}$ by

$$\begin{aligned} W^{\min}_{1'\to 2'} &= \int \rho(\boldsymbol{r},t)u(\boldsymbol{r})\mathrm{d}\boldsymbol{r} + \int \rho(\boldsymbol{r},t)\Phi_{\mathrm{ext}}(\boldsymbol{r},t)\mathrm{d}\boldsymbol{r} - \int \rho(\boldsymbol{r},t=0)\Phi_{\mathrm{ext}}(\boldsymbol{r},t=0)\mathrm{d}\boldsymbol{r} \\ &\quad + \int\int \frac{\partial \rho_{\mathrm{eq}}(\boldsymbol{r},\lambda)}{\partial\lambda}\frac{\delta\Omega[\rho_{\mathrm{eq}}(\boldsymbol{r},\lambda),\Phi_{\mathrm{ext}}(\boldsymbol{r})=0]}{\delta\rho_{\mathrm{eq}}(\boldsymbol{r},\lambda)}\mathrm{d}\boldsymbol{r}\mathrm{d}\lambda \\ &= \int \rho(\boldsymbol{r},t)u(\boldsymbol{r})\mathrm{d}\boldsymbol{r} + \int \rho(\boldsymbol{r},t)\Phi_{\mathrm{ext}}(\boldsymbol{r},t)\mathrm{d}\boldsymbol{r} - \int \rho(\boldsymbol{r},t=0)\Phi_{\mathrm{ext}}(\boldsymbol{r},t=0)\mathrm{d}\boldsymbol{r} \\ &\quad \Omega[\rho(\boldsymbol{r},t),\Phi_{\mathrm{ext}}(\boldsymbol{r})=0] - \Omega[\rho(\boldsymbol{r},t=0),\Phi_{\mathrm{ext}}(\boldsymbol{r})=0] \end{aligned} \tag{D.6}$$

Since the grand potential functional in the homogeneous system ($\Phi_{\mathrm{ext}}(\boldsymbol{r}) = 0$) is related to the grand potential functional in the presence of the external field $\Phi_{\mathrm{ext}}(\boldsymbol{r})$ [Eq. (2.21)]

$$\Omega[\rho(\boldsymbol{r},t=0),\Phi_{\mathrm{ext}}(\boldsymbol{r})] = \Omega[\rho(\boldsymbol{r},t=0),\Phi_{\mathrm{ext}}(\boldsymbol{r})=0] + \int \rho(\boldsymbol{r})\Phi_{\mathrm{ext}}(\boldsymbol{r})\mathrm{d}\boldsymbol{r}, \tag{D.7}$$

one can obtain

$$\begin{aligned} W^{\min}_{1'\to 2'} &= \int \rho(\boldsymbol{r},t)u(\boldsymbol{r})\mathrm{d}\boldsymbol{r} + \Omega[\rho(\boldsymbol{r},t),\Phi_{\mathrm{ext}}(\boldsymbol{r},t)] - \Omega[\rho(\boldsymbol{r},t=0),\Phi_{\mathrm{ext}}(\boldsymbol{r},t=0)] \\ &= \int \rho(\boldsymbol{r},t)u(\boldsymbol{r})\mathrm{d}\boldsymbol{r} + \Delta\Omega[\rho(\boldsymbol{r},t)]. \end{aligned} \tag{D.8}$$

Here, $\Delta\Omega[\rho(\boldsymbol{r},t)]$ is defined by $\Omega[\rho(\boldsymbol{r},t),\Phi_{\mathrm{ext}}(\boldsymbol{r},t)] - \Omega[\rho(\boldsymbol{r},t=0),\Phi_{\mathrm{ext}}(\boldsymbol{r},t=0)]$.

In the process from state 2. to 3., $u(\boldsymbol{r},\lambda(t))$ is varied with keeping the constant $\langle\hat{\rho}(\boldsymbol{r})\rangle_t = \rho(\boldsymbol{r},t)$. In state 2., $u(\boldsymbol{r},\lambda=0)$ is $u(\boldsymbol{r})$. In state 3., $u(\boldsymbol{r},\lambda=1)$ is 0. The work $W_{2\to 3}$ can be calculated by

$$\begin{aligned} W^{min}_{2\to 3} &= \int\int \rho(\boldsymbol{r},t)\frac{\partial u(\boldsymbol{r},\lambda)}{\partial\lambda}\mathrm{d}\boldsymbol{r}\mathrm{d}\lambda \\ &= \int \rho(\boldsymbol{r},t)\left[\int \frac{\partial u(\boldsymbol{r},\lambda)}{\partial\lambda}\mathrm{d}\lambda\right]\mathrm{d}\boldsymbol{r} \\ &= \int \rho(\boldsymbol{r},t)\left[u(\boldsymbol{r},\lambda=1) - u(\boldsymbol{r},\lambda=0)\right]\mathrm{d}\boldsymbol{r} \\ &= -\int \rho(\boldsymbol{r},t)u(\boldsymbol{r})\mathrm{d}\boldsymbol{r}. \end{aligned} \tag{D.9}$$

From Eqs (D.8) and (D.9), the work $W_{1\to 3}$ is

$$\begin{aligned} W_{1\to 3} &= W^{\min}_{1\to 2} + W_{2\to 3} \\ &= \Delta\Omega[\rho(\boldsymbol{r},t)]. \end{aligned} \tag{D.10}$$

Therefore, $\Delta\Omega[\rho(\boldsymbol{r},t)]$ is equal to be the work by using the virtual external potential $u(\boldsymbol{r})$.

References

[1] J. P. Abrahams, A. G. Leslie, R. Lutter, and J. E. Walker: Nature **370** (1994) 621.

[2] H. Noji, R. Yasuda, M. Yoshida, and K. Kinosita: Nature **386** (1997) 299.

[3] H. L. Sweeney and A. Houdusse: The EMBO Journal **23** (2004) 4527.

[4] K. Kitamura, M. Tokunaga, A. H. Iwane, and T. Yanagida: Nature **397** (1999) 129.

[5] A. L. Horwich, W. A. Fenton, E. Chapman, and A. G. W. Farr: Rev. Cell. Dev. Biol. **23** (2007) 115.

[6] P. J. B. D. K. Clare, H. van Heerikhuizen, S. M. van der Vies, and H. R. Saibil: Nature **457** (2009) 107.

[7] R. Kanno, A. Koike-Takeshita, K. Yokoyama, H. Taguchi, and K. Mitsuoka: Structure **17** (2009) 287.

[8] S. Asakura and F. Oosawa: J. Chem. Phys **22** (1954) 1255.

[9] S. Asakura and F. Oosawa: J. Polym. Sci **33** (1958) 183.

[10] J. P. Hansen and I. R. McDonald: *Theory of Simple Liquids 3rd ed.* (Academic Press, London, 2006)

[11] D. Beglov and B. Roux: J. Chem. Phys. **103** (1995) 360.

[12] Y. Harano, R. Roth, Y. Sugita, M. Ikeguchi, and M. Kinoshita: Chem. Phys. Lett. **437** (2007) 112.

[13] T. Yoshidome, Y. Ito, M. Ikeguchi, , and M. Kinoshita: J. Am. Chem. Soc **137** (2011) 035102.

[14] T. Yoshidome, Y. Ito, N. Matubayasi, M. Ikeguchi, and M. Kinoshita: J. Chem. Phys **137** (2012) 035102.

[15] H. Mishima, H. Oshima, S. Yasuda, and M. Kinoshita: J. Phys. Chem. B **119** (2015) 3423.

[16] P.-M. König, R. Roth, and K. R. Mecke: Phys. Rev. Lett. **93** (2004) 160601.

[17] K. Amano and M. Kinoshita: Chem. Phys. Lett. **488** (2010) 1.

[18] K. Amano and M. Kinoshita: Chem. Phys. Lett. **504** (2011) 22.

[19] K. Amano, H. Oshima, and M. Kinoshita: J. Chem. Phys. **135** (2011) 185101.

[20] K. Amano and M. Kinoshita: private cominications, the potential of mean force between a large-sphere and a cylindrical vessel is calculated by integral equational theory (2015).

[21] K. Amano, T. Yoshidome, M. Iwaki, M. Suzuki, and M. Kinoshita: J. Chem. Phys. **133** (2010) 045103.

[22] H. Mishima, H. Oshima, S. Yasuda, K. Amano, and M. Kinoshita: J. Chem. Phys. **139** (2013) 205102.

[23] H. Mishima, H. Oshima, S. Yasuda, K. Amano, and M. Kinoshita: Chem. Phys. Lett. **561** (2013) 159.

[24] R. Kubo, M. Toda, and N. Hashitsume: *Statistical Physics II Nonequilibrium Statistical Mechanics* (Springer-Verlag, Berlin Heidelberg, 1991)

[25] U. M. B. Marconi and P. Tarazona: J. Chem. Phys **110** (1999) 8032.

[26] A. Yoshimori: J. Theor. Comput. Chem. **3** (2004) 117.

[27] A. Yoshimori: Phys. Rev. E **71** (2005) 031203.

[28] R. Akiyama, Y. Karino, H. Obama, and A. Yoshifuku: Phys. Chem. Chem. Phys. **12** (2010) 3096.

[29] H. N. W. Lekkerkerker and R. Tuinier: *Colloids and the Depletion Interaction* (Springer-Verlag, Dordrecht, 2011)

[30] R. F. T. Jr, I. D. K. Jr, and F. A. Petsko: Biochemistry **23** (1984) 2849.

[31] G. J. Ewing and S. Maestas: J. Phys. Chem **74** (1970) 2341.

[32] Y. Shingh: Phys. Rep. **207** (1991) 351.

[33] T. V. Ramakrishan and M. Yussouff: Phys. Rev. B **19** (1979) 2775.

[34] T. Morita: Prog. Theor. Phys. **23** (1960) 829.

[35] T. Morita and K. Hiroike: Prog. Theor. Phys. **25** (1961) 537.

[36] L. Verlet and D. Levesque: Physica **28** (1962) 1124.

[37] T. Yoda, Y. Sugita, and Y. Okamoto: Chem. Phys. Lett. **386** (2004) 460.

[38] R. Kodama, R. Roth, Y. Harano, and M. Kinoshita: J. Chem. Phys **135** (2011) 045103.

[39] Y. Harano: Entropy **14** (2012) 1443.

[40] Y. Harano, R. Roth, Y. Sugita, M. Ikeguchi, and M. KinoshitaI: Chem. Phys. Lett. **437** (2007) 112.

[41] T. imai, Y. Harano, M. Kinoshita, A. Kovalenko, and F. Hirata: J. Chem. Phys **125** (2006) 024911.

[42] T. Yu, O. S. Lee, and G. C. Schatz: J. Phys. Chem. A **117** (2013) 7453.

[43] S. Khalid, P. J. Bond, J. Holyoake, R. W. Hawtin, and M. S. P. Sansom: J. R. Soc. Interface **5** (2008) 241.

[44] A. A. Broyles: J. Chem. Phys **33** (1960) 456.

[45] A. Mulero, M. I. P. C. A. Galȧn, and F. Cuadros: *Theory and Simulation of Hard-Sphere Fluids and Related Systems* (Springer-Verlag, Berlin Heidelberg, 2008)

[46] Y. Ito, T. Oroguchi, and M. Ikeguchi: J. Am. Chem. Soc. **133** (2011) 3372.

[47] S. Hayashi, H. Ueno, A. R. Shaikh, M. Umemura, M. Kamiya, Y. Ito, M. Ikeguchi, Y. Komoriya, R. Iino, and H. Noji: J. Am. Chem. Soc. **134** (2012) 8447.

[48] Y. Ito, T. Yoshidome, N. Matubayasi, M. Kinoshita, and M. Ikeguchi: J. Phys. Chem. B. **117** (2013) 3298.

[49] T. Yoshidome, Y. Ito, M. Ikeguchi, and M. Kinoshita: J. Am. Chem. Soc. **133** (2011) 4030.

[50] T. Yoshidome, Y. Ito, N. Matubayasi, M. Ikeguchi, and M. Kinoshita: J. Chem. Phys. **137** (2012) 035102.

[51] S. Phongphanphanee, T. Rungrotmongkol, N. Yoshida, S. Hannongbua, and F. Hirata: J. Am. Chem. Soc. **132** (2010) 9782.

[52] R. Akiyama: Seibutsubuturi **51** (2011) 036.

[53] A. Kovalenko and F. Hirata: Chem. Phys. Lett. **290** (1998) 237.

[54] H. S. Rye, A. M. Roseman, S. Chen, K. Furtak, W. A. Fenton, H. R. Saibil, and A. L. Horwich: Cell **97** (1999) 325.

[55] G. D. Hahn: Int. J. Number. Meth. Eng. **32** (1991) 943.

[56] S. Takahashi, Y. Ching, J. Wang, and D. L. Rousseau: J. Biol. Chem. **270** (1995) 8405.

[57] T. Yoshidome, M. Kinoshita, S. Hirota, N. Baden, and M. Terazima: J. Chem. Phys **128** (2008) 225104.

[58] S. Takahashi, Y. Ching, J. Wang, and D. L. Rousseau: J. Biol. Chem **270** (1995) 8405.

[59] R. M. Ballew and McCammon: Proc. Natl. Acad. Sci **93** (1996) 5759.

[60] W. A. Eaton, V. Munõzz, S. J. Hagen, G. S. J. Lisa, J. L. Eric, R. Henry, and J. Hofrichter: Annu. Rev. Biophys. Biomol. Struct **29** (2000) 327.

[61] W. Saburi, H. Hondoh, Y. M. Kim, H. Mori, M. Okuyama, and A. Kimura: Biologia **63** (2008) 1000.

[62] J. Araki and T. Munakata: Phys. Rev. E **52** (1995) 2577.

[63] M. Bier, R. van Roij, M. Dijkstra, and P. van der Schoot: Phys. Rev. Lett **101** (2008) 215901.

[64] K. Fuchizaki and K. Kawasaki: J. Phys. Soc. Jpn **67** (1998) 1505.

[65] B. Bagchi and A. Chandra: Proc. Indian. Acad. Sci **100** (1988) 353.

[66] A. Chandra and B. Bagch: J. Chem. Phys **94** (1991) 8367.

[67] B. Bagchi and A. Chandra: J. Chem. Phys **97** (1992) 5126.

[68] S. Roy, S. Komath, and B. Bagchi: J. Chem. Phys **99** (1993) 3139.

[69] B. Bagchi: J. Chem. Phys **100** (1994) 6658.

[70] A. Yoshimori: J. Chem. Phys **105** (1996) 5971.

[71] A. Yoshimori, T. J. F. Day, and G. N. Patey: J. Chem. Phys **108** (1998) 6378.

[72] A. Yoshimori, T. J. F. Day, and G. N. Patey: J. Chem. Phys **109** (1998) 3222.